Introduction to

Polarimetric

SAR Tomography

Laurent Ferro-Famil

University of Rennes 1

Laurent.Ferro-Famil@univ-rennes1.fr

Laurent Ferro-Famil

Laurent.Ferro-Famil@univ-rennes1.fr

INSTITUT D'ÉLECTRONIQUE ET DE TÉLÉCOMMUNICATIONS DE RENNES

University of Rennes 1
IETR SHINE Team
Rennes France

SHINE

SAR & Hyperspectral multi-modal Imaging and sigNal processing, Electromagnetic modeling

UNIVERSITÉ DE RENNES 1

Contents

UiT THE ARCTIC UNIVERSITY OF NORWAY
POLITECNICO MILANO
CHALMERS
enveo
esa

SAR Tomography basics

SAR imaging:
resolution improvement based on signal diversity

2-D imaging limitations over 3-D scenes:
SAR interferometry

2-D SAR and inSAR imaging limitations over complex (really 3-D) scenes:
SAR tomography

Radar response model

Born approximation at order 1:

valid for media with weak dielectric contrast

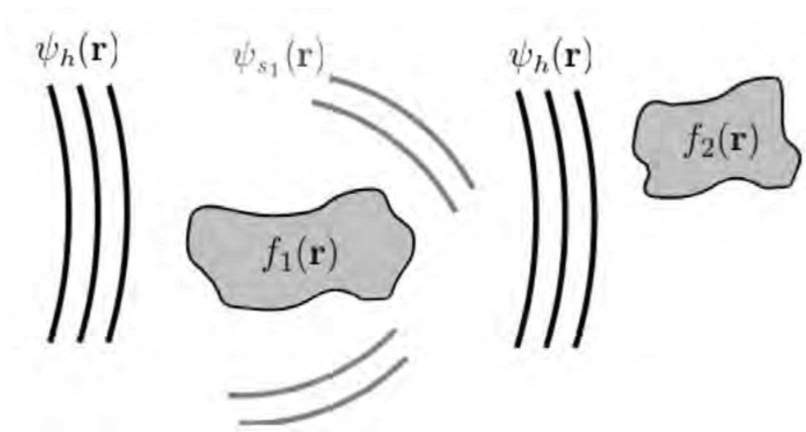

$$\psi_{s_i}(\mathbf{r}) \approx \int_{V_i} f_i(\mathbf{r}')\psi_h(\mathbf{r}')\frac{e^{jk|\mathbf{r}-\mathbf{r}'|}}{|\mathbf{r}-\mathbf{r}'|}\mathrm{d}(\mathbf{r}')$$

Consequence: linear response model

(does not account for multiple interactions)

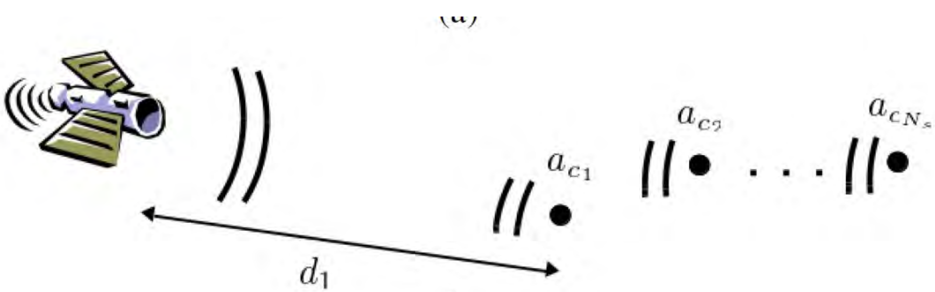

$$\boxed{s_r(\tau) = \sum_i a_{c_i} u(\tau - \tau_i)\, e^{-j\omega_c \tau_i}}$$

1-D imaging using SPECTRAL diversity

1 scatterer located at distance d_0

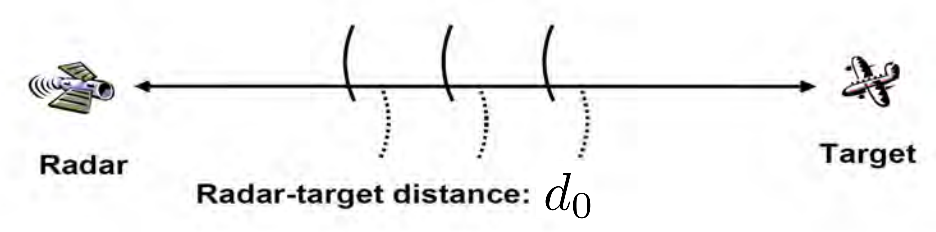

- mono-chromatic waveform $u(\tau) = 1$

$$s_r(\tau) = a_c\,\mathrm{e}^{-j\omega_c\tau_0} \in \mathbb{C} \quad \xrightarrow{?} \quad \begin{cases} a_c & \in \mathbb{C} \\ d_0 & \in \mathbb{R} \end{cases}$$

No, ill-conditioned estimation

- bi-chromatic waveform $u(\tau) = \mathrm{e}^{-j\pm\Delta\omega\tau}$

$$\begin{cases} s_{r_1} &= a_c\,\mathrm{e}^{-j(\omega_c\pm\Delta\omega)\tau_0} \\ s_{r_2} &= a_c\,\mathrm{e}^{-j(\omega_c\pm\Delta\omega)\tau_0} \end{cases} \longrightarrow d_0, a_c$$

2 frequencies for 1 scatterer

1-D imaging using SPECTRAL diversity

Several scatterers

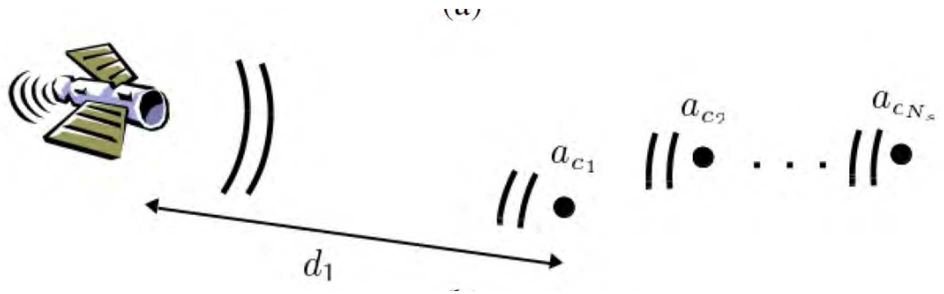

$$s_r(\tau) = \sum_i a_{c_i} u(\tau - \tau_i)\, e^{-j\omega_c \tau_i}$$

- measurements at many spectral locations $\omega_0, \omega_1, \ldots$

- wide bandwidth (rich spectrum) waveform

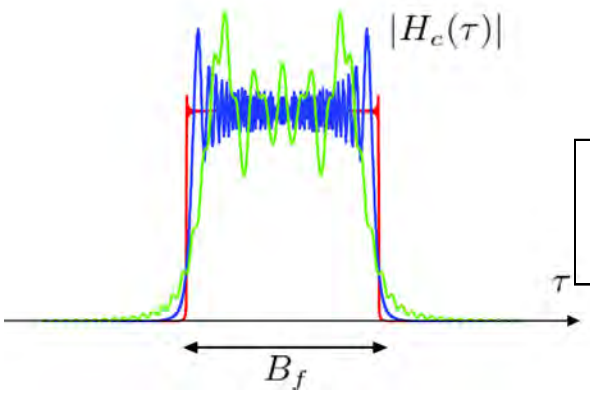

$$\boxed{\delta d = \frac{c}{2B_f}}$$

Large B_f

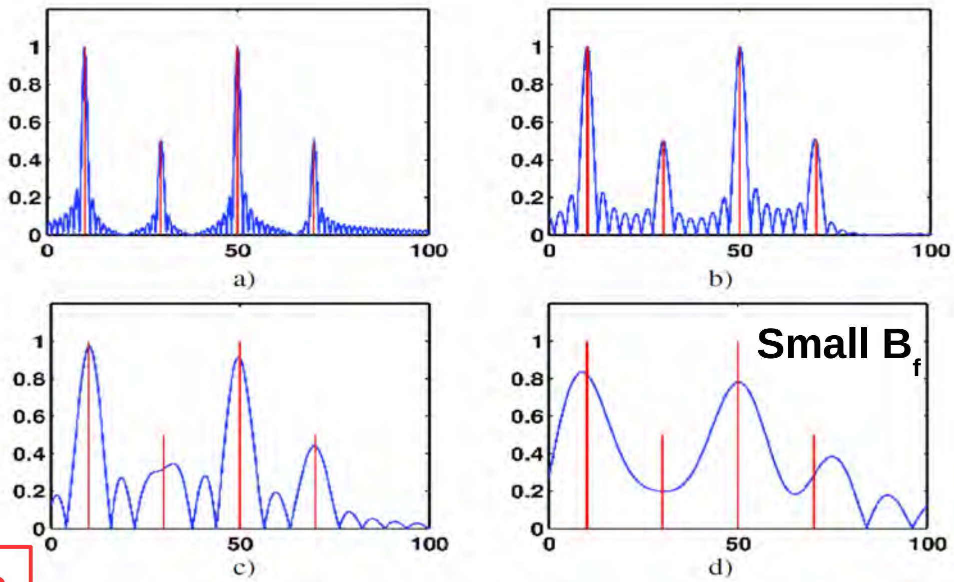

Small B_f

Several scatterers → many frequencies

1-D imaging using SPATIAL diversity

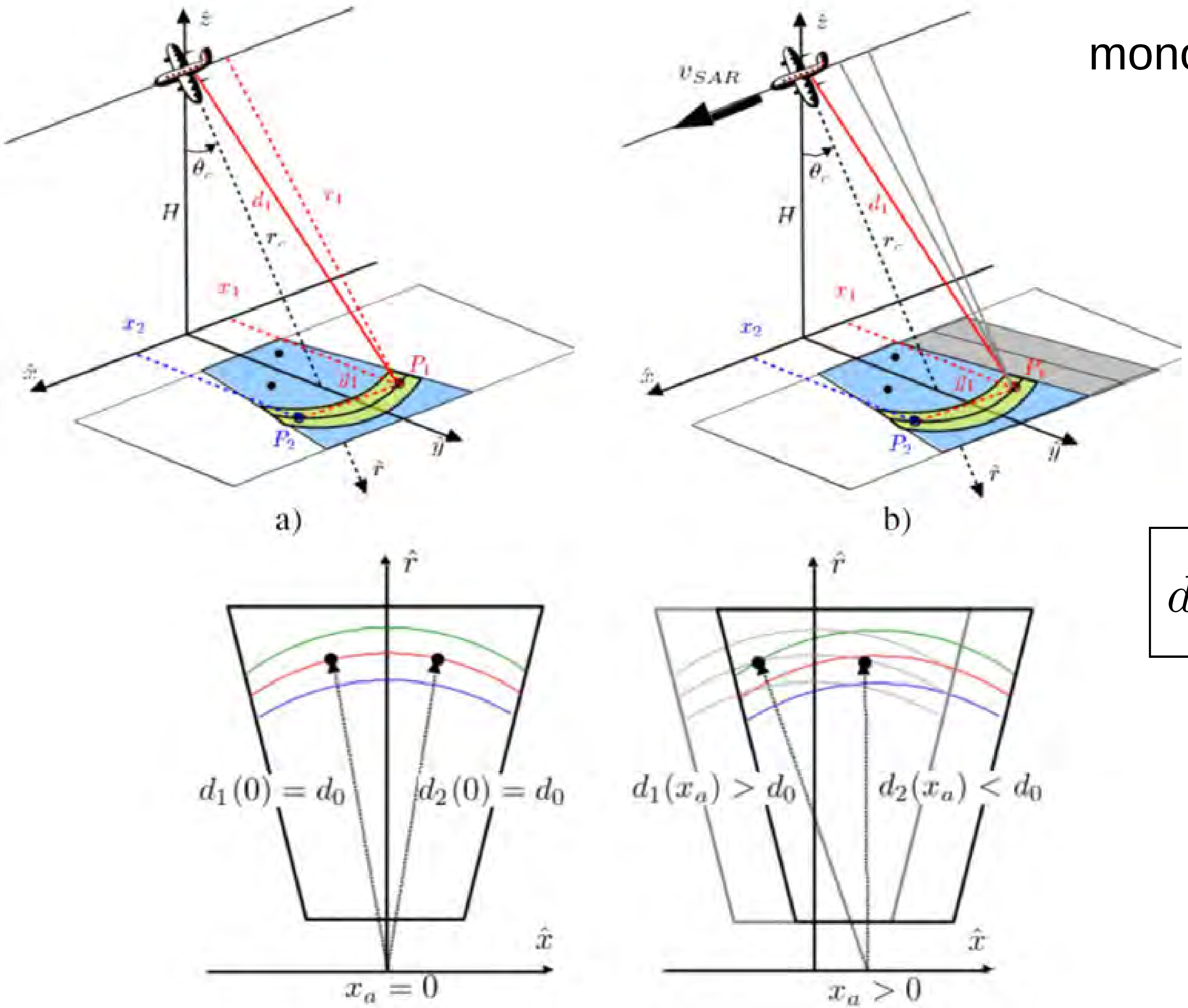

mono-chromatic waveform $u(\tau) = 1$

$$s_{r_i}(x_a) = a_{c_i}\, \mathrm{e}^{-j\omega_c \tau_i(x_a)}$$
$$= a_{c_i}\, \mathrm{e}^{-jkd_i(x_a)}$$

2-way wavenumber $k = \dfrac{4\pi}{\lambda}$

$$\boxed{d_i(x_a) = \sqrt{r_i^2 + (x_i - x_a)^2}}$$

1-D imaging using SPATIAL diversity

1 scatterer located at distance x_0: 2 azimuth positions

$$\mathrm{s}_{r_i}(\pm\Delta x_a) = a_{c_i}\,\mathrm{e}^{-jk\sqrt{r_i^2+(x_0\mp\Delta x_a)^2}} \longrightarrow x_0, a_c$$

Several scatterers: many azimuth positions

$$\delta x = \frac{\lambda_c}{4\sin\left(\frac{\Delta\phi}{2}\right)}$$

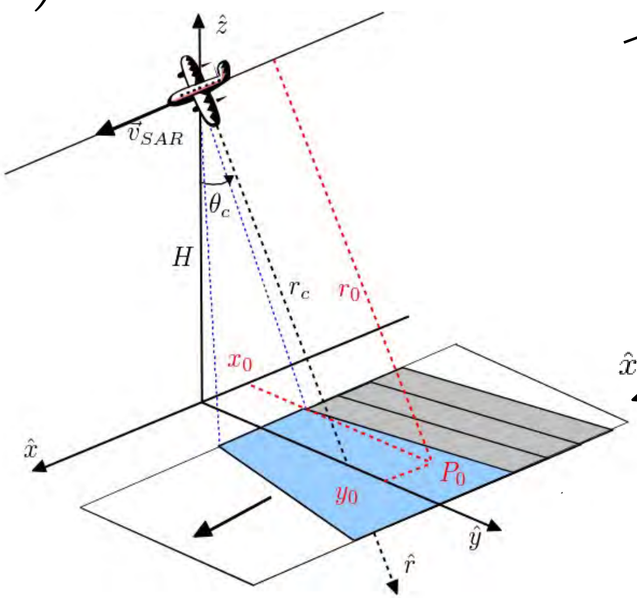

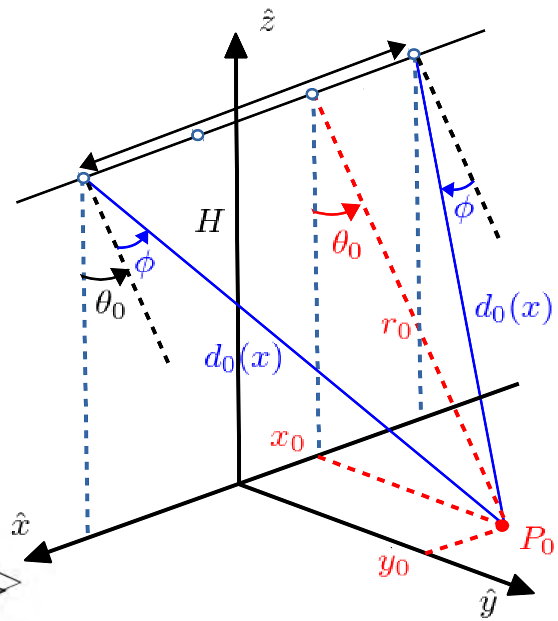

2-D SAR imaging

2-D imaging of several scatterers

- 1-D range imaging using **spectral diversity** (wide bandwith waveform)

+

- 1-D imaging in azimuth using **spatial diversity** (wide azimuth aperture)

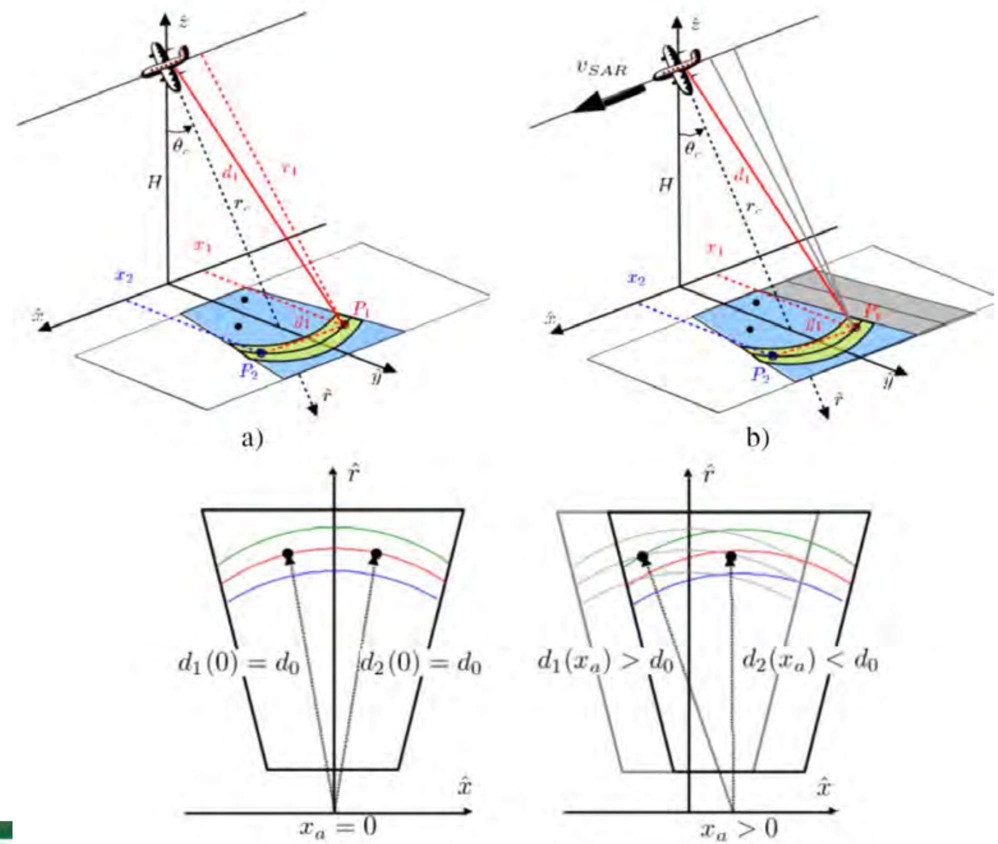

2-D SAR imaging

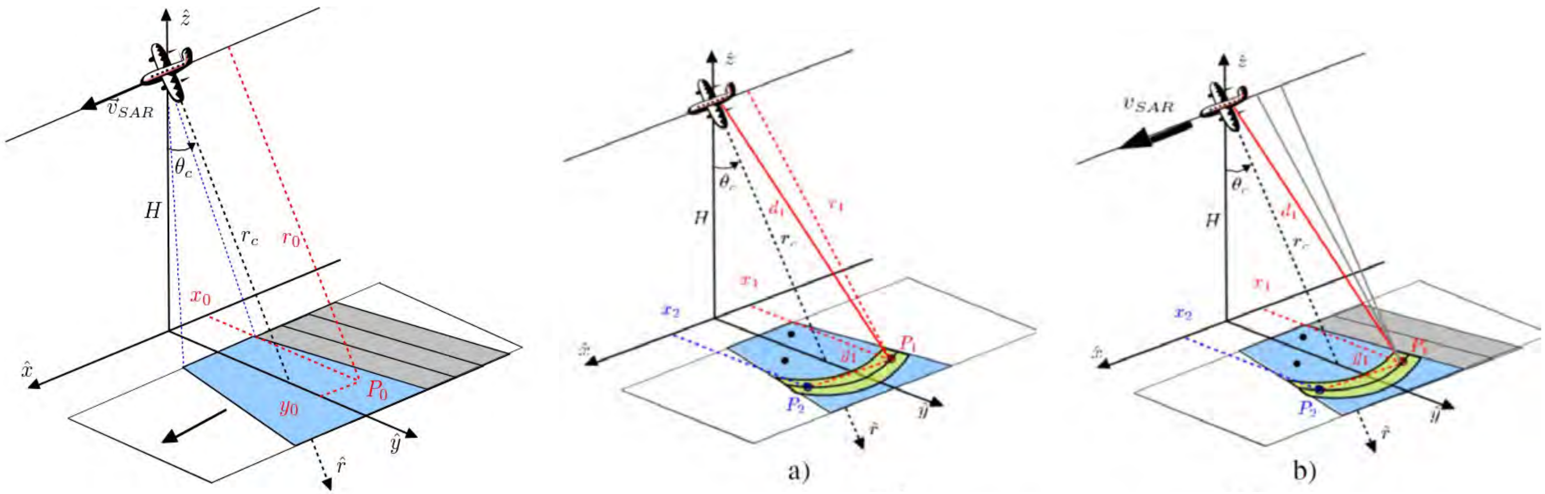

Raw Data → **Range Focusing** → **Integration**

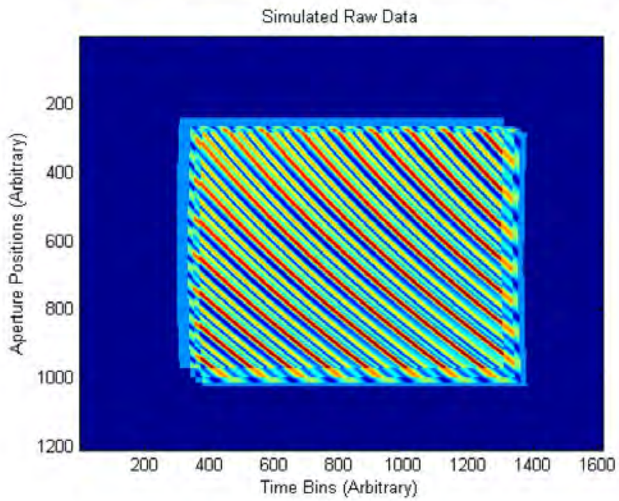

$$s_r(x_a, \tau)$$

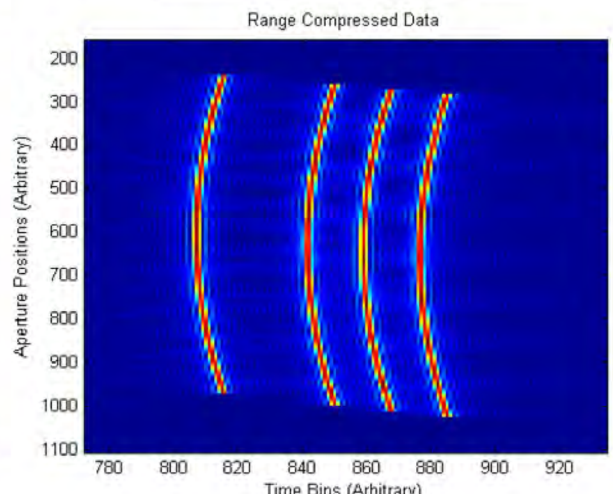

$$s_{rf}(x_a, d)$$

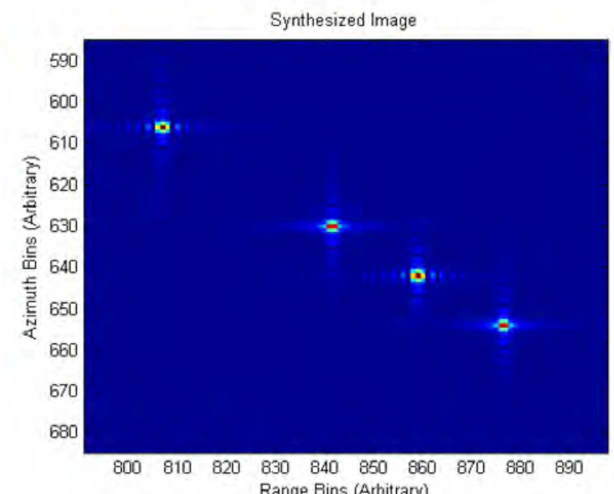

$$s_{raf}(x, r)$$

2-D SAR imaging

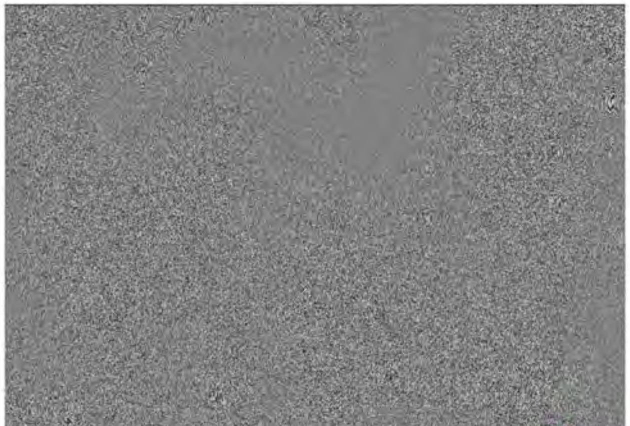

SAR raw data

SAR image

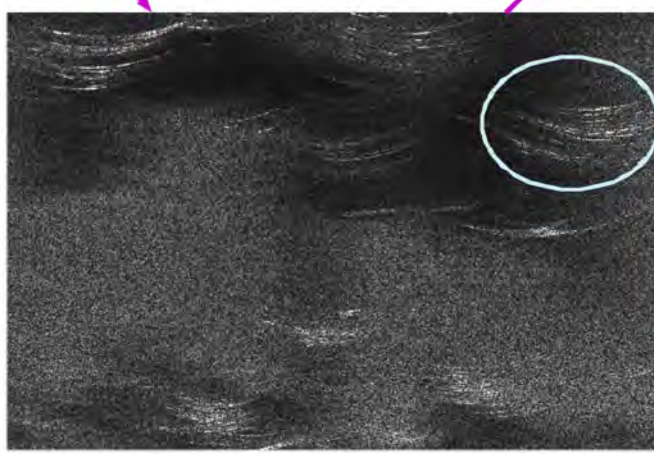

range distance variation
during azimuth illumination
(range cell migration or RCM)

Range compressed SAR image

SAR Tomography basics

SAR imaging:
resolution improvement based on signal diversity

2-D imaging limitations over 3-D scenes:
SAR interferometry

2-D SAR and inSAR imaging limitations over complex (really 3-D) scenes:
SAR tomography

SAR images of 3-D scenes

3-D reflectivity		2-D raw data		2-D image
$\gamma(x, y, z)$	$\Rightarrow$	$s_r(x, \tau)$	$\Rightarrow$	$s(x, r)$

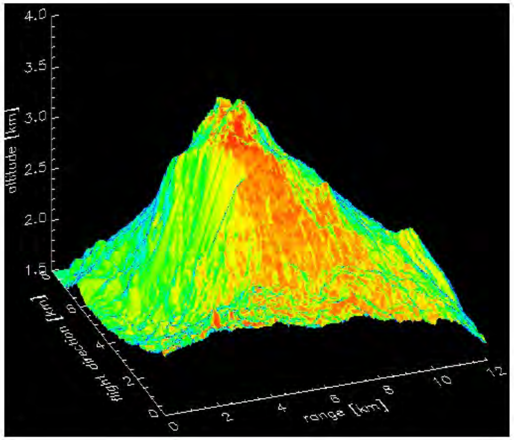

DEM of Mt Etna, Italy

$$\Longrightarrow$$

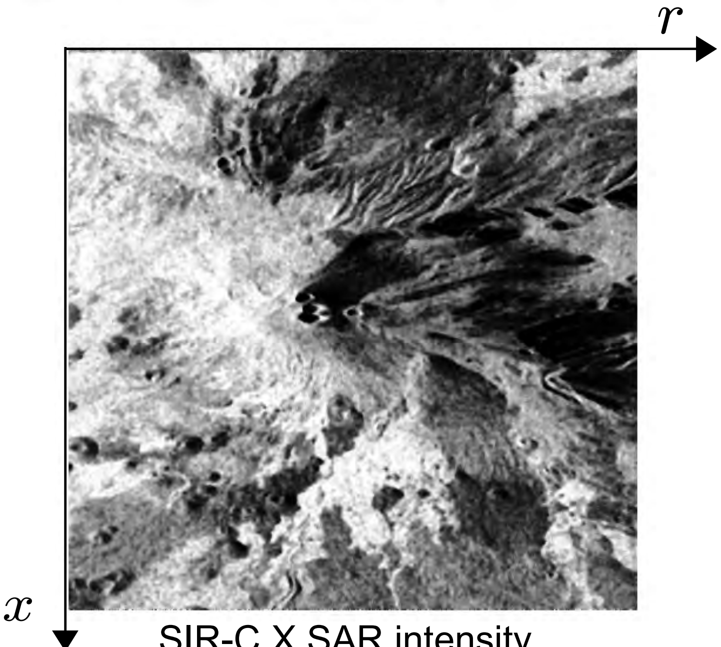

SIR-C X SAR intensity

Loss of a dimension

2-D SAR imaging: cylindrical ambiguity

$$r_i = \sqrt{(H - z_i)^2 + y_i^2}$$

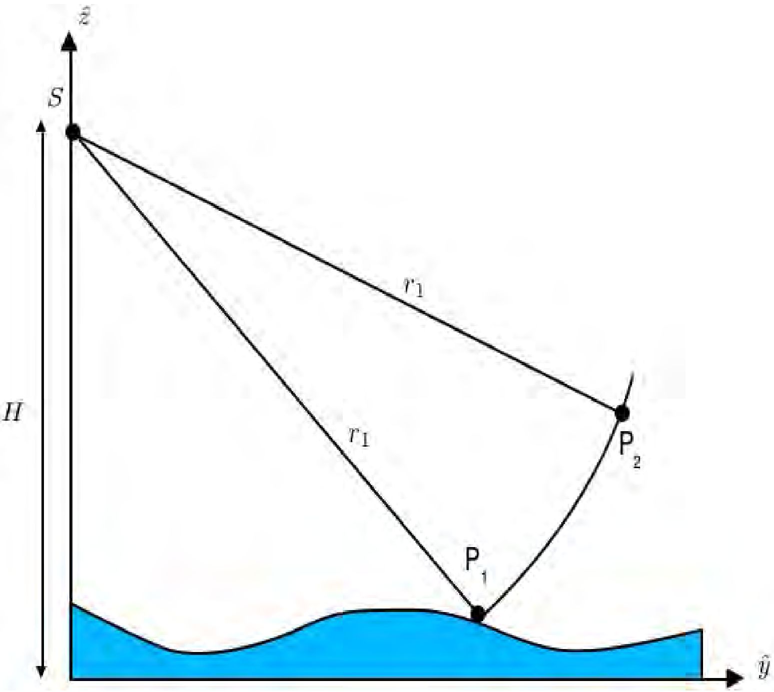

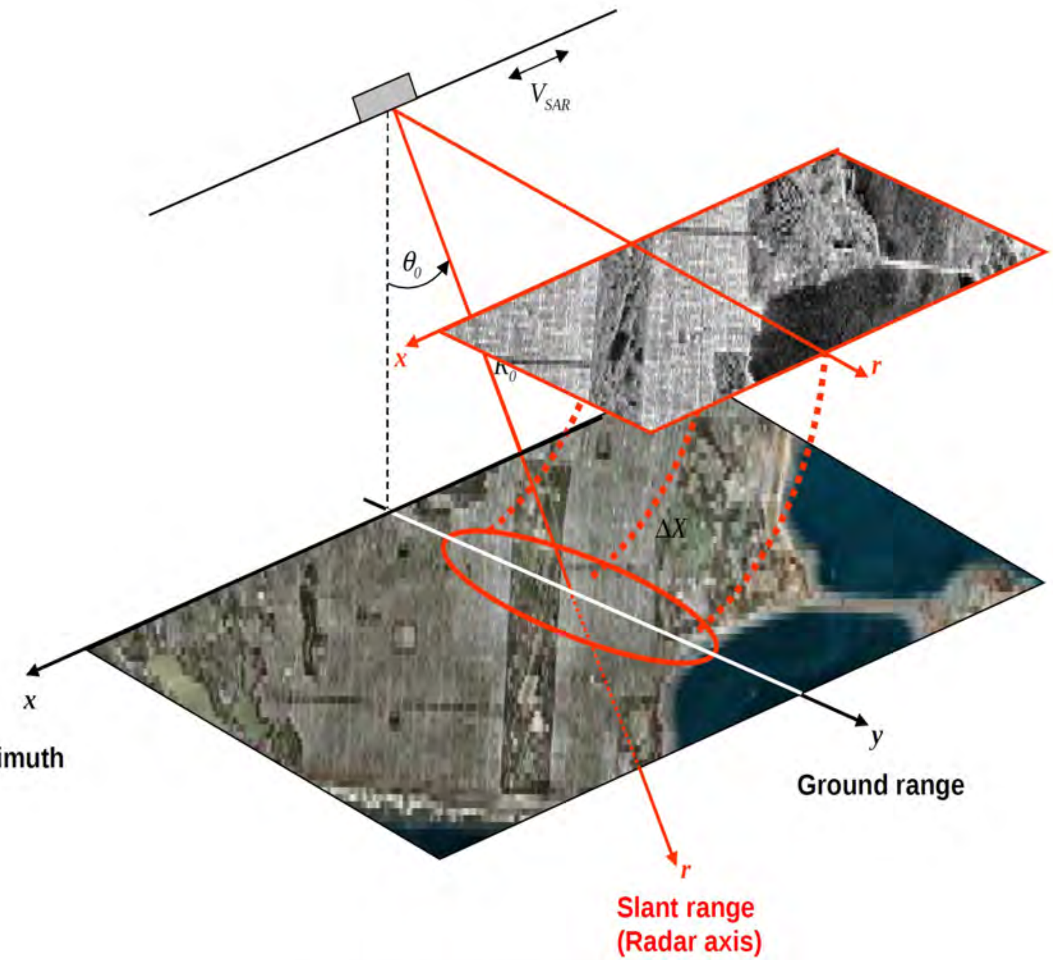

Broadside geometry

Additional spatial diversity

1 scatterer → 2 positions: SAR interferometry

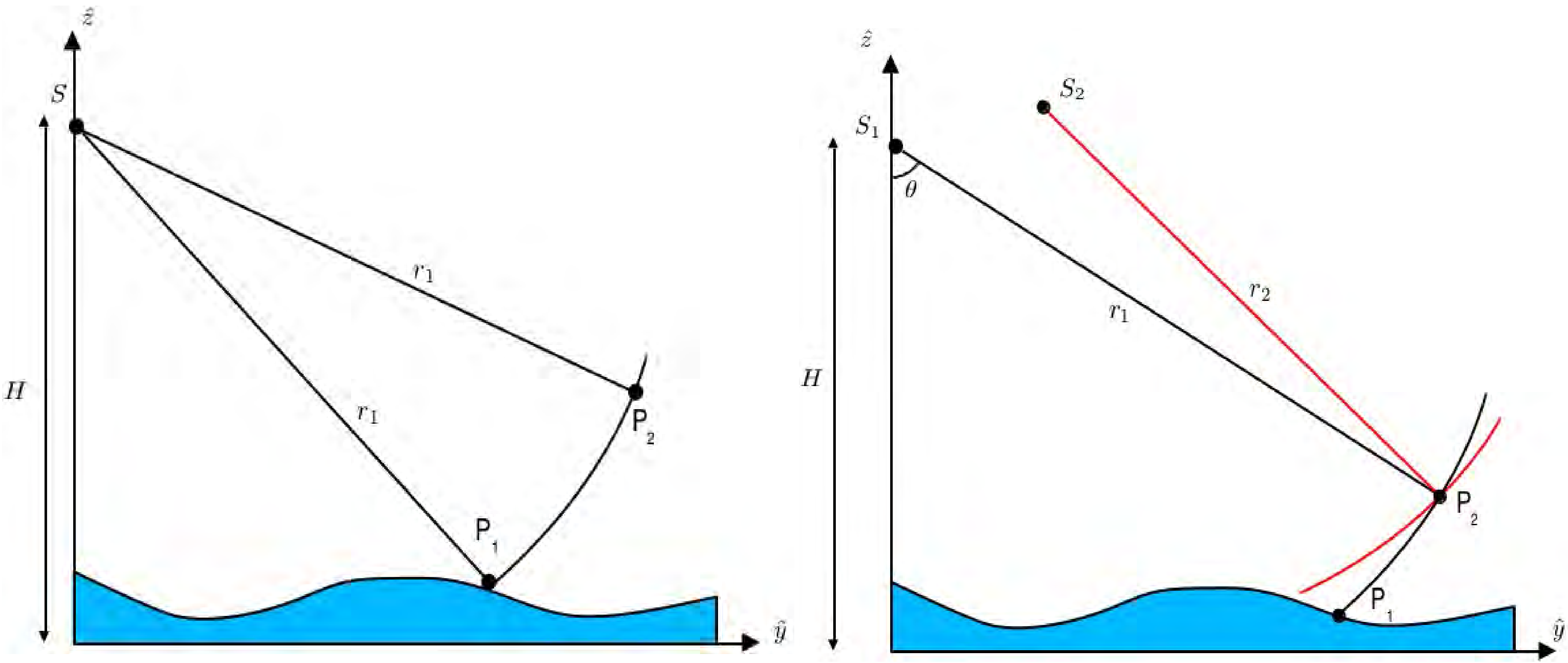

SAR interferometry

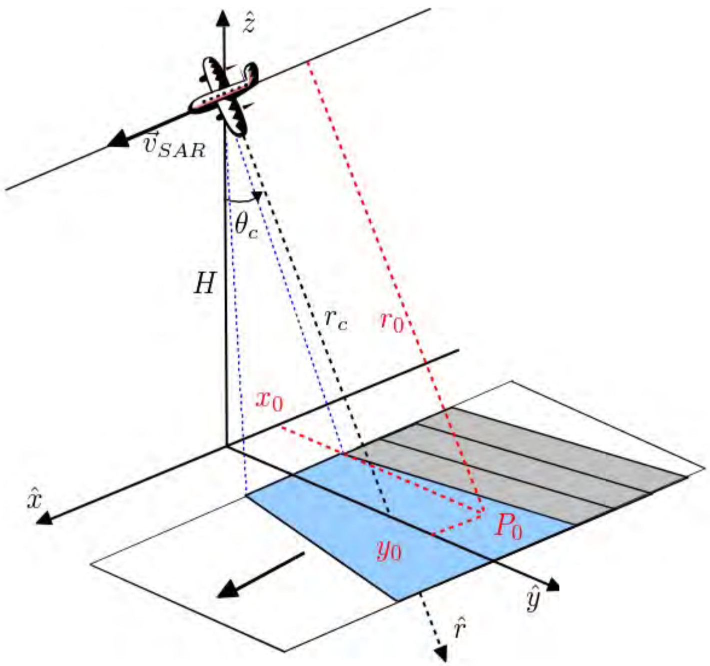

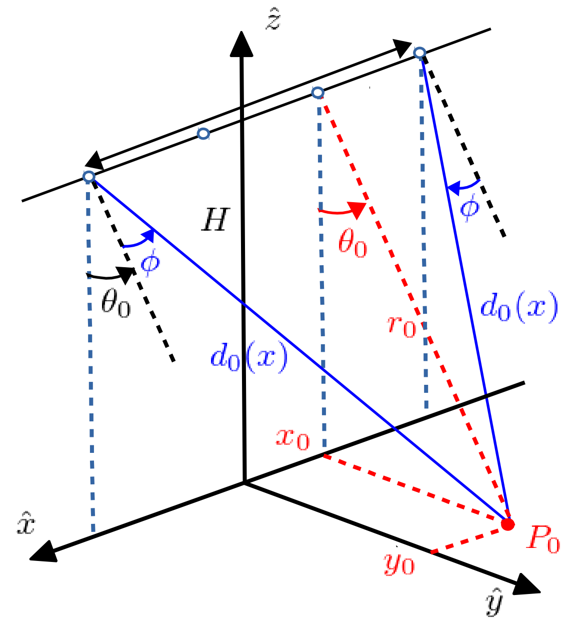

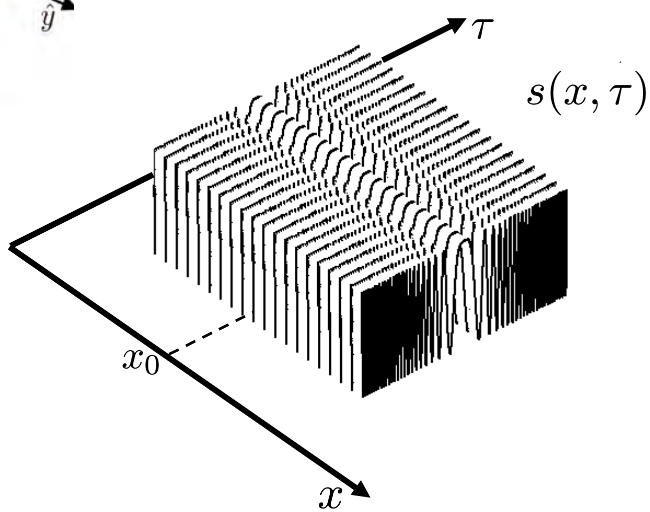

Acquired signal (x-τ domain)

Delay: $\tau = \dfrac{2d}{c}$

Baseband pulse: $p(\tau)\,\mathrm{rect}\left(\dfrac{\tau}{T_p}\right)$

SAR interferometry

Range focused signal (x-d domain)

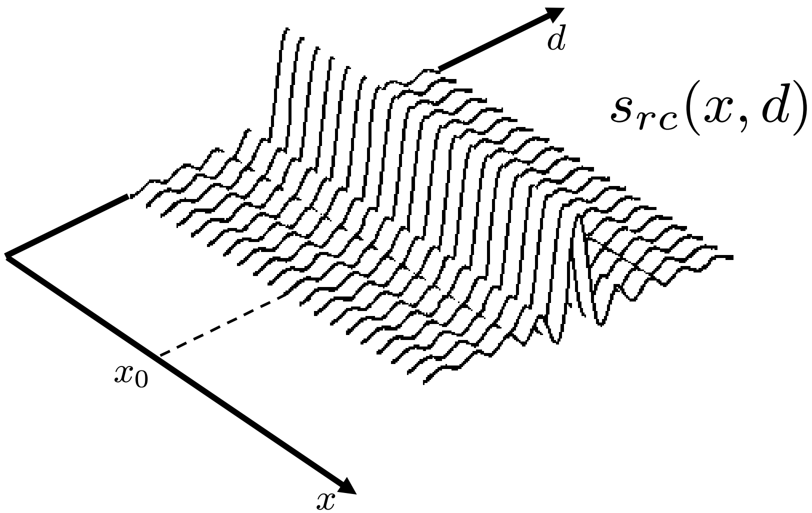

2-D focused signal (x-r domain)

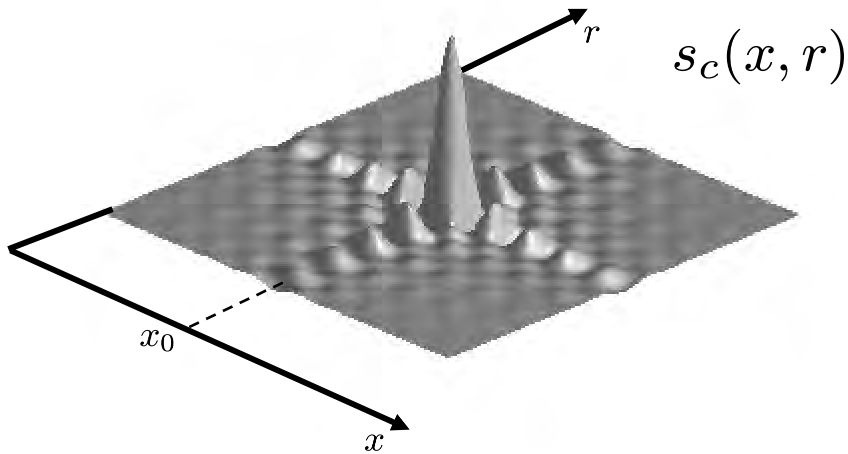

$$
\begin{aligned}
s(x,r) = \quad & a_c && \rightarrow \textbf{complex reflection coefficient} \\
& h_r(d - r_0) && \rightarrow \text{delayed range impulse response} \\
& h_a(x - x_0) && \rightarrow \text{delayed azimuth impulse response} \\
& \exp(-j\tfrac{4\pi}{\lambda_c} r_0) && \rightarrow \textbf{two-way propagation phase}
\end{aligned}
$$

Relating InSAR phase to height

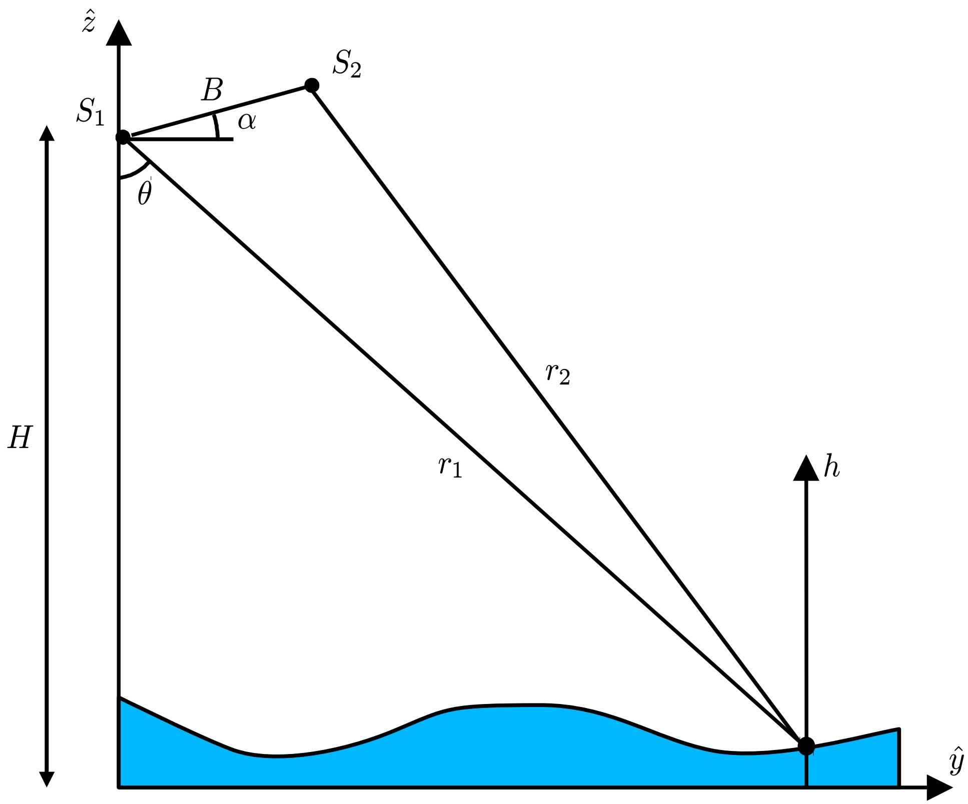

Coherent information

$$s_1 = |a_{c_1}| \exp\left(-j\frac{4\pi}{\lambda_c} r_1 + j + \phi_{obj_1}\right)$$
$$s_2 = |a_{c_2}| \exp\left(-j\frac{4\pi}{\lambda_c} r_2 + j + \phi_{obj_2}\right)$$

InSAR assumptions (small B)

$$|a_{c_1}| \approx |a_{c_2}|, \quad \phi_{obj_1} \approx \phi_{obj_2}$$

InSAR phase difference

$$\phi_{12} = \arg(s_1 s_2^*) = \frac{4\pi}{\lambda_c}(r_2 - r_1) = k_c \Delta r_{12}$$

Relating InSAR phase to height

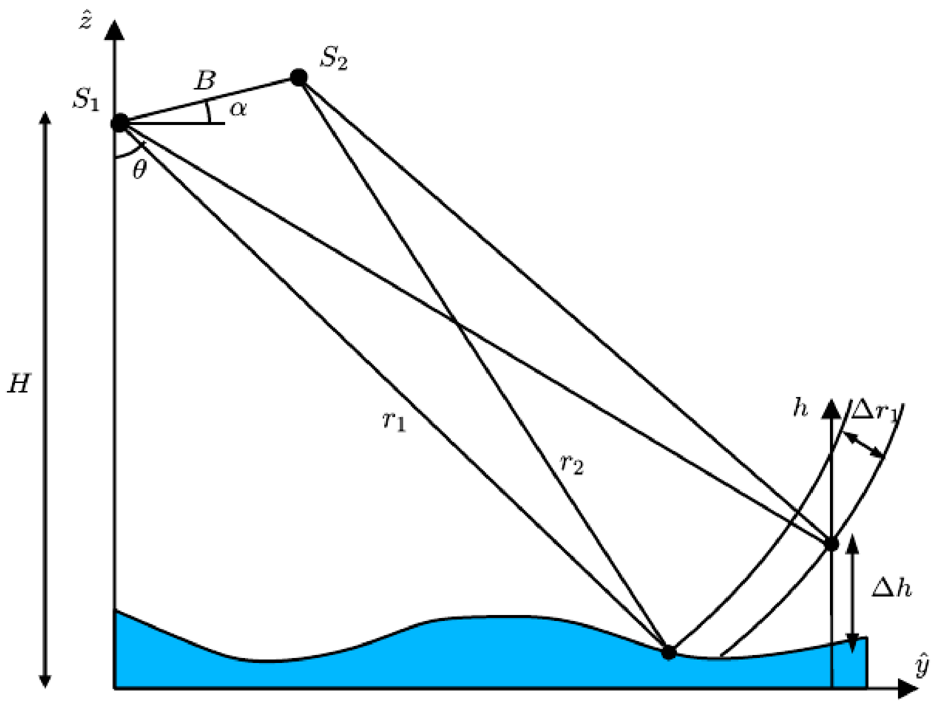

Far-field expression (r_1 >> B)

$$\phi_{12} = k_c B \sin(\alpha - \theta)$$

Sensitivity to terrain geometry

$$\theta = f(H, r_1, h)$$

Local linearization

$$\boxed{\begin{aligned} \Delta\phi_{12} &= k_z \Delta h + k_{fe} \Delta r_1 \\ &= \Delta\phi_{topo} + \Delta\phi_{fe} \end{aligned}}$$

$$k_z = \frac{k_c B_\perp}{r_1 \sin\theta}, \quad k_{fe} = k_z \cos\theta$$

InSAR topography estimation

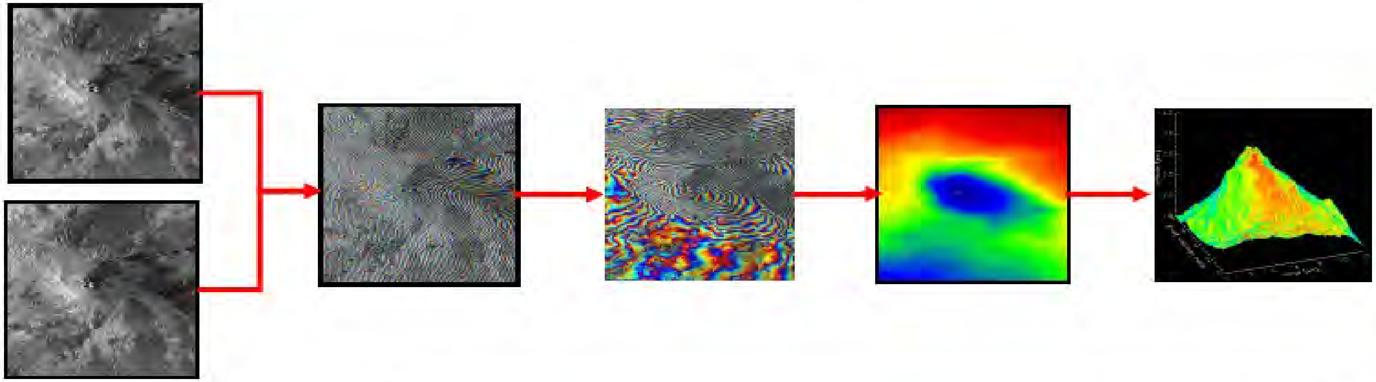

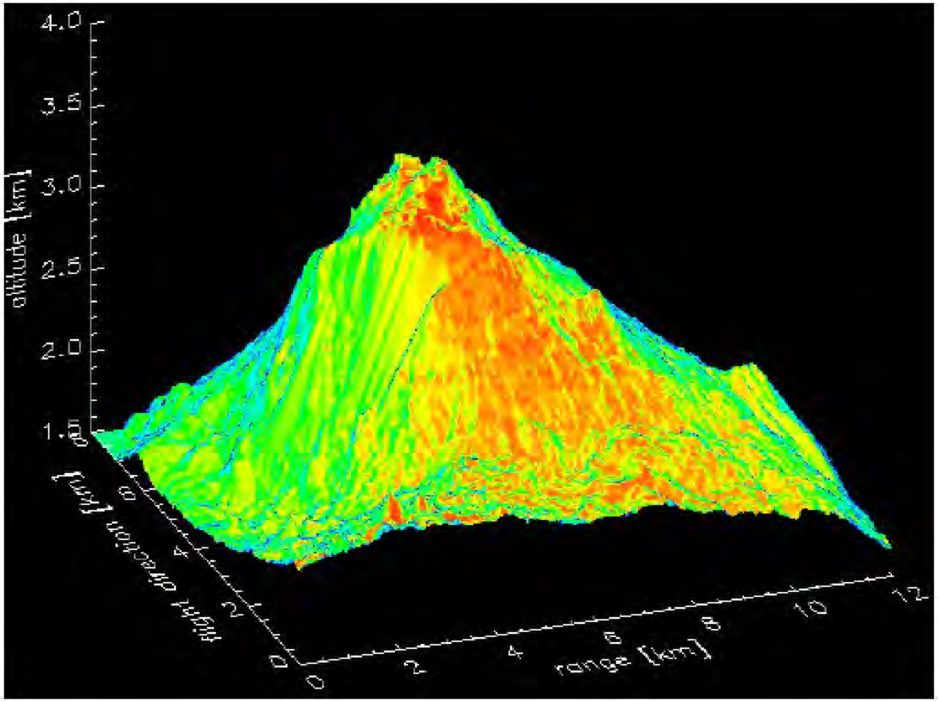

SAR Tomography basics

SAR imaging:
resolution improvement based on signal diversity

2-D imaging limitations over 3-D scenes:
SAR interferometry

*2-D SAR and inSAR imaging limitations over complex (**really 3-D**) scenes:*
SAR tomography

SAR imaging of 3-D scenes

Urban areas

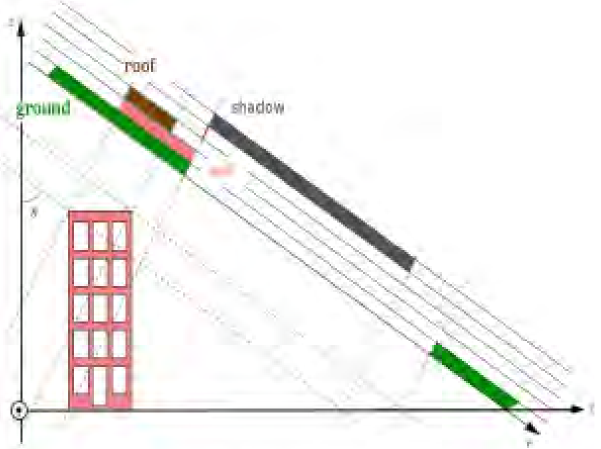

Mixture of **several contributions** in the elevation direction

Pauli-coded SAR image

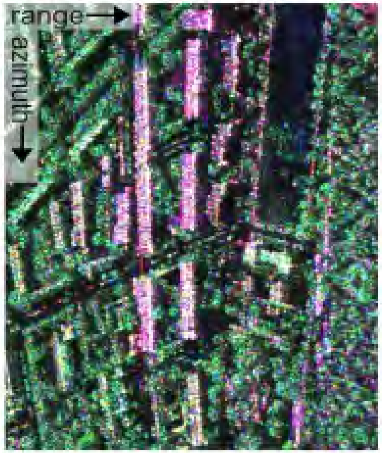

Optical image

BIOSAR II, Boreal forest, L band

Forest height [m]

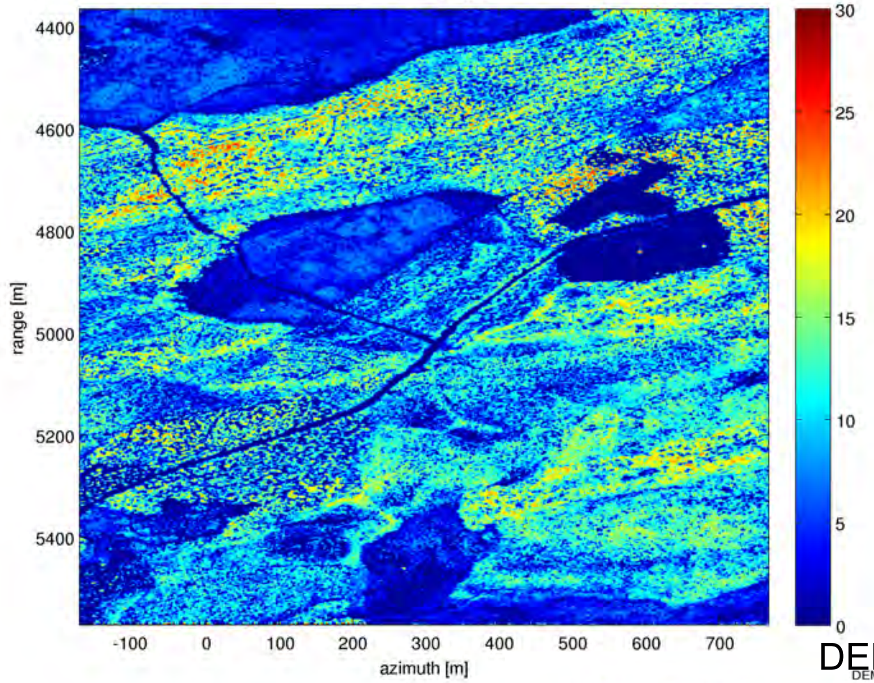

HH intensity [dB]

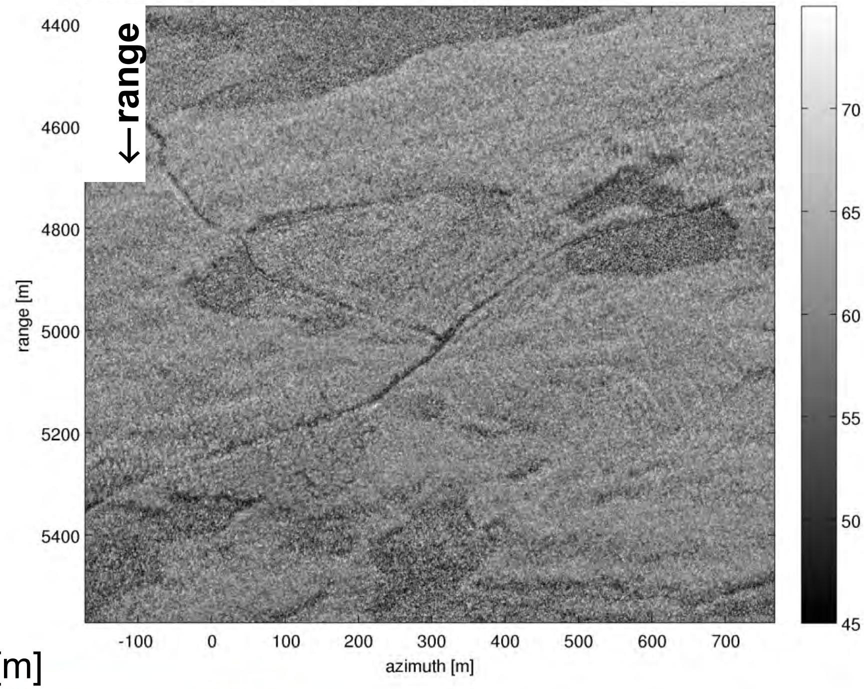

DEM [m]

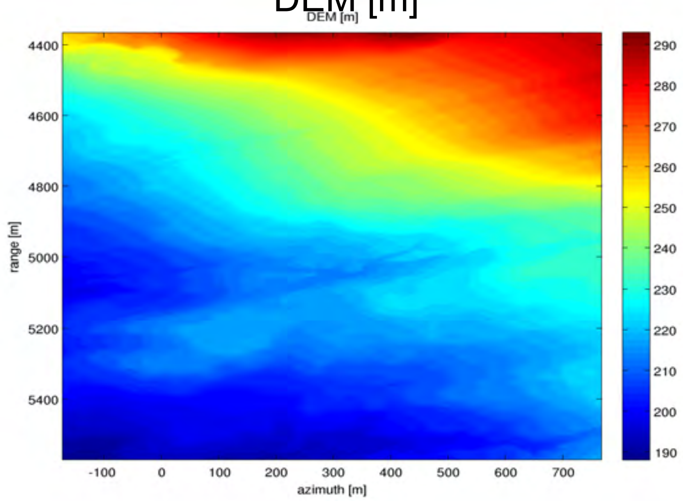

Mixture of
numerous contributions
in the elevation direction

Multibaseline InSAR (MB-InSAR) tomography

Several mixed scatterers → many across-track positions

Acquisition geometry

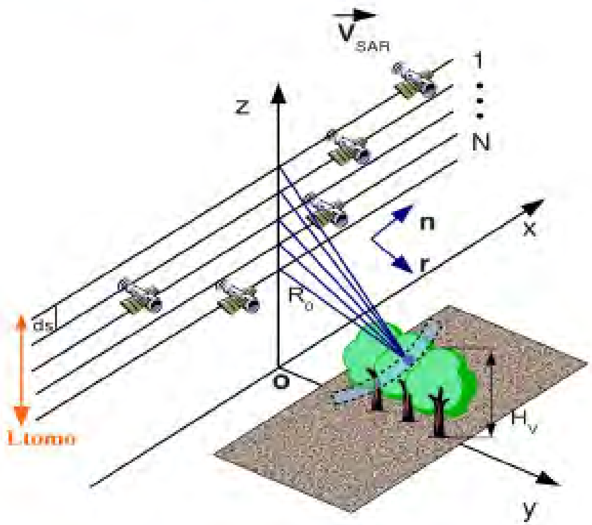

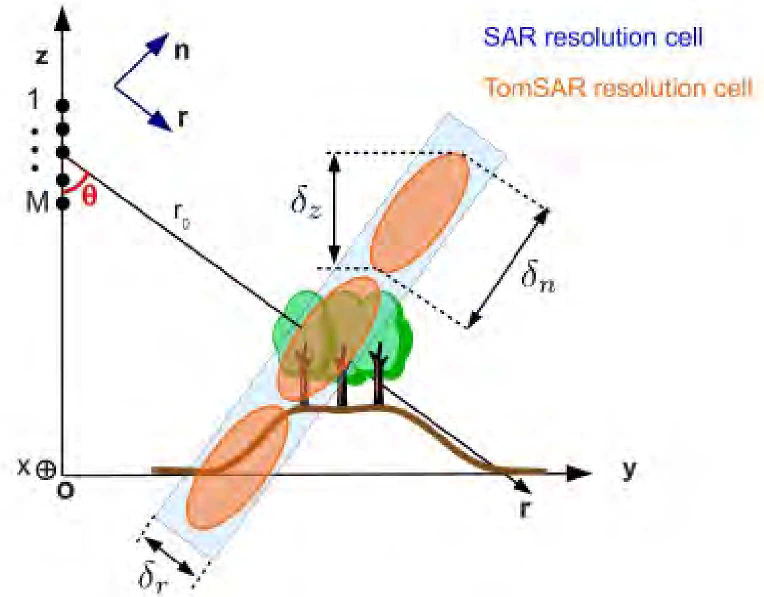

Vertical focusing

- Vertical aperture : L_{tomo}
- Resolution : $\delta_z = \delta_n \sin\theta$ with $\delta_n = \frac{\lambda R_0}{2L_{tomo}}$

Multibaseline InSAR (MB-InSAR) tomography

Several mixed scatterers → many across-track positions

Acquisition geometry

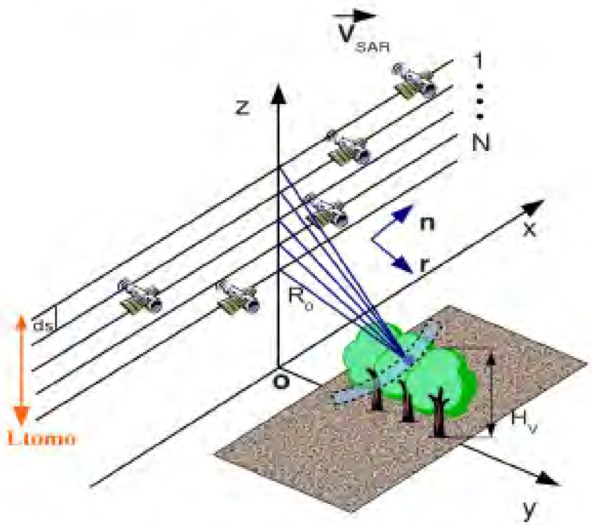

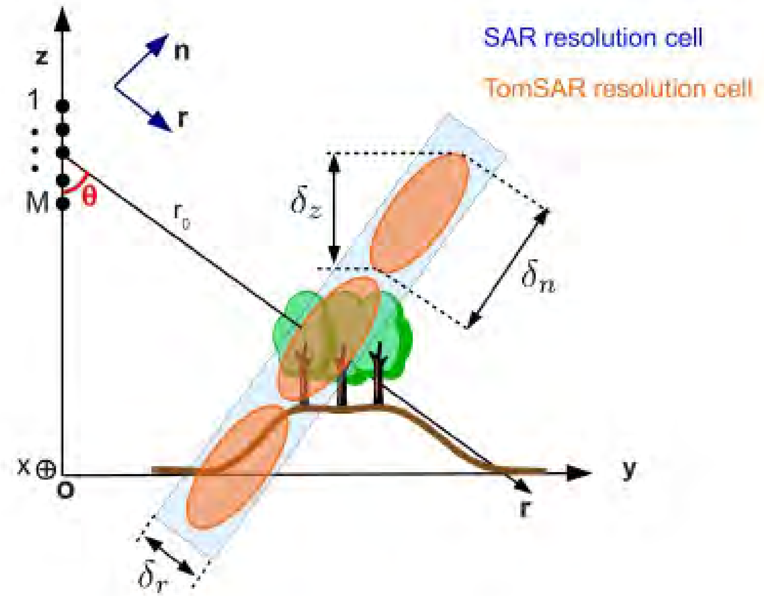

Processing options

- **Direct 3-D imaging**: coherent combination of M SAR acquisitions

- **M x 2-D focusing** & **coherent processing** of M-InSAR quantities

SAR imaging of 3-D scenes

Direct 3-D imaging of an Alpine glacier at L band

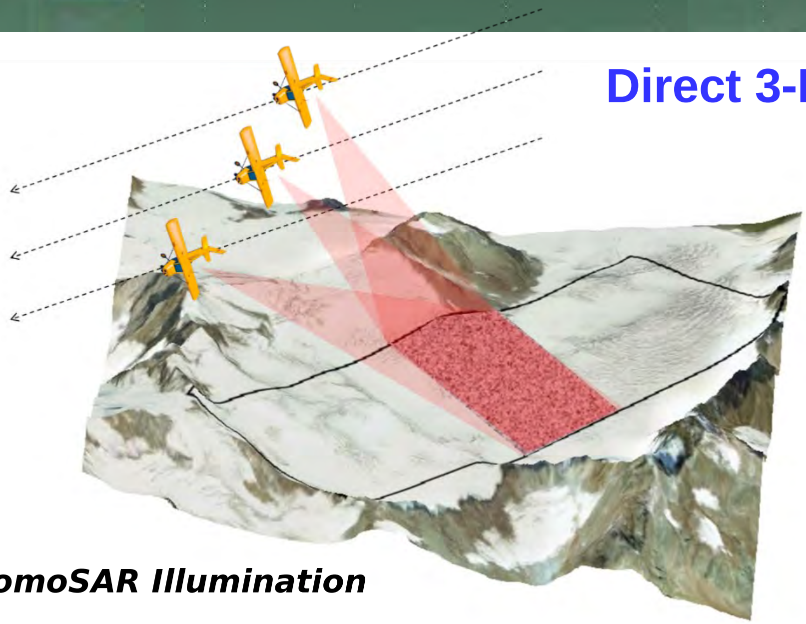

TomoSAR Illumination

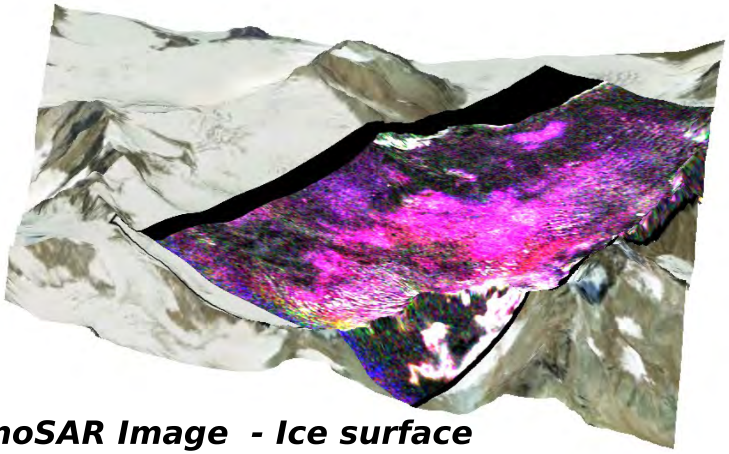

TomoSAR Image - Ice surface

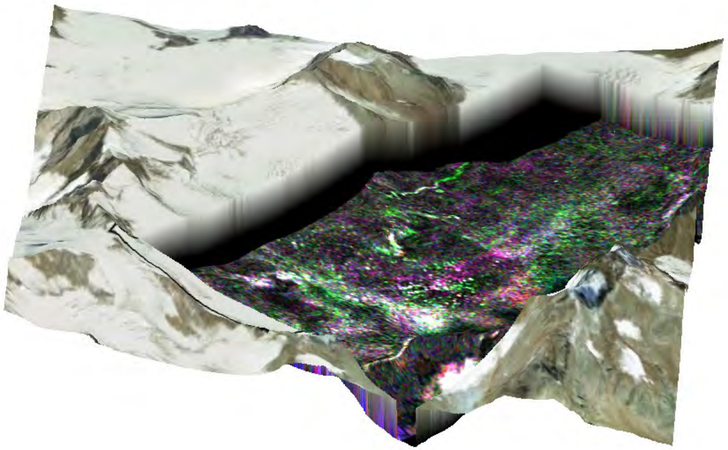

TomoSAR Image - 25 m below the Ice surface

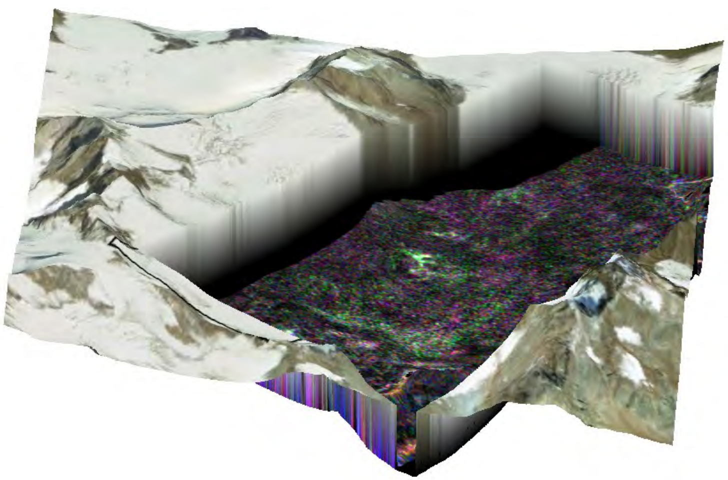

TomoSAR Image - 50 m below the Ice surface

SAR imaging of 3-D scenes

M x 2-D imaging of a Boreal forest at L band

SAR: 2D Imaging

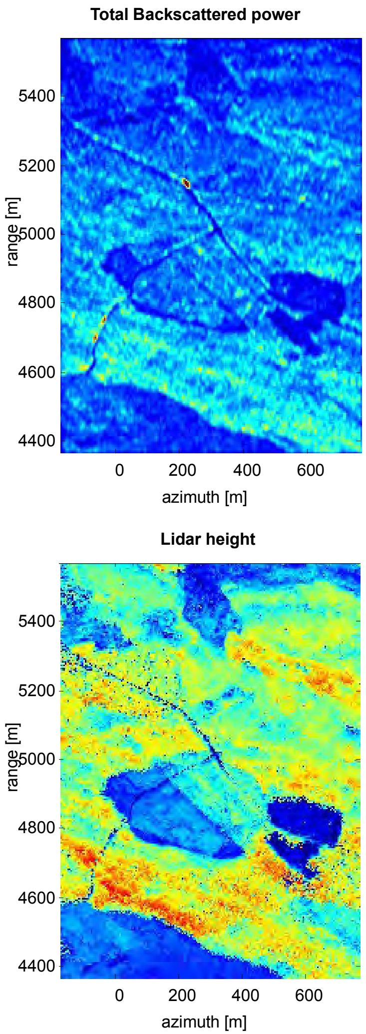

TomoSAR: 3D Imaging

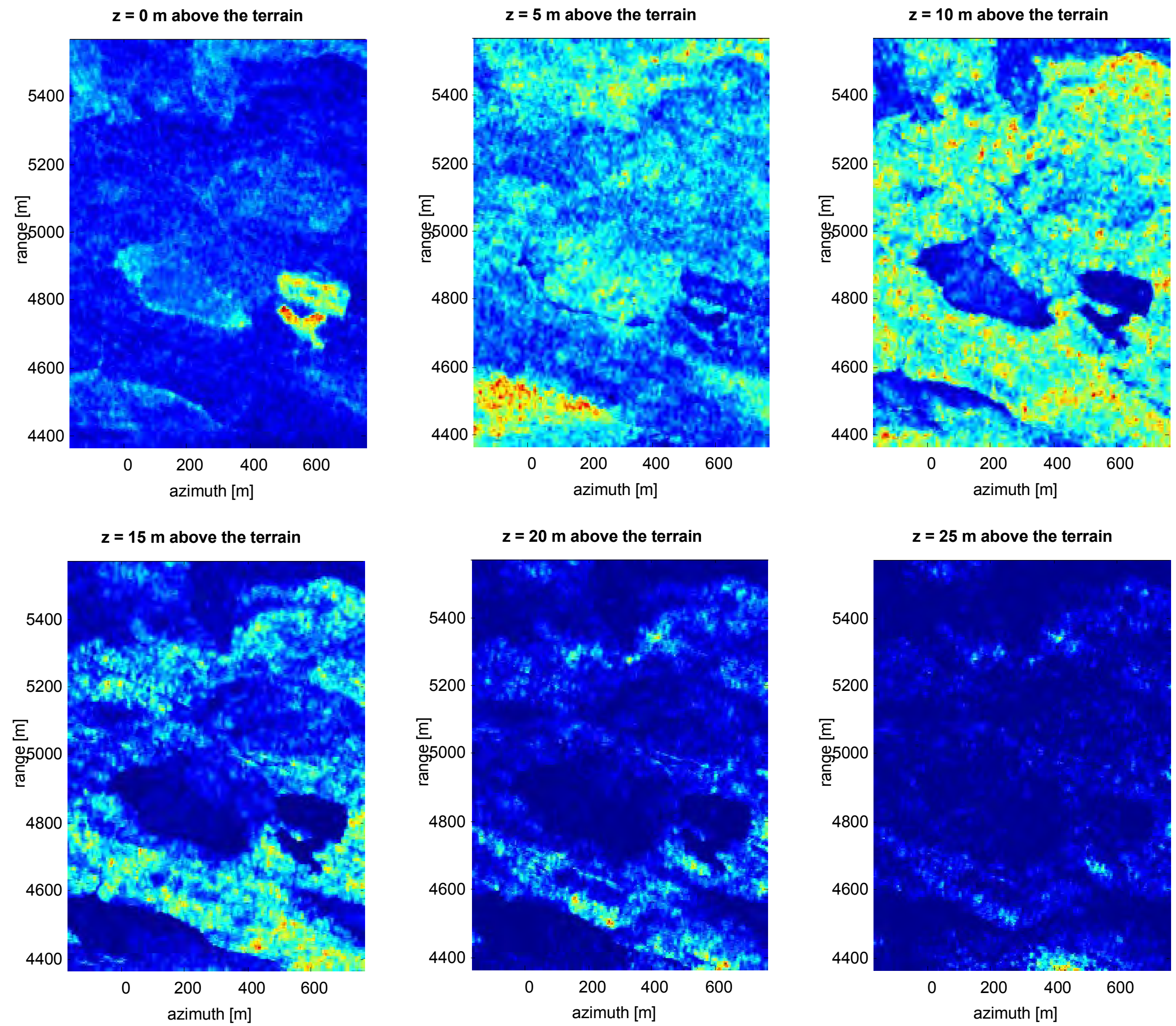

- Power distribution in height direction
- Full-resolution CAPON

Multiple baselines : Illumination from multiple points of view

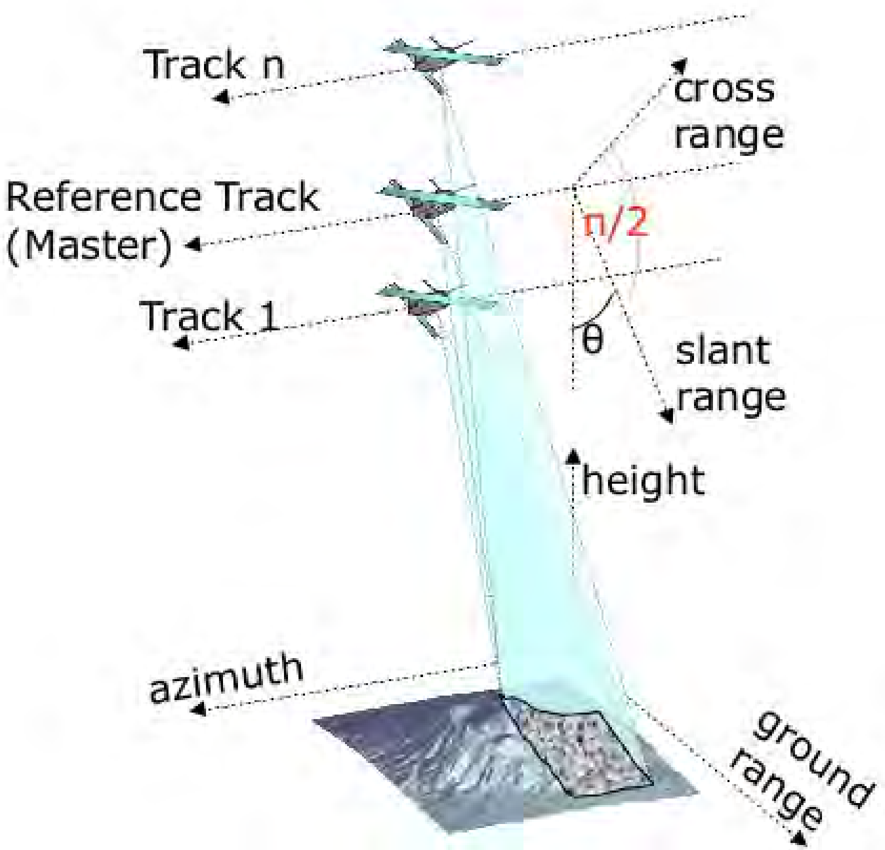

Multiple baselines : Illumination from multiple points of view

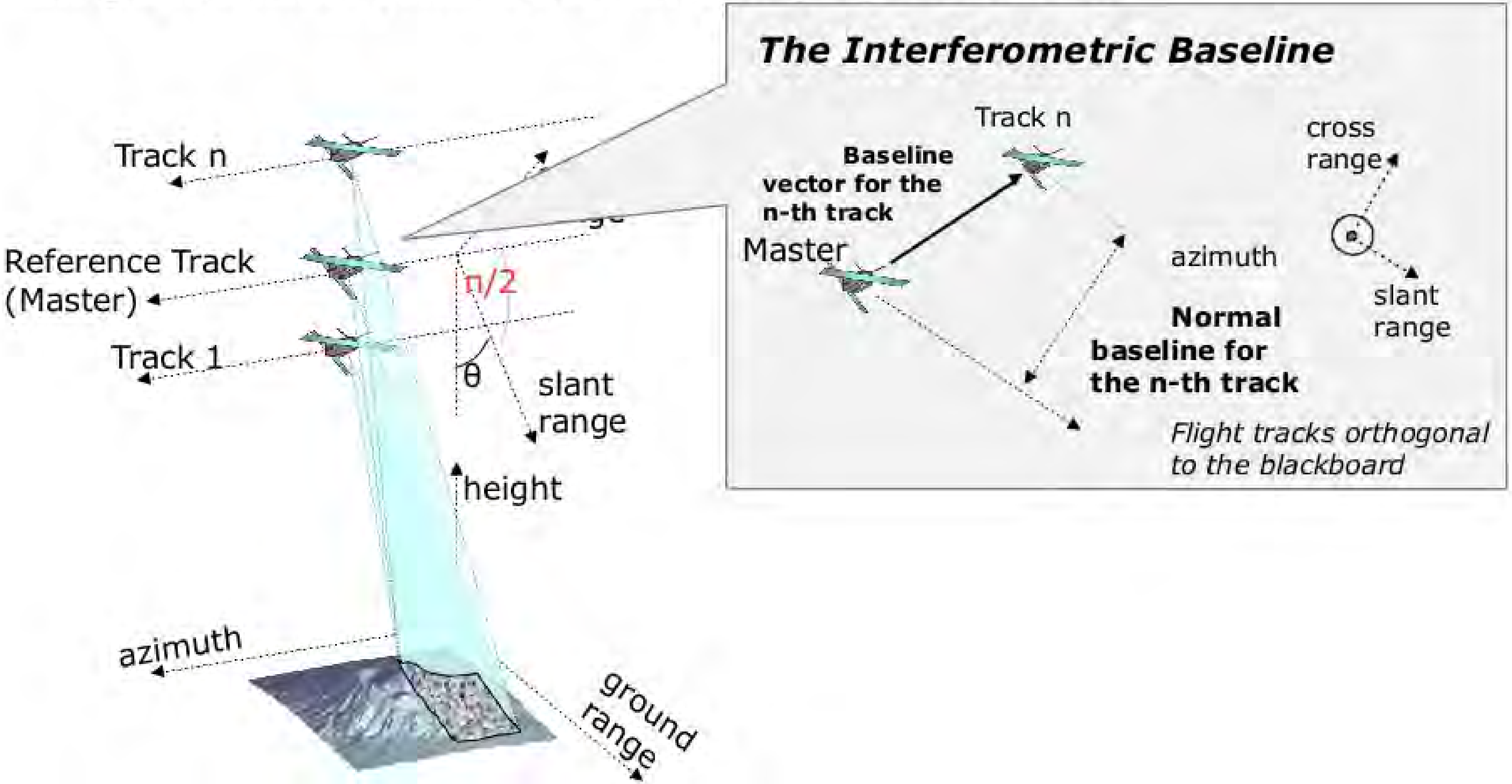

TomoSAR Focusing

Multiple baselines : Illumination from multiple points of view

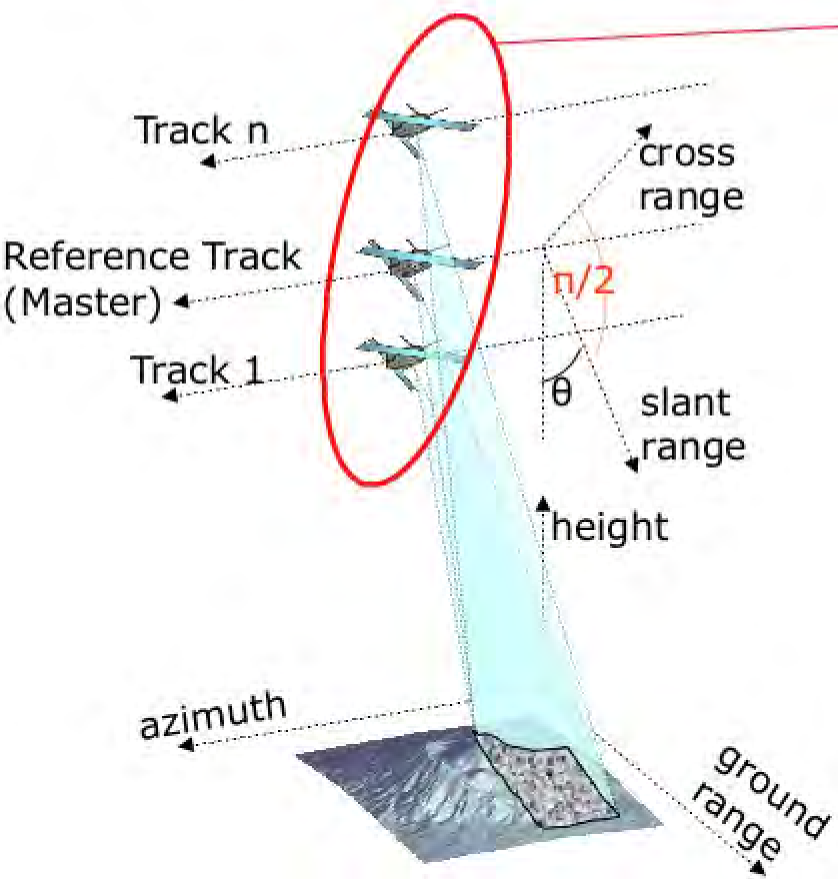

Aperture Synthesis in the cross-range direction

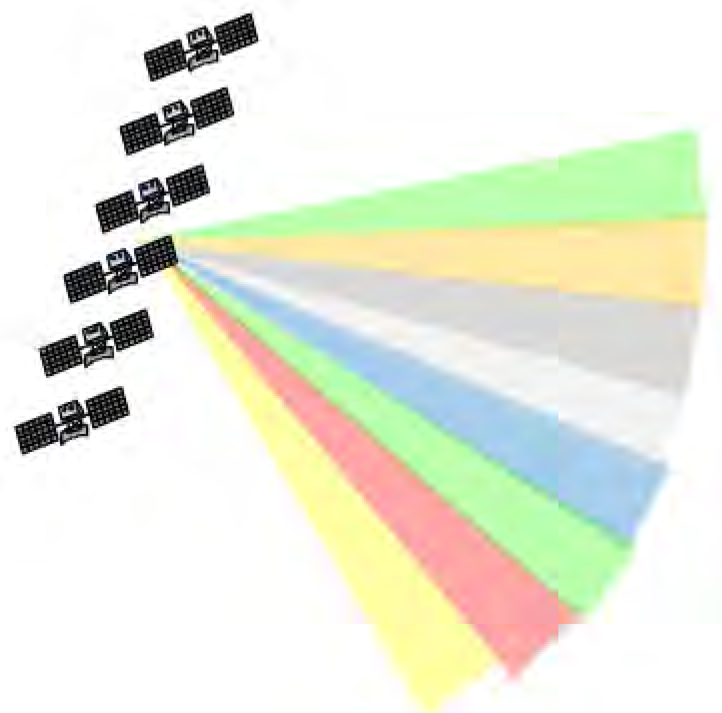

Multiple baselines : Illumination from multiple points of view

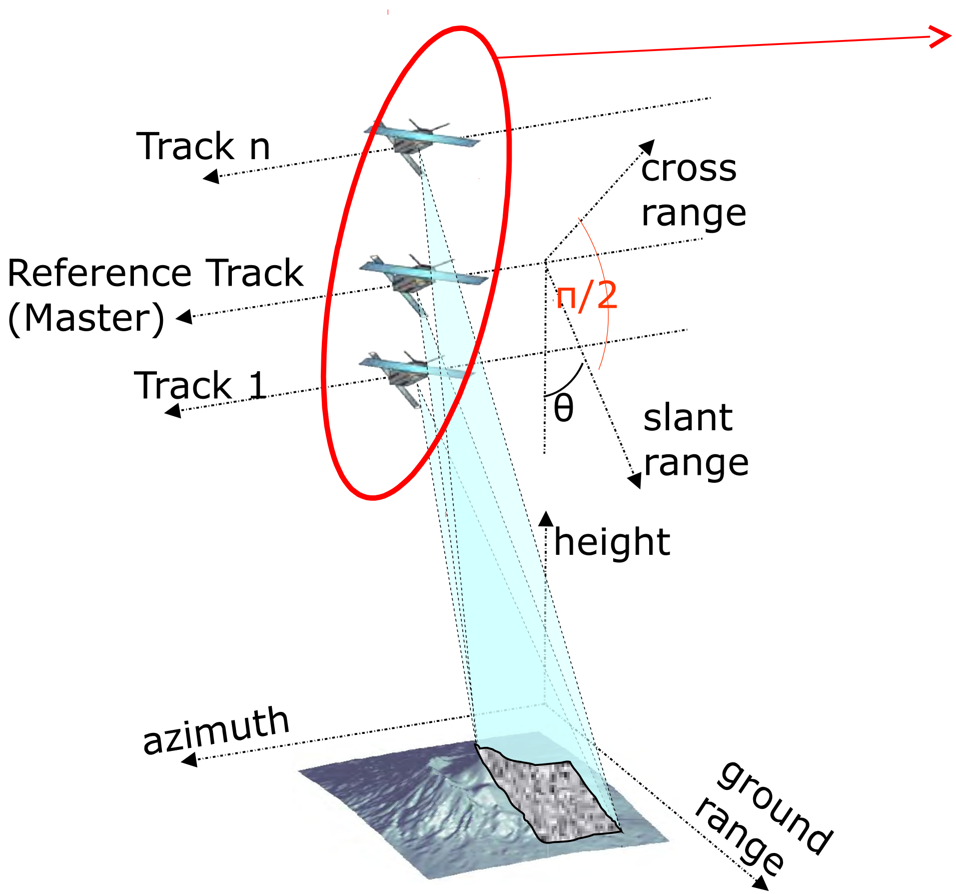

Aperture Synthesis in the cross-range direction

⇒ ***Cross-range resolution capabilities***

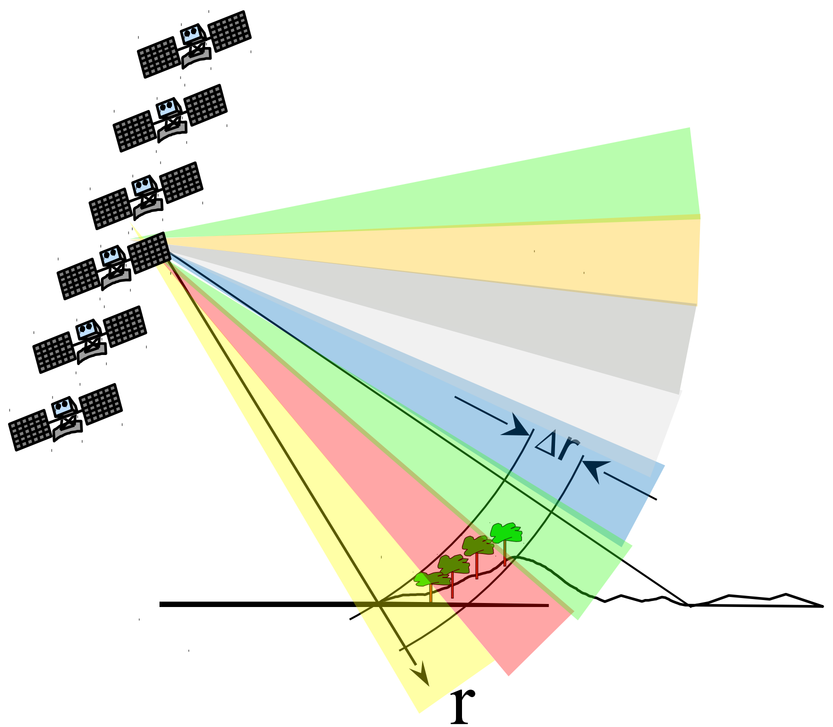

TomoSAR Resolution

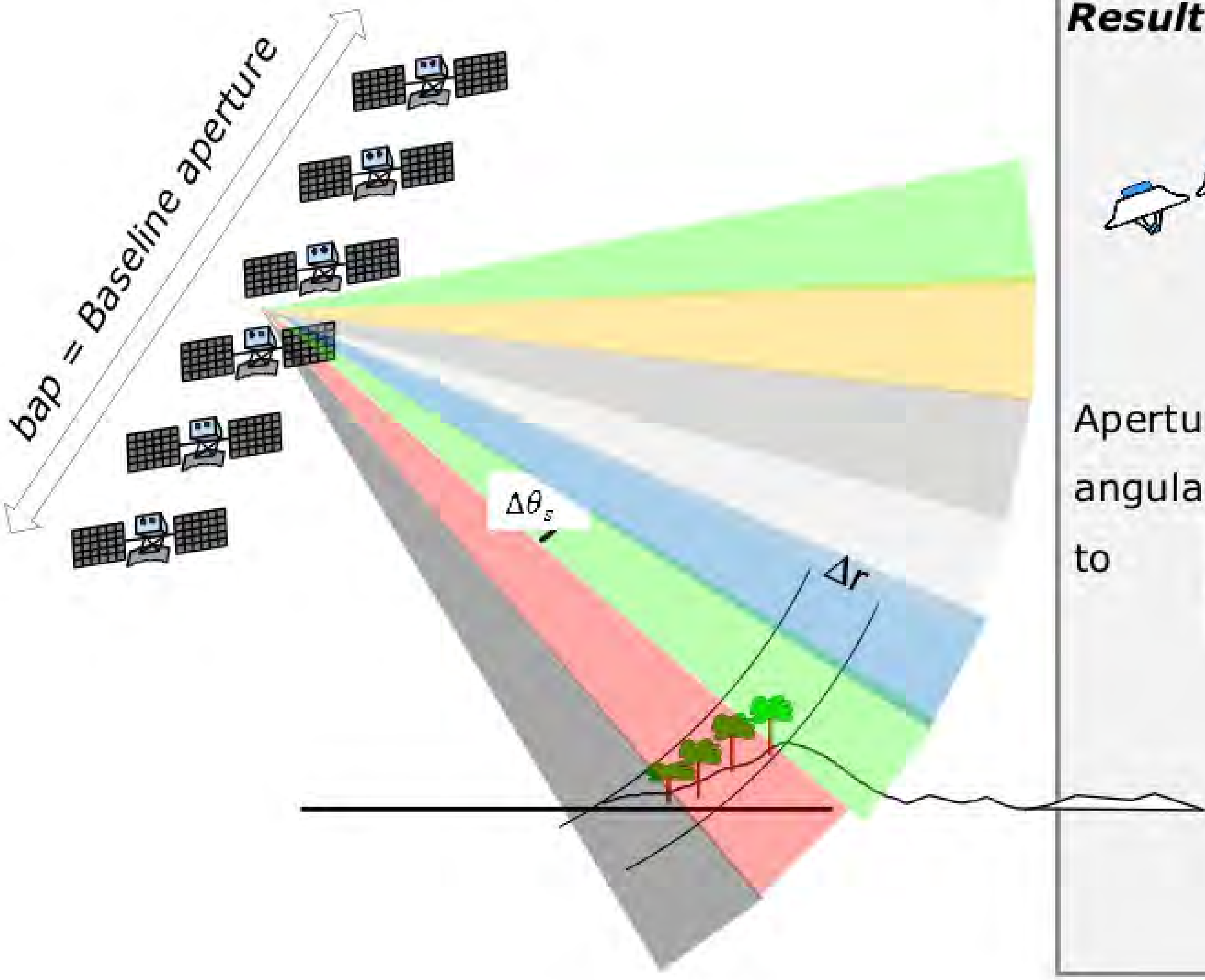

Result from array theory

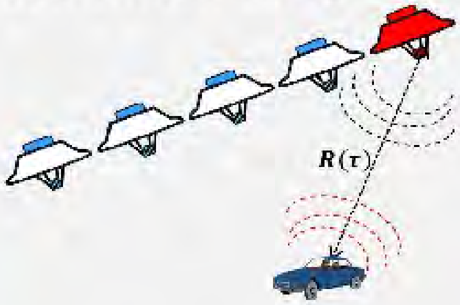

Aperture length translates to angular resolution according to

$$\Delta\theta_s \cong \frac{\lambda}{2b_{ap}}$$

TomoSAR Resolution

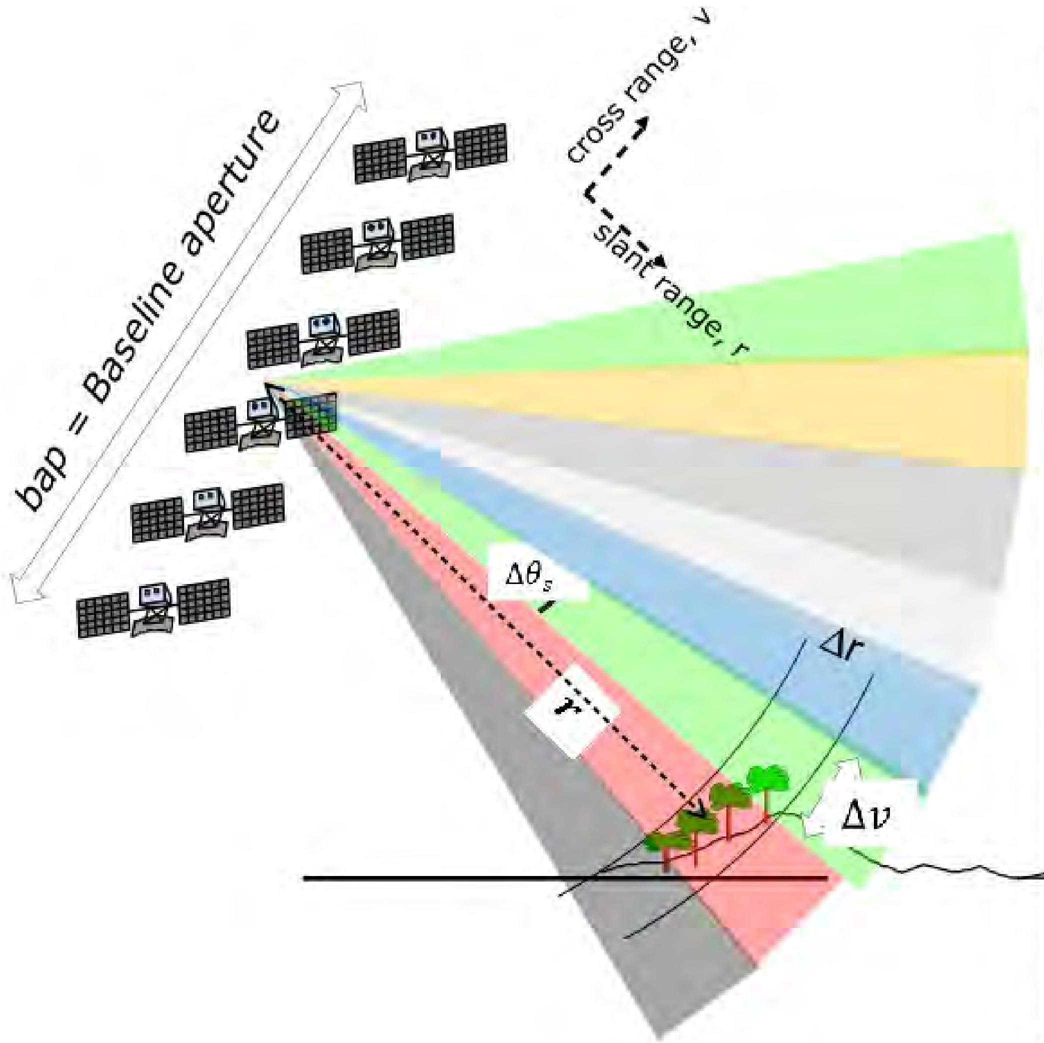

Result from array theory

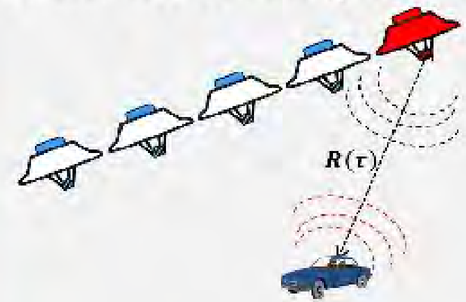

Aperture length translates to angular resolution according to

$$\Delta\theta_s \cong \frac{\lambda}{2b_{ap}}$$

Angular resolution translates into **cross-range** resolution according to

$$\Delta v \cong \Delta\theta_s \cdot r$$

TomoSAR Resolution

Resolution is determined by

- Pulse bandwidth along the slant range direction
- Along-track synthetic aperture length in the azimuth direction
- Baseline aperture in the cross range direction

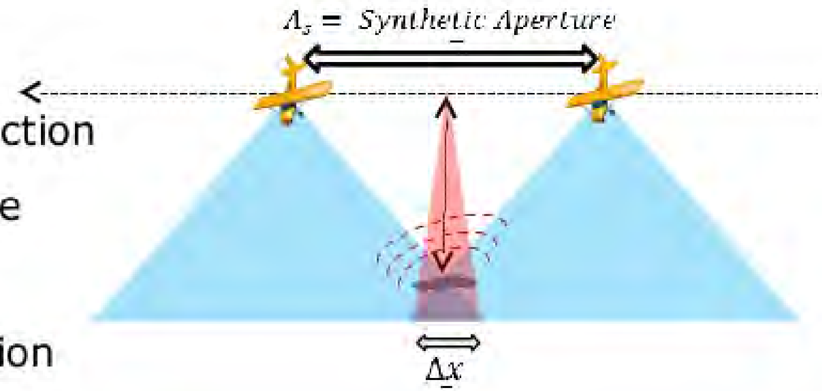

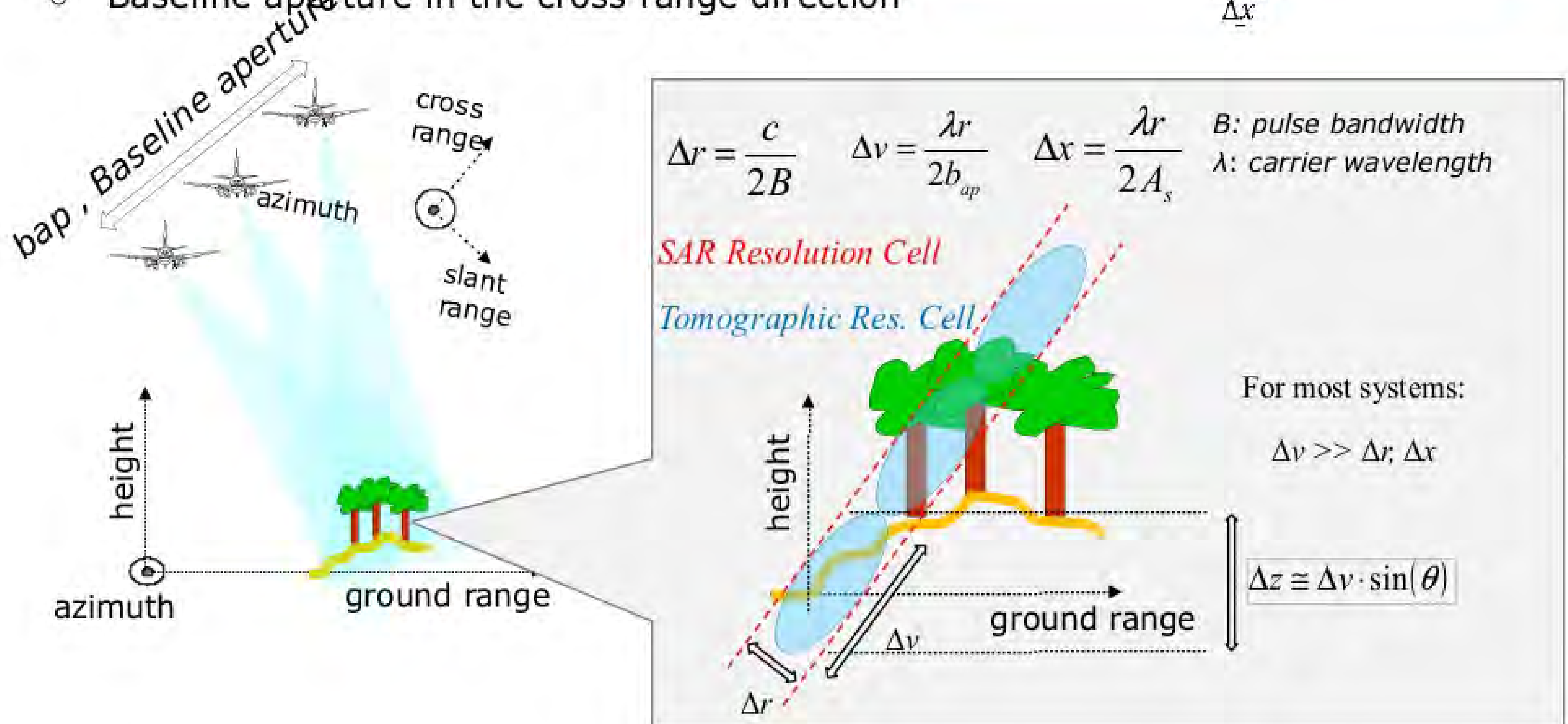

TomoSAR Processing

Modeling of a TomoSAR response

$$I(r,x) = \int_C A(x,y,z) \cdot e^{-j\frac{4\pi}{\lambda}R(x,y,z)} dxdydz$$

C = resolution cell

SAR pixel = Integral of all contributions within the resolution cell

- Each elementary scatterer is phase-rotated according to its distance from the Radar

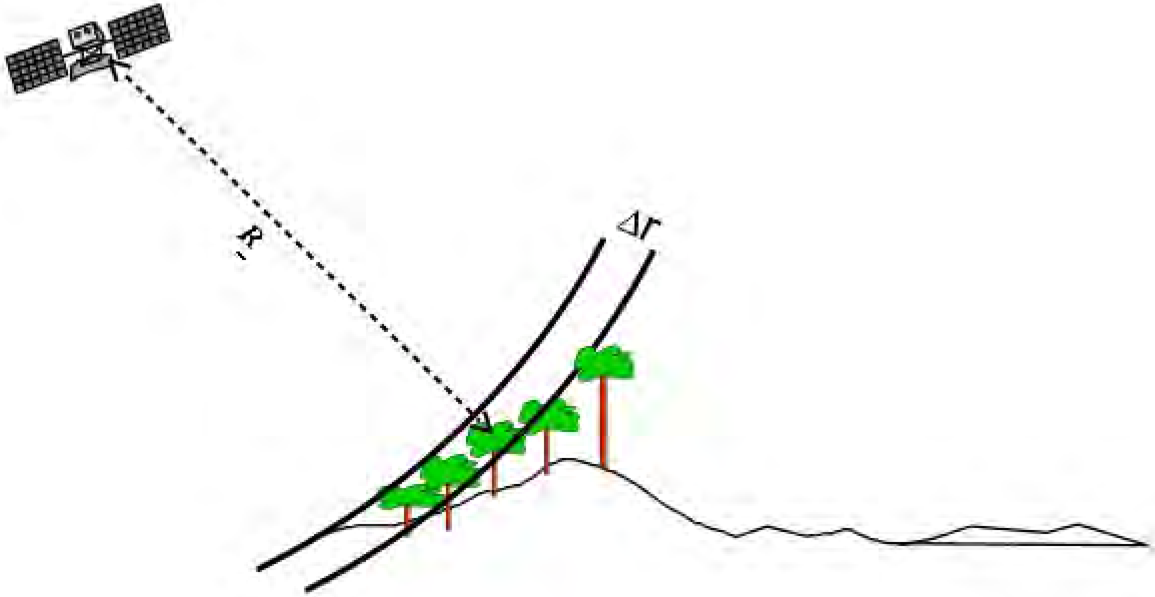

Modeling of a TomoSAR response

$$I_n(r,x) = \int_{Cn} A(x,y,z) \cdot e^{-j\frac{4\pi}{\lambda}R_n(x,y,z)}\,dxdydz$$

Cn = resolution cell for the n-th view point

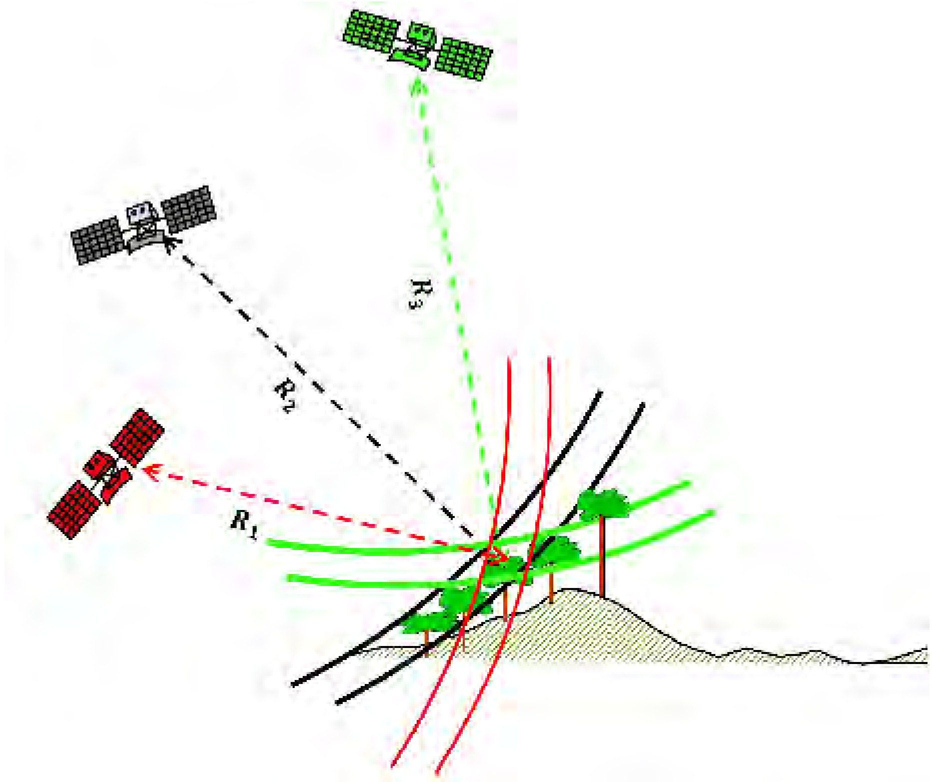

SAR pixel = Integral of all contributions within the resolution cell

- Each elementary scatterer is phase-rotated according to its distance from the Radar

Multiple baselines

- Resolution cell is oriented at different angles for different baselines
- ⇔ ***Range migration:*** Targets at different cross-range positions appear at different range positions for different baselines

Exact TomoSAR focusing requires 3D Back-Projection

Hyp 1: range migration is negligible

small aperture, small bandwidth, targets are distributed in a small angular sector

$$I_n(r,x) = \int_C A(x,y,z) \cdot e^{-j\frac{4\pi}{\lambda}R_n(x,y,z)} dxdydz$$

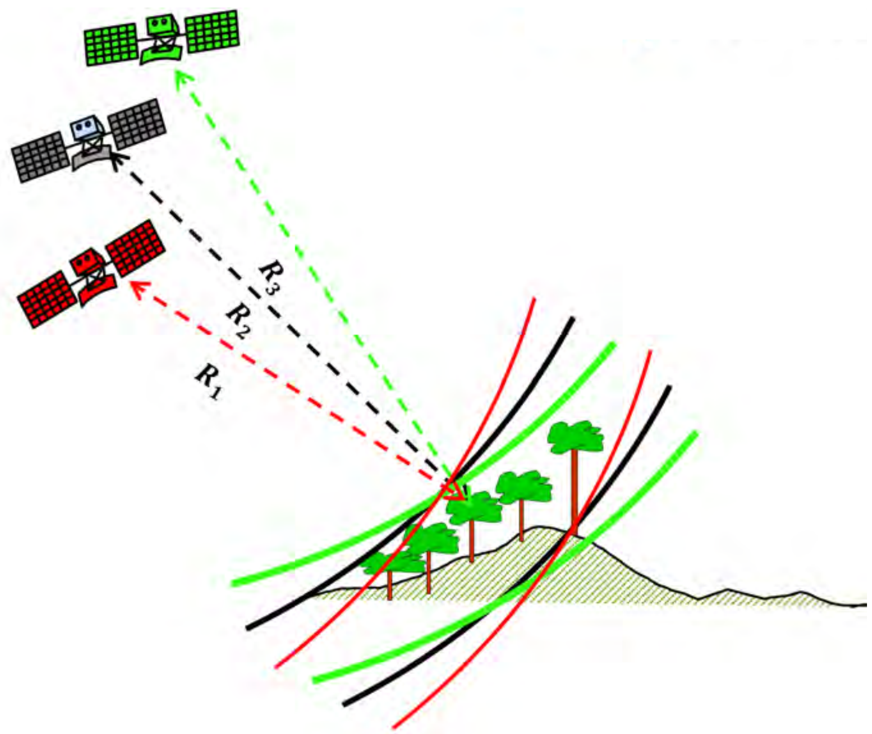

C = resolution cell

Only phase terms vary

w.r.t. baselines

Relaxing the model...

Hyp 2 : locally-plane wave approximation *(across-track scene extent << R)*

b_n = ***normal baseline*** *of the n-th view w.r.t. the Master view* $b_n = (\theta_n - \theta_M) \cdot R_M(ref)$

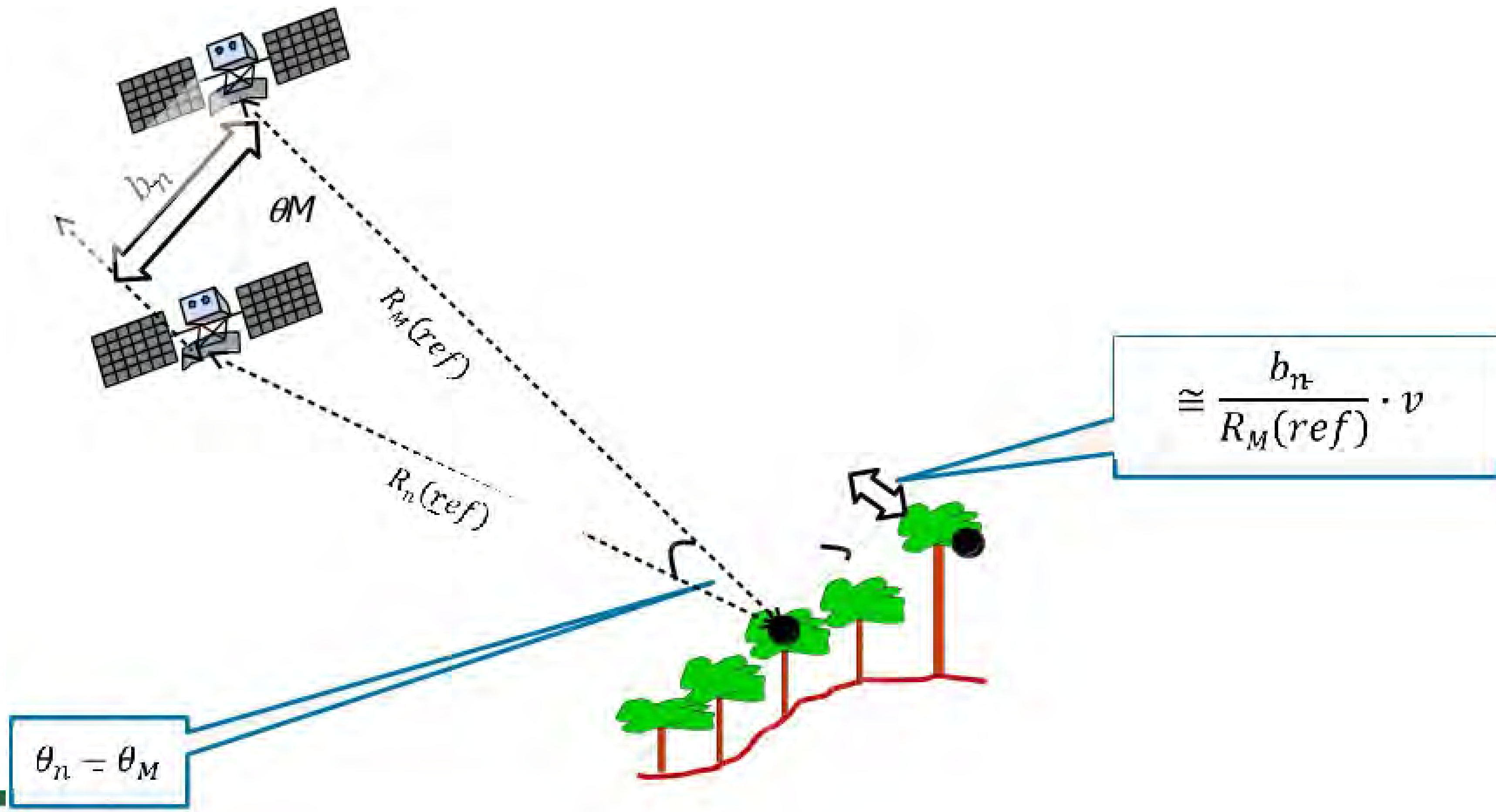

Relaxed model

$$I_n(r,x) = exp\left\{-j\frac{4\pi}{\lambda}R_n(ref)\right\}\cdot\int_C A(r',x',v)exp\left\{-j\frac{4\pi}{\lambda}r'\right\}\cdot exp\left\{-j\frac{4\pi}{\lambda}\frac{b_n}{r}v\right\}dx'dr'dv$$

Common terms for all baselines

Solving the integral w.r.t. r′ and x′ one gets

$$\boxed{I_n(r,x) = exp\left\{-j\frac{4\pi}{\lambda}R_n(ref)\right\}\cdot\int_C s(r,x,v)\cdot exp\left\{-j\frac{4\pi}{\lambda}\frac{b_n}{r}v\right\}dv}$$

Flat earth phase (w.r.t. reference)

s(r,x,v) = cross-range projection of target reflectivity within the SAR resolution cell at (r,x)

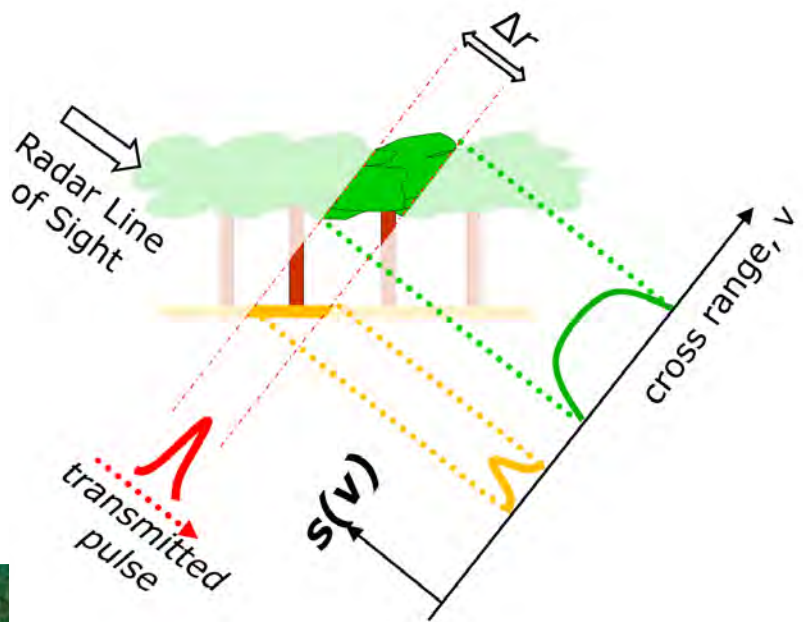

SAR Tomography as a Fourier imaging process: M-Fwd 2-D imaging

Focused SLC SAR image

Fourier Transform of s(r,x,v) the scene complex reflectivity

(cross-range coord.)

$$\boxed{I_n(r,x) = \int_C s(r,x,v)\cdot exp\left\{-j\frac{4\pi}{\lambda}\frac{b_n}{r}v\right\}dv}$$

$I_n(r,x)$: SLC pixel in the *n-th* image

s(r,x,*v*): cross-range projection of target reflectivity within the SAR resolution cell at (*r*,*x*)

b_n : normal baseline for the *n-th* image

λ : carrier wavelength

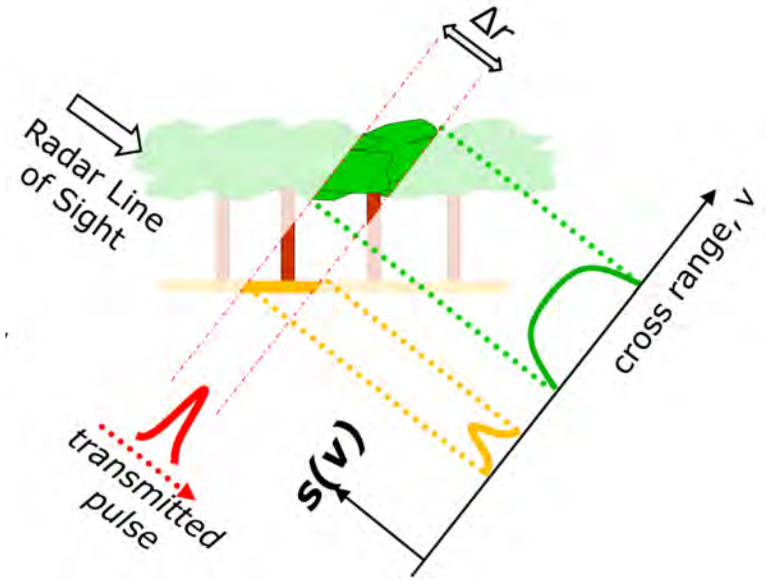

SAR Tomography as a Fourier imaging process: Backwd 3D imaging

⇒ The cross-range distribution of the complex reflectivity can be retrieved by Fourier transforming SLC data with respect to the normal baseline

$$\hat{s}(r,x,v) = DFT\{I_n(r,x)\}$$

DFT = Discrete Fourier Transform **over the b_ns**

In other words…

$$I_n(r,x) = \int s(r,x,v)\exp\left(-j\frac{4\pi}{\lambda r}b_n v\right)dv$$

⇨

$$\hat{s}(r,x,v) = \sum_n I_n(r,x)\exp\left(+j\frac{4\pi}{\lambda r}b_n v\right)$$

$I_n(r,x)$ = observation

$s(r,x,v)$ = unknown

$\hat{s}(r,x,v)$ = estimate

TomoSAR focusing – examples

$$\boxed{I_n(r,x) = \int_C s(r,x,v) \cdot exp\left\{-j\frac{4\pi}{\lambda}\frac{b_n}{r}v\right\}dv}$$

$$\hat{s}(r,x,v) = \sum_n I_n(r,x)\exp\left(+j\frac{4\pi}{\lambda r}b_n v\right)$$

Case 1: one point target

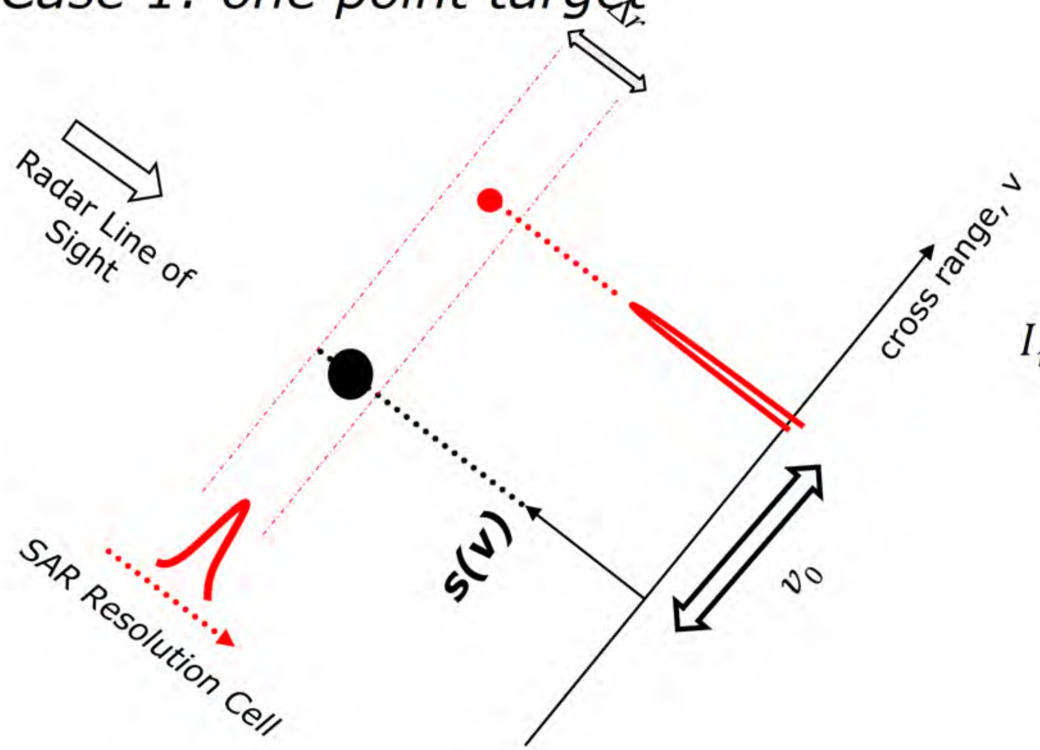

$$I_n(r,x) = s_0 \cdot exp\left\{-j\frac{4\pi}{\lambda}\frac{b_n}{r}v_0\right\}$$

● = reference position

TomoSAR focusing – examples

$$\boxed{I_n(r,x) = \int_C s(r,x,v) \cdot exp\left\{-j\frac{4\pi}{\lambda}\frac{b_n}{r}v\right\}dv}$$

$$\hat{s}(r,x,v) = \sum_n I_n(r,x)\exp\left(+j\frac{4\pi}{\lambda r}b_n v\right)$$

Case 1: one point target

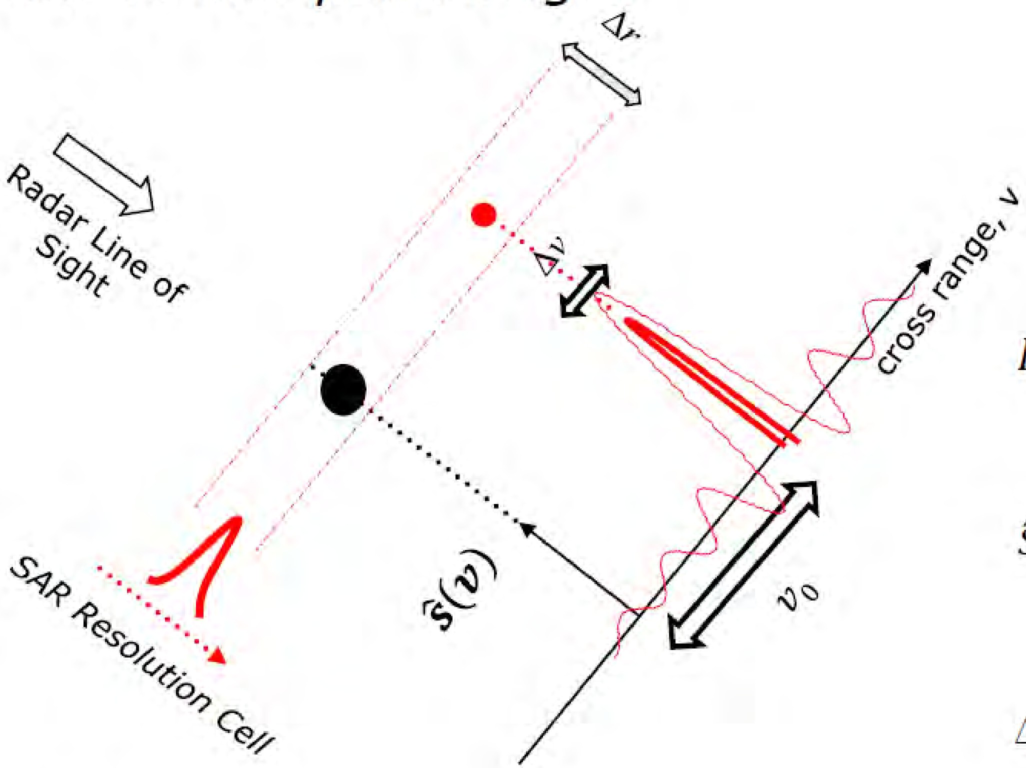

$$I_n(r,x) = s_0 \cdot exp\left\{-j\frac{4\pi}{\lambda}\frac{b_n}{r}v_0\right\}$$

$$\hat{s}(r,x,v) = s_0 \cdot sinc\left(\frac{v-v_0}{\Delta v}\right)$$

$$\Delta v = \frac{\lambda r}{2b_{ap}}$$

● = reference position

Note: Constant amplitude factors omitted

TomoSAR focusing – examples

$$I_n(r,x) = \int_C s(r,x,v) \cdot exp\left\{-j\frac{4\pi}{\lambda}\frac{b_n}{r}v\right\}dv$$

$$\hat{s}(r,x,v) = \sum_n I_n(r,x)\exp\left(+j\frac{4\pi}{\lambda r}b_n v\right)$$

Case 2: two point targets

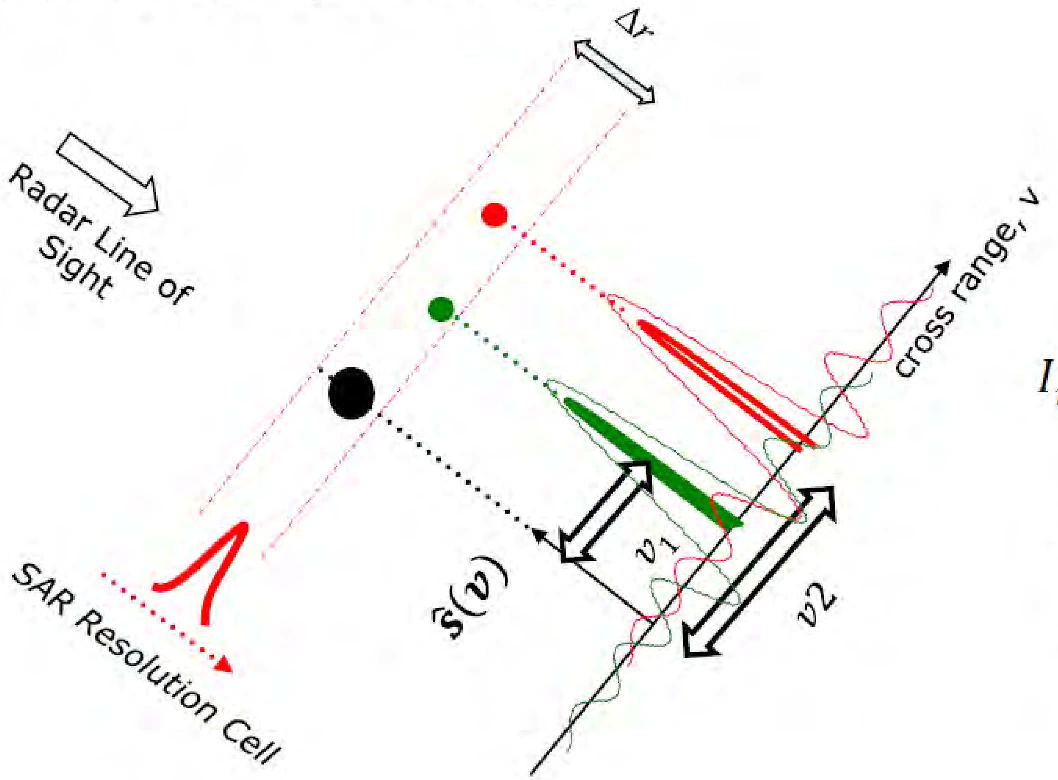

$$I_n(r,x) = \sum_{p=1}^{2} s_p \cdot exp\left\{-j\frac{4\pi}{\lambda}\frac{b_n}{r}v_p\right\}$$

$$\hat{s}(r,x,v) = \sum_{p=1}^{2} s_p \cdot sinc\left(\frac{v-vp}{\Delta v}\right)$$

● = reference position

Note: Constant amplitude factors omitted

TomoSAR focusing – examples

$$\boxed{I_n(r,x) = \int_C s(r,x,v)^{-} \cdot exp\left\{-j\frac{4\pi}{\lambda}\frac{b_n}{r}v\right\}dv}$$

$$\hat{s}(r,x,v) = \sum_n I_n(r,x)\exp\left(+j\frac{4\pi}{\lambda r}b_n v\right)$$

Case 3: terrain

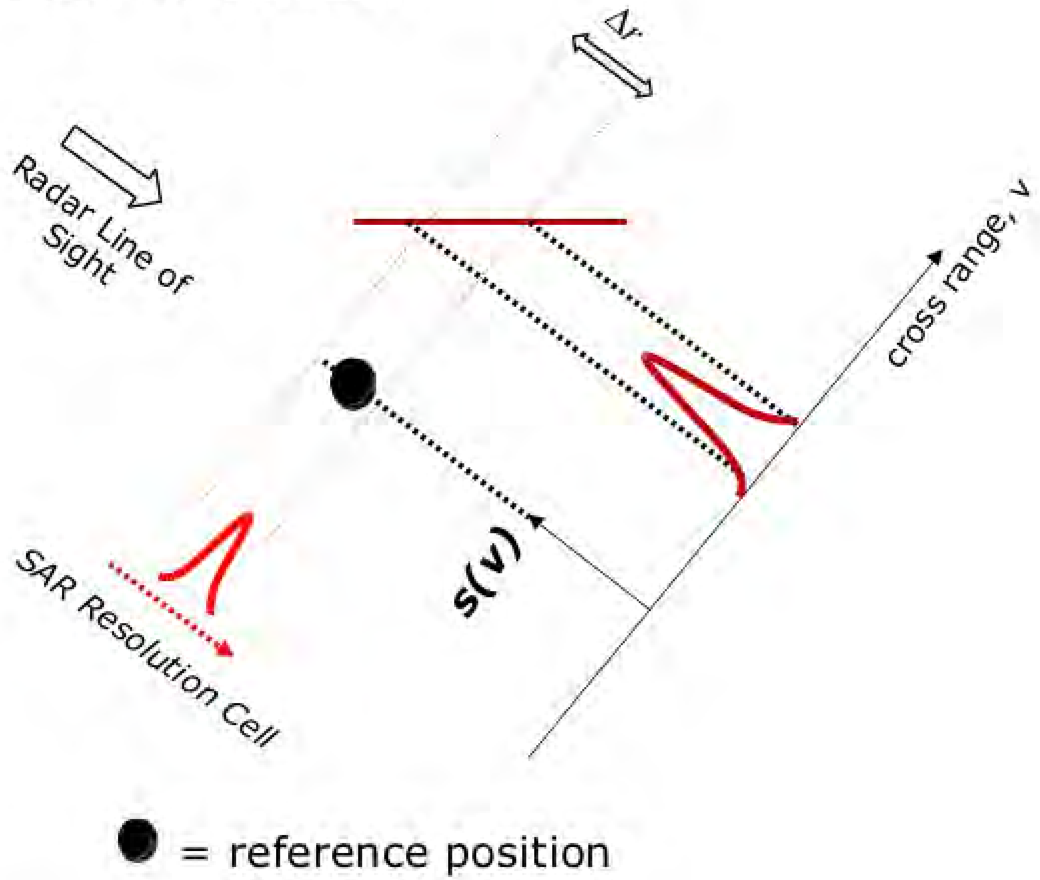

Terrain = extended target

⇔ *It does not project into a peak*

⇔ *Cross-range spread*

TomoSAR focusing – examples

$$\boxed{I_n(r,x) = \int_C s(r,x,v) \cdot exp\left\{-j\frac{4\pi}{\lambda}\frac{b_n}{r}v\right\}dv}$$

$$\hat{s}(r,x,v) = \sum_n I_n(r,x)\exp\left(+j\frac{4\pi}{\lambda r}b_n v\right)$$

Case 3: terrain

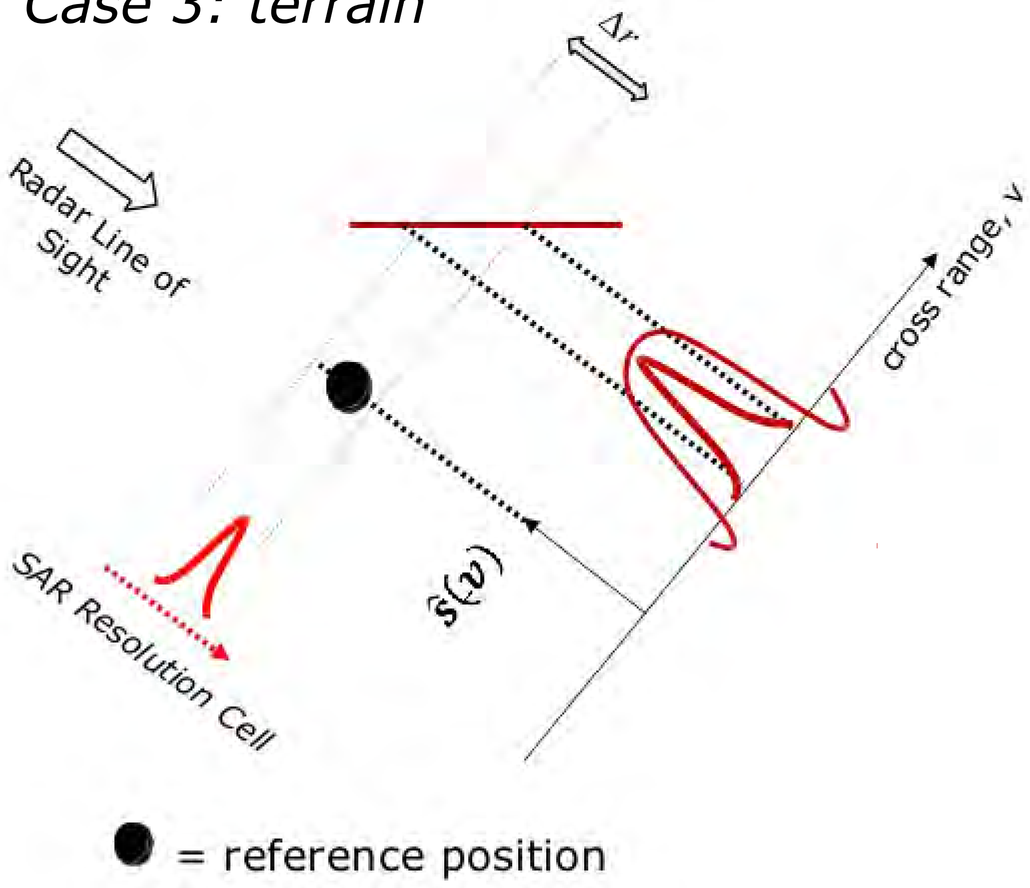

TomoSAR focusing – examples

$$\boxed{I_n(r,x) = \int_C s(r,x,v) \cdot exp\left\{-j\frac{4\pi}{\lambda}\frac{b_n}{r}v\right\}dv}$$

$$\hat{s}(r,x,v) = \sum_n I_n(r,x)\exp\left(+j\frac{4\pi}{\lambda r}b_n v\right)$$

Case 3: terrain

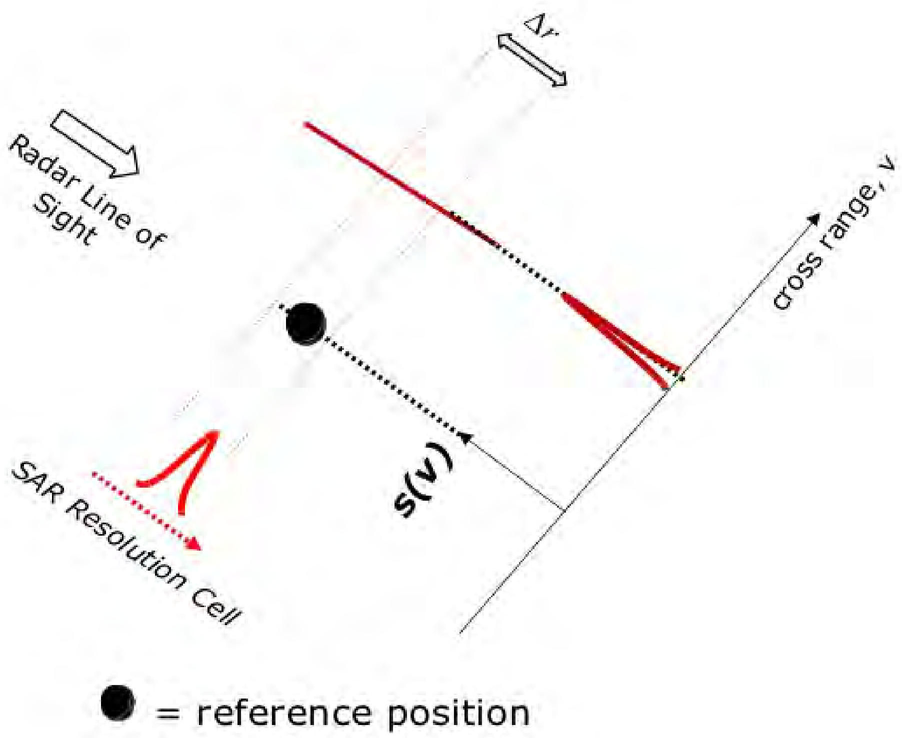

Terrain = extended target

⇔ *Cross-range spread depends on terrain slope*

TomoSAR focusing – examples

$$\boxed{I_n(r,x) = \int_C s(r,x,v) \cdot exp\left\{-j\frac{4\pi}{\lambda}\frac{b_n}{r}v\right\}dv}$$

$$\hat{s}(r,x,v) = \sum_n I_n(r,x)\exp\left(+j\frac{4\pi}{\lambda r}b_n v\right)$$

Case 3: terrain

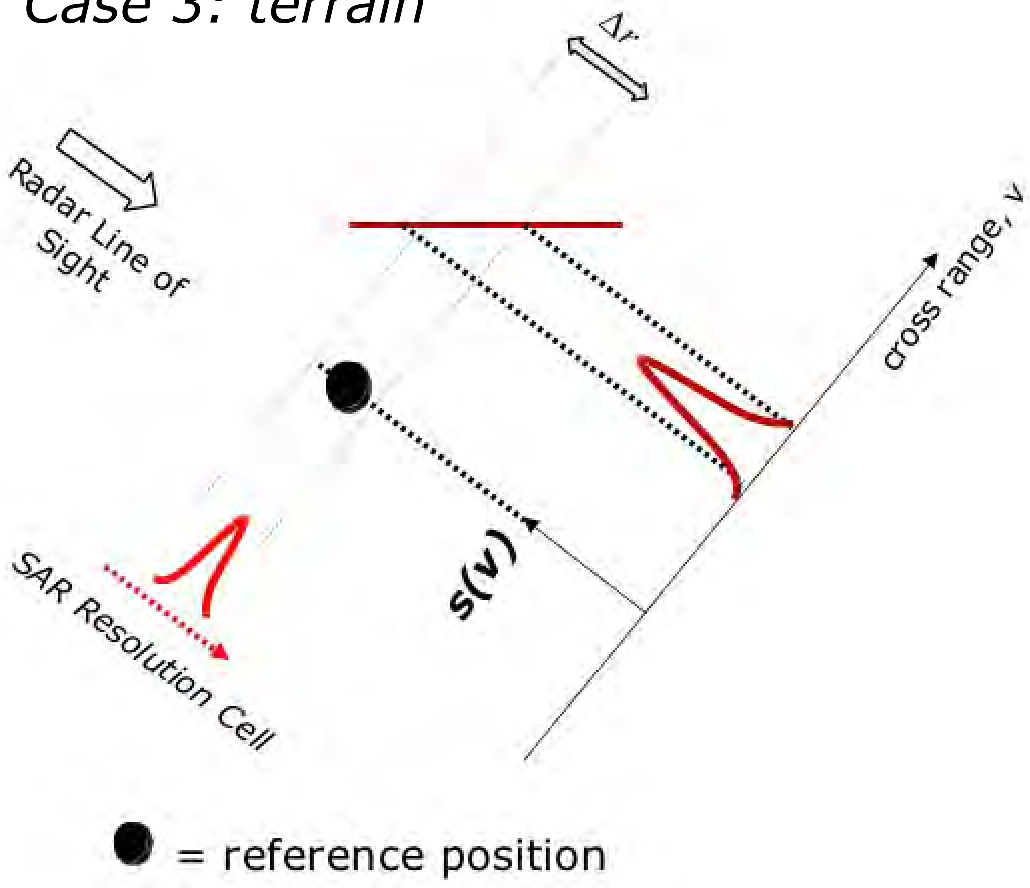

Terrain = extended target

⇔ *Cross-range spread depends on terrain slope*

TomoSAR focusing – examples

$$\boxed{I_n(r,x) = \int_C s(r,x,v) \cdot exp\left\{-j\frac{4\pi}{\lambda}\frac{b_n}{r}v\right\}dv}$$

$$\hat{s}(r,x,v) = \sum_n I_n(r,x)\exp\left(+j\frac{4\pi}{\lambda r}b_n v\right)$$

Case 3: terrain

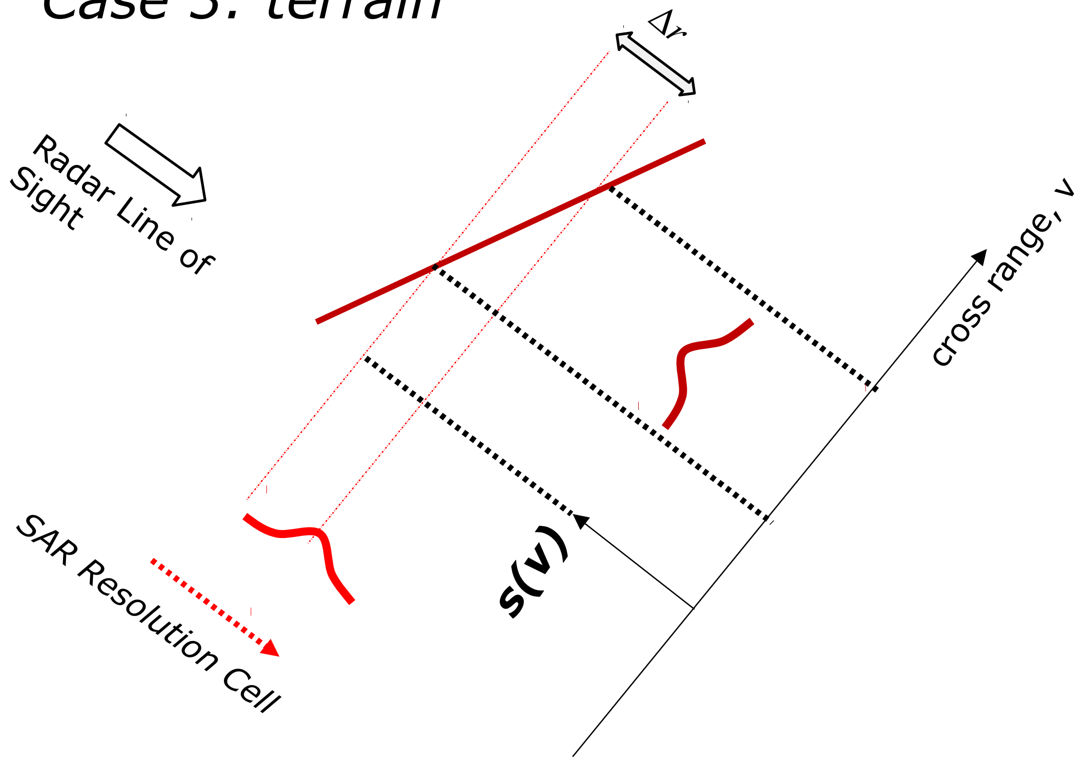

Terrain = extended target

⇔ *Cross-range spread*

depends on terrain slope

= reference position

TomoSAR focusing – examples

$$\boxed{I_n(r,x) = \int_C s(r,x,v) \cdot exp\left\{-j\frac{4\pi}{\lambda}\frac{b_n}{r}v\right\}dv}$$

$$\hat{s}(r,x,v) = \sum_n I_n(r,x)\exp\left(+j\frac{4\pi}{\lambda r}b_n v\right)$$

Case 4: terrain + forest

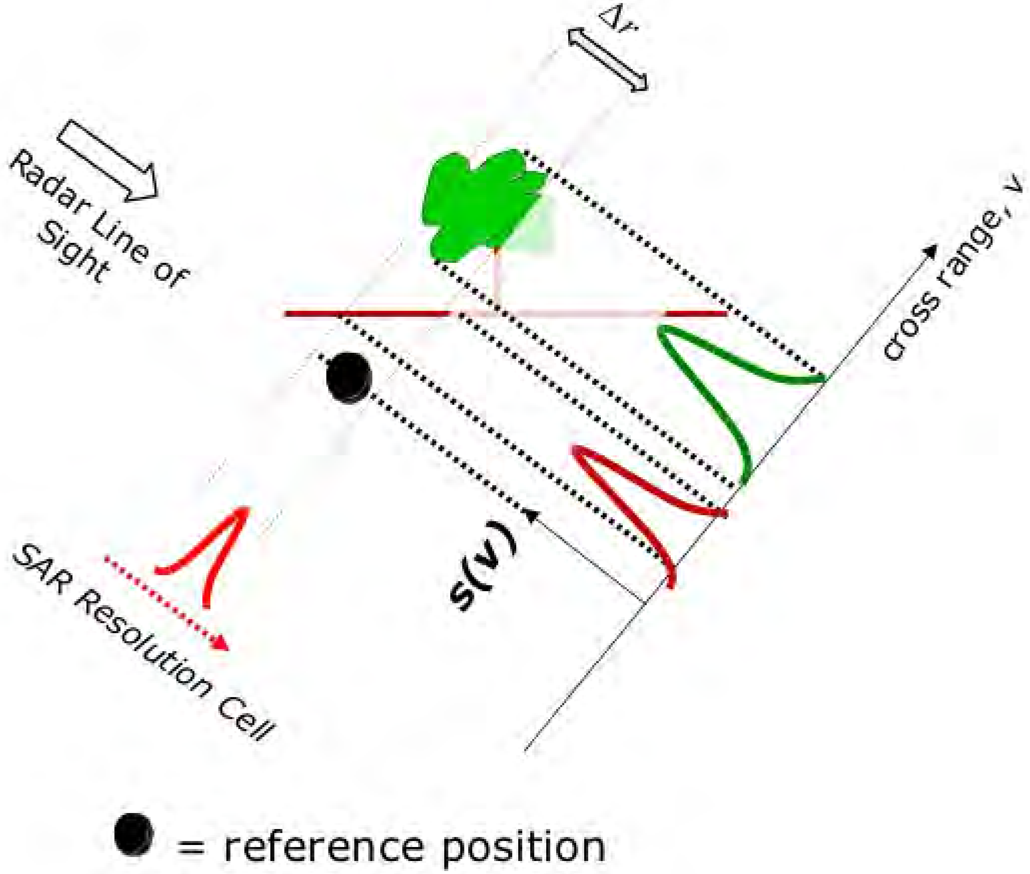

TomoSAR focusing – examples

$$I_n(r,x) = \int_C s(r,x,v) \cdot exp\left\{-j\frac{4\pi}{\lambda}\frac{b_n}{r}v\right\}dv$$

$$\hat{s}(r,x,v) = \sum_n I_n(r,x)\exp\left(+j\frac{4\pi}{\lambda r}b_n v\right)$$

Case 4: terrain + forest

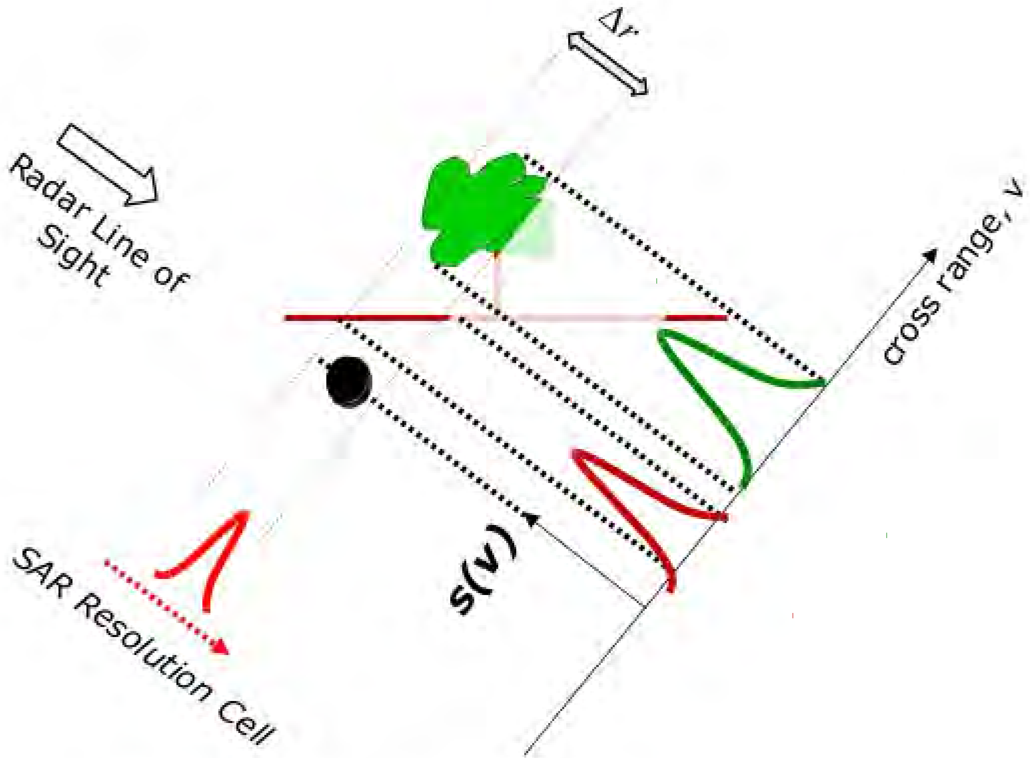

= reference position

Ambiguity

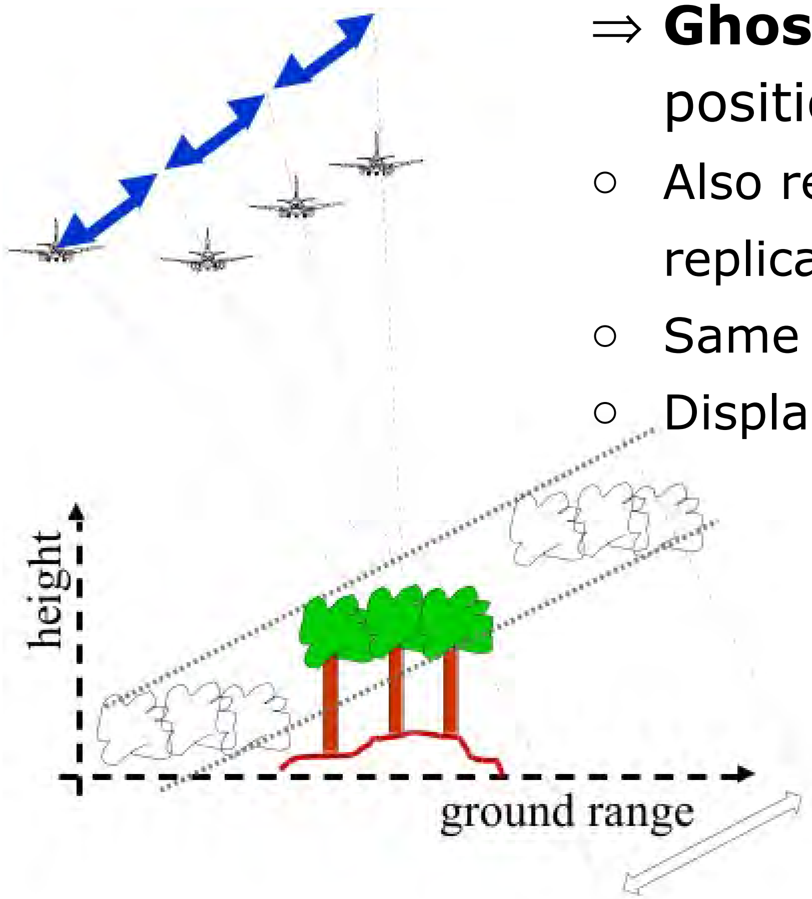

DFT produces ***periodic*** results

⇒ **Ghost** targets appearing at known position w.r.t. the real one

- Also referred to as ambiguous targets, or replicas
- Same range as the real target
- Displaced in cross-range

Baseline design

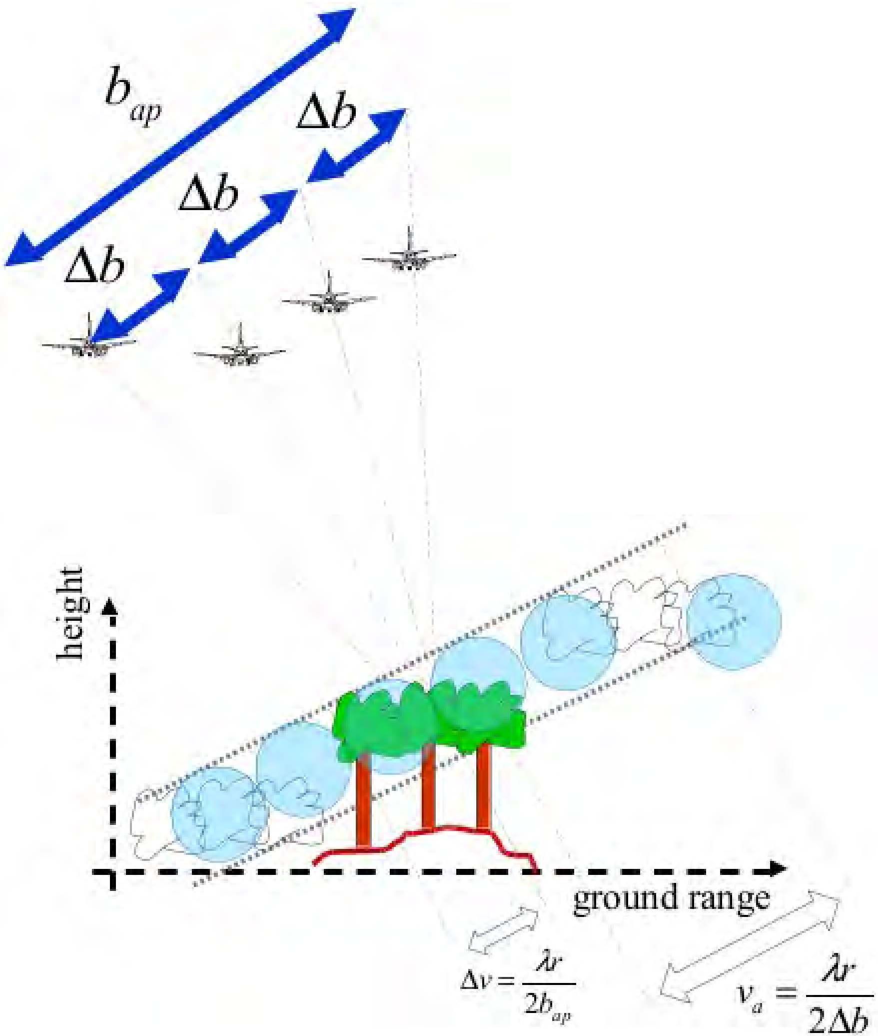

Baseline design tips

- Ambiguity ≥E baseline spacing
- Resolution ≥E baseline aperture

⇒ Baseline spacing: small enough to ensure that ambiguous targets stay away from the real ones

⇒ Baseline aperture: large enough to meet resolution requirement

⇒ How many passes ?

$$N \geq \frac{b_{ap}}{\Delta b} = \frac{v_a}{\Delta v}$$

Projection in the vertical direction

TomoSAR forward model

$$I_n(r,x) = \int_C s(r,x,v) \cdot \exp\left\{-j\frac{4\pi}{\lambda}\frac{b_n}{r}v\right\}dv$$

$I_n(r,x)$: SLC pixel in the *n-th* image

$s(r,x,v)$: cross-range projection of target reflectivity within the SAR resolution cell at (r,x)

b_n : normal baseline for the *n-th* image

λ : carrier wavelength

Change of variable from cross range to height

$$z = v \cdot \sin\theta$$

$$\Downarrow$$

$$I_n(r,x) = \int_C s(r,x,z) \cdot \exp\{-jk_z(n)z\}dz$$

k_z is usually referred to as **vertical wavenumber** or **phase to height conversion factor**

$$k_z(n) = \frac{4\pi}{\lambda r}\frac{b_n}{\sin\theta}$$

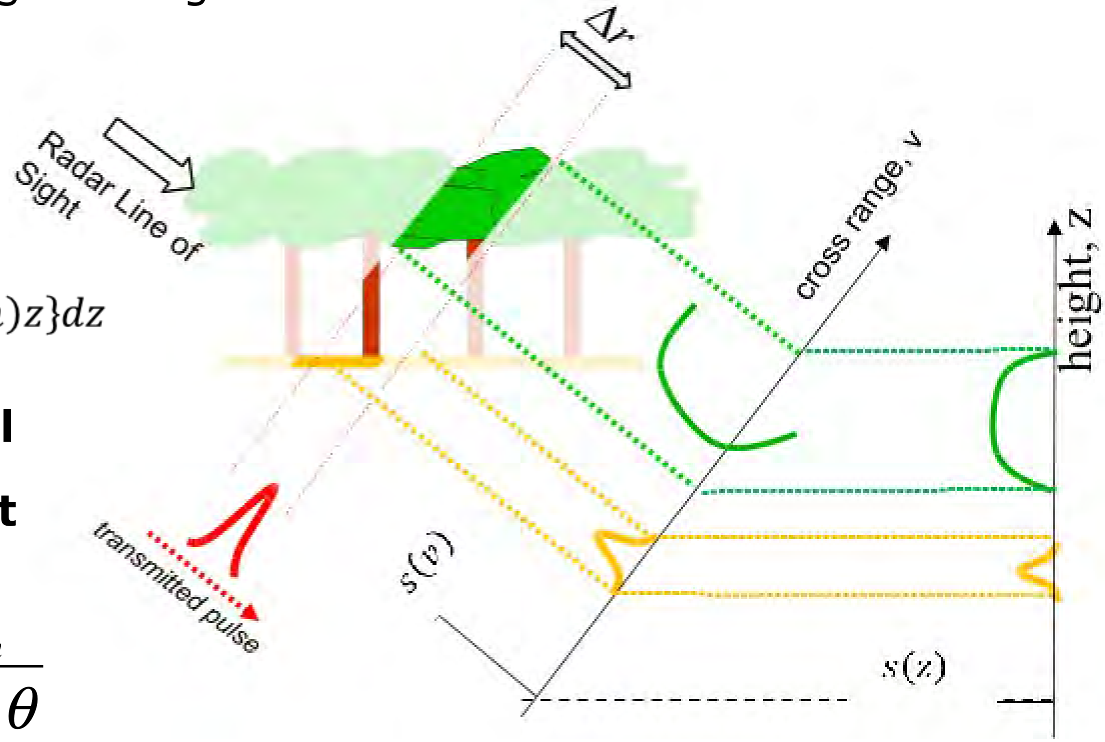

3-D SAR imaging

Co-registration on a reference plane

Valid for $z \in z_{ref} \pm \Delta z_{val}/2$

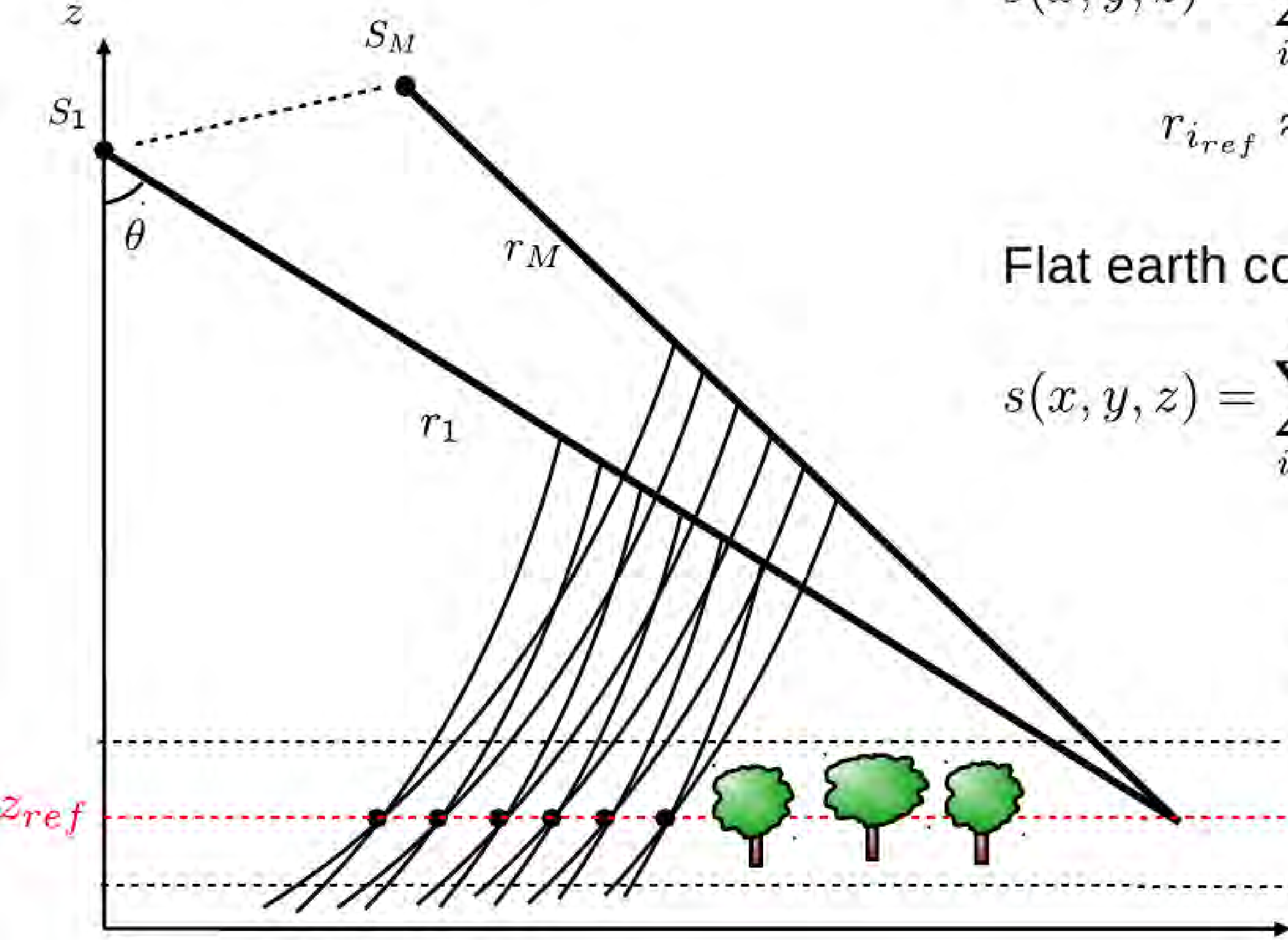

Δz_{val}

$$s(x,y,z) = \sum_{i=1}^{M} s_i(x, r_{i_{ref}})\, \mathrm{e}^{jk_c r_{i_{ref}}}$$

$$r_{i_{ref}} \approx r_{1_{ref}} + k_{z_i} z$$

Flat earth compensation

$$s(x,y,z) = \sum_{i=1}^{M} s_{i_{flat}}(x, r_{i_{ref}})\, \mathrm{e}^{jk_{z_i} z}$$

$$k_{z_i} = \frac{4\pi}{\lambda_c} \frac{B_{\perp_i}}{r_{1_{ref}} \sin\theta_{ref}}$$

Height-to-phase conversion number [rad/m]

3-D SAR imaging

3-D Synthetic Aperture imaging

$$s(x,y,z) = \sum_{i=1}^{M} s_i(x, r_{i_{ref}})\, \mathrm{e}^{jk_{z_i} z}$$

Beamformer-like formulation

SLC data

$$\Rightarrow \quad \mathbf{y} = [y_1, \ldots, y_M]^T$$

Steering vector

$$\mathbf{a} = [1, \mathrm{e}^{-jk_{z_2} z}, \ldots, \mathrm{e}^{-jk_{z_M} z}]^T$$

$$\boxed{s(z) = \mathbf{a}(z)^{\dagger}\mathbf{y}}$$

3-D Fourier imaging is equivalent to the Beamformer spectral analysis method

Principles of spectral analysis

Example: sum of monochromatic signals

$$s(t) = \sum_{i=1}^{N_s} a_i \, \mathrm{e}^{j2\pi f_i t} \qquad \hat{S}(f) = \int_{-\frac{\Delta T}{2}}^{+\frac{\Delta T}{2}} s(t)\, \mathrm{e}^{-j2\pi f t}\, \mathrm{d}t$$

Discrete-time signal $s_s(t) = \sum_{i=-M/2}^{M/2-1} s(t_i)\delta(t-t_i) \quad \tilde{S}(f) = \sum_{-M/2}^{M/2-1} s_i \, \mathrm{e}^{-j2\pi f t_i}$

$$\boxed{t_i = t_0 + iT_s \Longrightarrow \tilde{S}(f) = \frac{1}{T_s}\sum_k S\left(f - \frac{k}{T_s}\right)}$$

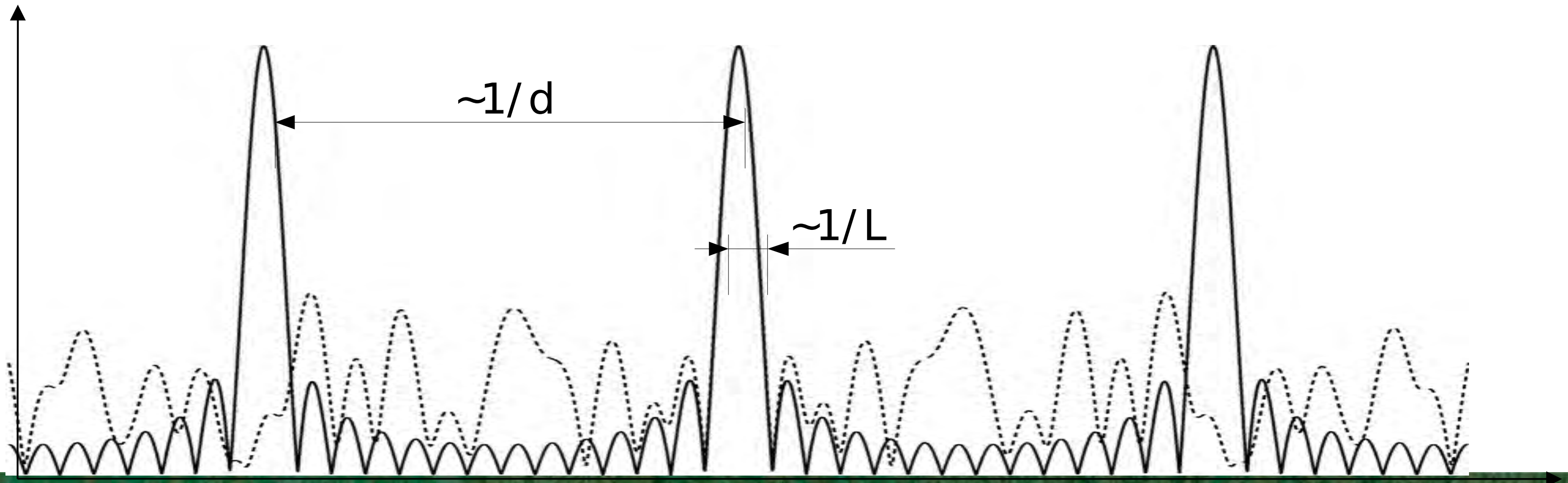

Discrete-time signal

$$\tilde{S}(f) = \sum_{-M/2}^{M/2-1} s_i \, \mathrm{e}^{-j2\pi f t_i}$$

Tomographic equivalence

$$s_m = \sum_{i=1}^{N_s} a_{c_i} \, \mathrm{e}^{j k_{z_m} z} \qquad m = 1, \ldots, M$$

$$\tilde{S}(z) = \sum_{-M/2}^{M/2-1} s_m \, \mathrm{e}^{-j2\pi k_{z_m} z}$$

Irregular baseline sampling

Limited bandwidth Δk_z

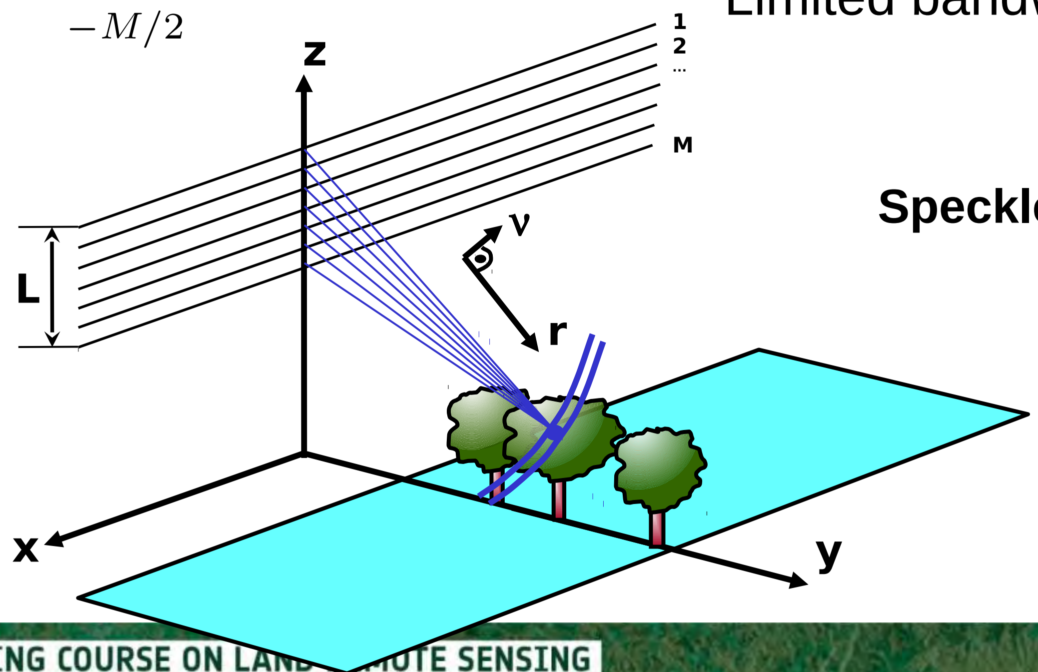

Speckle effect ?

Principles of spectral analysis

Stationary signal $\mathrm{E}(|s(t)|^2) = I \quad \forall t \qquad \rho_{ss}(\tau) = ACF(s(t))$

$$\hat{\Phi}(f) = \mathrm{E}(|\hat{S}(f)|^2) = I \int_{-\frac{\Delta T}{2}}^{+\frac{\Delta T}{2}} \rho_{ss}(\tau)\, \mathrm{e}^{-j2\pi f\tau}\, \mathrm{d}\tau$$

Tomographic equivalence $s_m = \sum_{i=1}^{N_s} a_c(z)\, \mathrm{e}^{jk_{z_m} z} \qquad m = 1, \dots, M$

$$\tilde{\Phi}_{ss}(z) = \mathrm{E}(|a_c(z)|^2) = I \sum_{m=-M/2}^{M/2-1} \gamma_{1m}\, \mathrm{e}^{-j2\pi k_{z_m} z}$$

$$\gamma_{mn} = \frac{\mathrm{E}(s_m s_n^*)}{\sqrt{\mathrm{E}(|s_m|^2\, \mathrm{E}\, |s_n|^2)}} \quad \Longrightarrow \quad \mathbf{R} = \begin{bmatrix} 1 & \gamma_{12} & \cdots & \gamma_{1N} \\ \gamma_{21} & 1 & & \\ \vdots & & \ddots & \vdots \\ \gamma_{N1} & & \cdots & 1 \end{bmatrix}$$

Current paradigm for forested areas: **retrieve the *vertical distribution of backscattered power* based on the observed *InSAR coherences***

SLC data

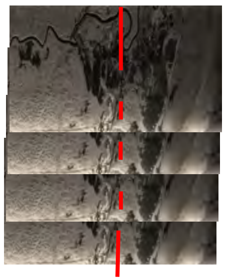

Complex data vector (Nx1)

$$\mathbf{d} = \begin{bmatrix} d_1 \\ d_2 \\ \vdots \\ d_N \end{bmatrix}$$

$\Rightarrow$

Coherence estimation (spatial multilooking)

$$\gamma_{nm} = \frac{\langle d_n d_m^* \rangle_L}{\sqrt{\langle |d_n|^2 \rangle_L \langle |d_m|^2 \rangle_L}}$$

$\Rightarrow$

Coherence matrix (NxN)

$$\mathbf{R} = \begin{bmatrix} 1 & \gamma_{12} & \cdots & \gamma_{1N} \\ \gamma_{21} & 1 & & \vdots \\ \vdots & & \ddots & \\ \gamma_{N1} & & \cdots & 1 \end{bmatrix}$$

$\Downarrow$

TomoSAR processing

$\Downarrow$

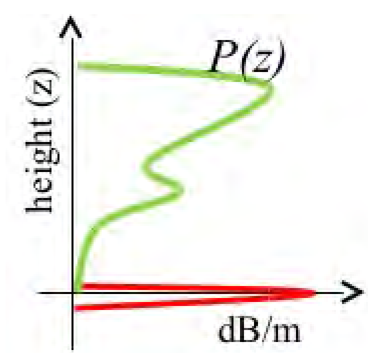

Why?

⇒*Improved performance by using Spectral Analysis*

- **Super-resolution** (super = finer than the limit from baseline aperture)
- **Side-lobe rejection**
- **Rejection of ambiguous targets** (using irregular baseline spacing)

Tomographic imaging using specan

Acquired signal (single scatterer)

$$\mathbf{y} = a_c\,\mathbf{a}(z_0) + \mathbf{n}$$

with $\mathbf{a}(z_0) = [1, \mathrm{e}^{jk_{z_2} z_0}, \ldots, \mathrm{e}^{jk_{z_M} z_0}]^T$

Used approach: linear filtering

$$f(\mathbf{w}) = \mathbf{w}^\dagger \mathbf{y} = \sum_{i=1}^{M} w_i^* y_i$$

Beamformer

$$\boxed{\mathbf{w}_{BF} = \frac{\mathbf{a}(z)}{M}}$$

- (Fast) filter maximizing the output SNR
- SNR maximized at z = z_0 :
- Use: compute

$$P_B(z) = |\mathbf{w}_B^\dagger(z)\mathbf{y}|^2$$

estimate parameters from the max

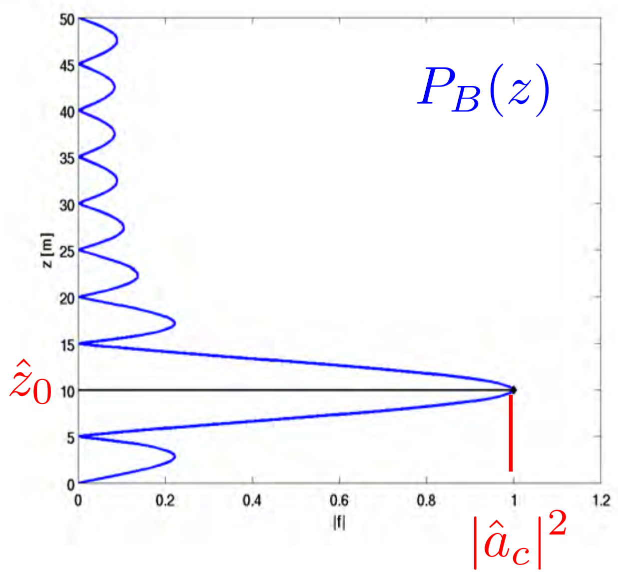

Tomographic imaging using specan

Uniform baseline sampling $\mathbf{a}(z) = [1, \mathrm{e}^{j\mathrm{d}k_z z}, \dots, \mathrm{e}^{j(M-1)\mathrm{d}k_z z}]^T$

Fast: resolution

$$|f(z)| = |a_c| \frac{\mathbf{a}^\dagger(z)\mathbf{a}(z_0)}{N} = \frac{|a_c|}{M} \frac{|\sin(\pi \Delta k_z (z - z_0))|}{|\sin(\pi \mathrm{d}k_z (z - z_0))|}$$

Slow: ambiguity

Spatial features of a tomogram

- **rapidly varying: resolution**
- **band-limited: sidelobes**
- **sampled: ambiguities**

$$\boxed{\delta z = \frac{2\pi}{\Delta k}, \quad z_{amb} = \frac{2\pi}{\mathrm{d}k}, \quad \delta z = \frac{z_{amb}}{M}}$$

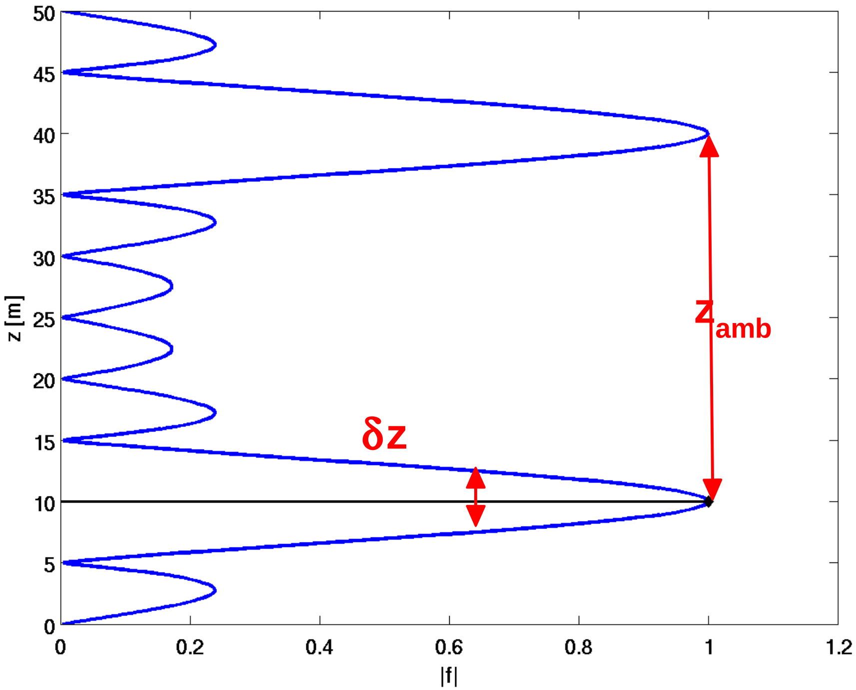

M=6

Tomographic imaging using specan

M=6

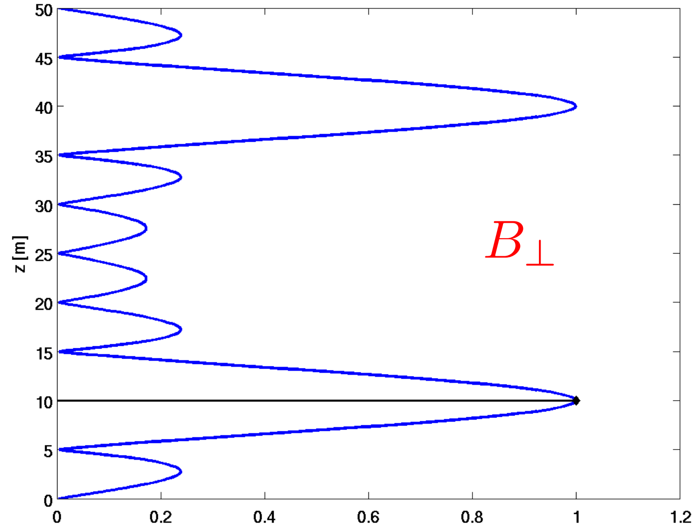

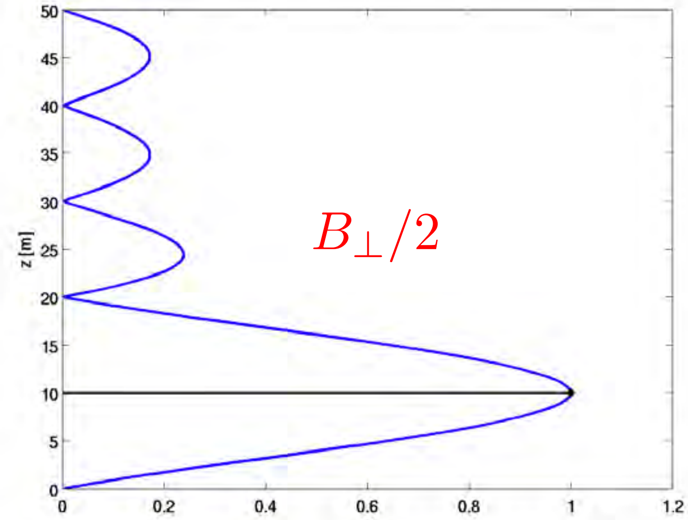

M=12

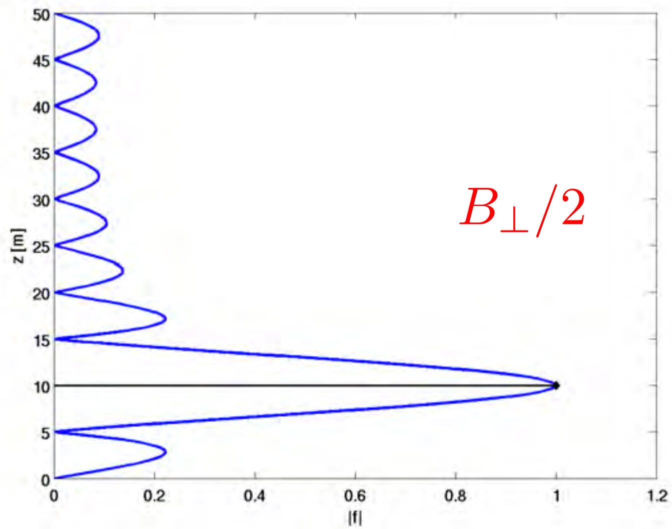

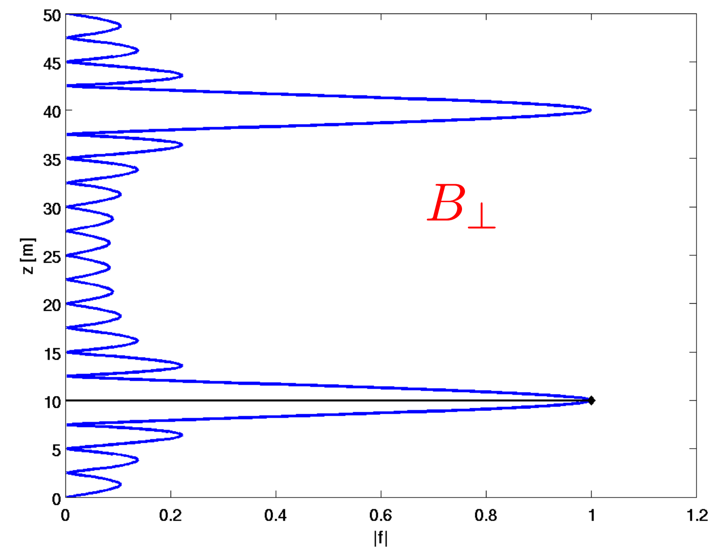

M=6

M=12

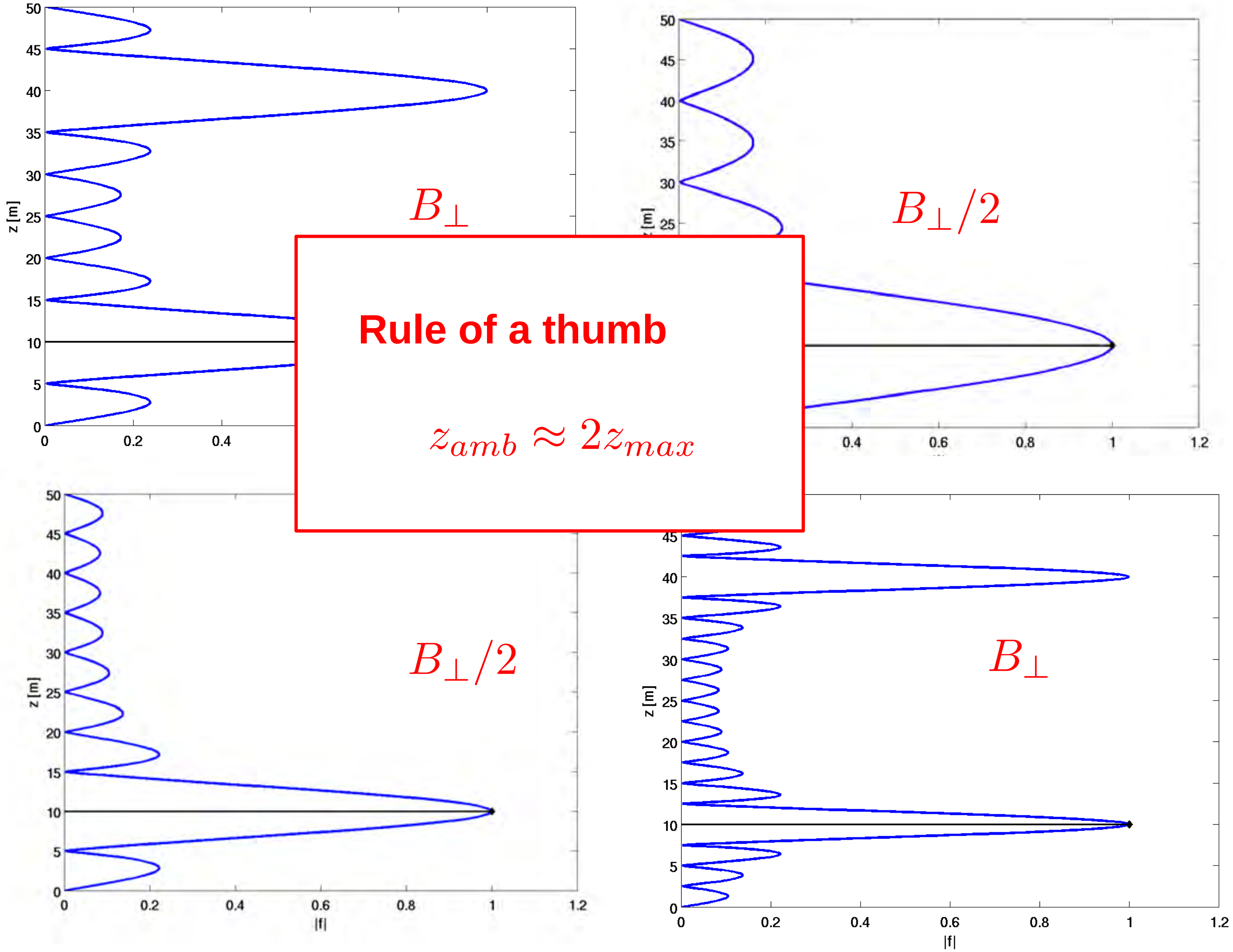

Rule of a thumb

$$z_{amb} \approx 2 z_{max}$$

Beamformer features

- Excellent statistical accuracy
- Fourier resolution (depends on Δk)
- Cannot handle closely spaced scatterers

Capon's approach

- Linear filter (fast)
- Aims to minimize spatial perturbations & sidelobes

Capon's solution

$$\mathbf{w}_C = \arg\min_{\mathbf{w}} \mathrm{E}(|\mathbf{w}^\dagger \mathbf{y}|^2) \quad \text{s.t,} \quad \mathbf{w}^\dagger \mathbf{a}(z) = 1$$

$$\mathbf{w}_C = \frac{\mathbf{R}^{-1}\mathbf{a}(z)}{\mathbf{a}^\dagger(z)\,\mathbf{R}^{-1}\mathbf{a}(z)}, \quad \mathbf{R} = \mathrm{E}(\mathbf{y}\mathbf{y}^\dagger)$$

$$\widehat{\mathbf{R}} = \frac{1}{L}\sum_{l=1}^{L} \mathbf{y}(l)\mathbf{y}^\dagger(l)$$

Tomographic imaging using specan

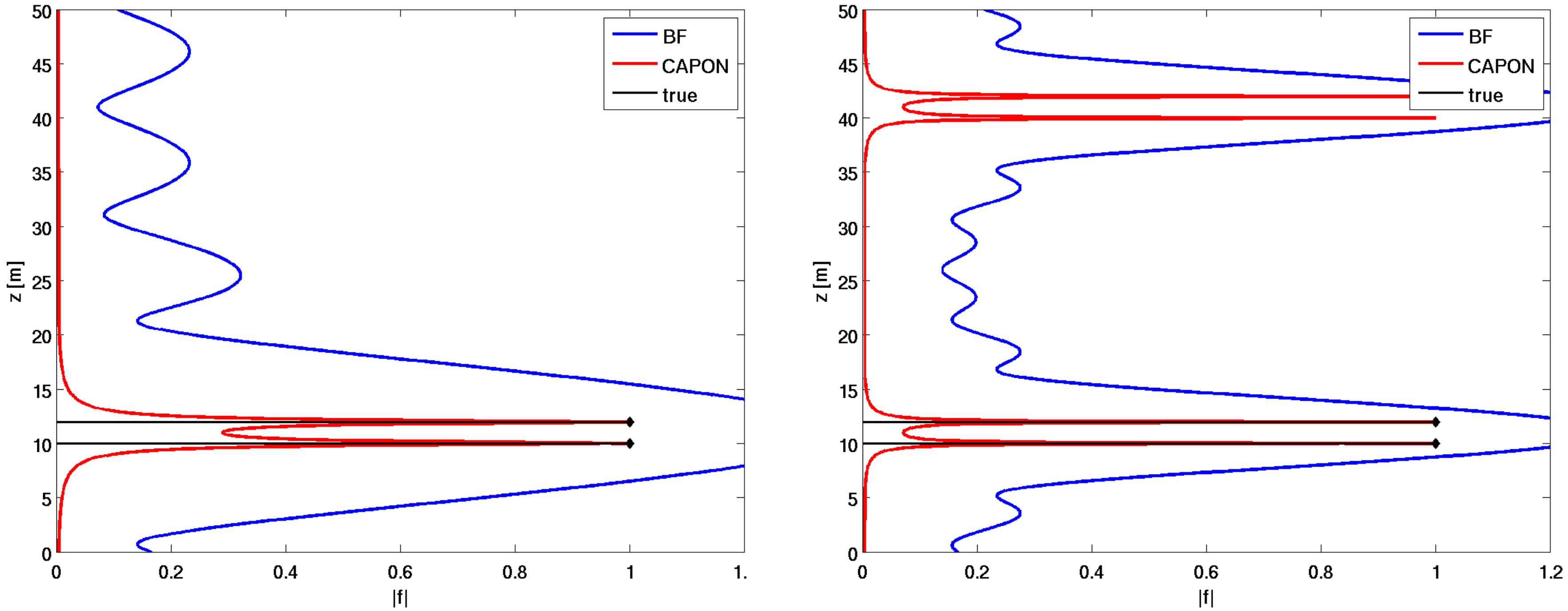

- **Capon: significantly improved resolution**
- **For regular baselines, BF & Capon are equally affected by ambiguities**

Irregular baseline sampling: logscale distribution

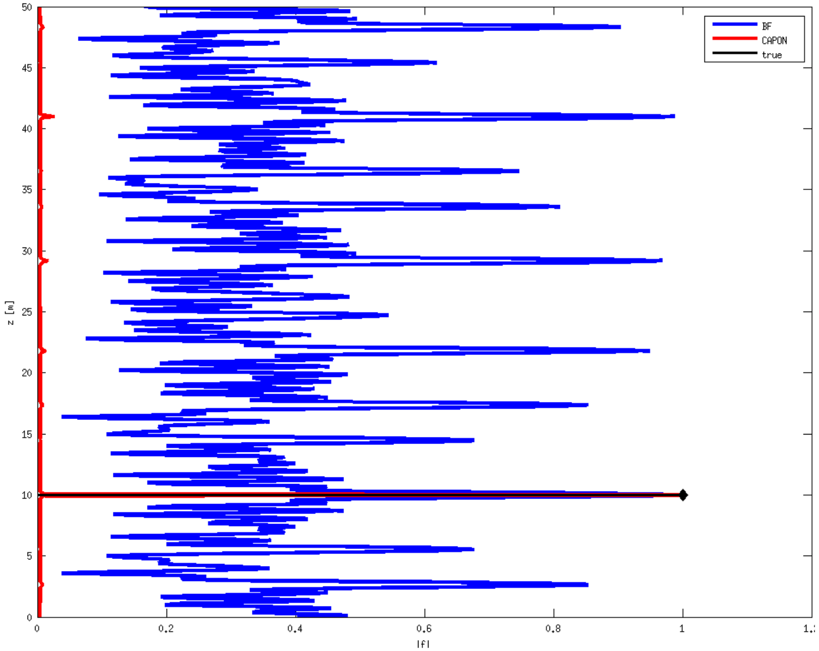

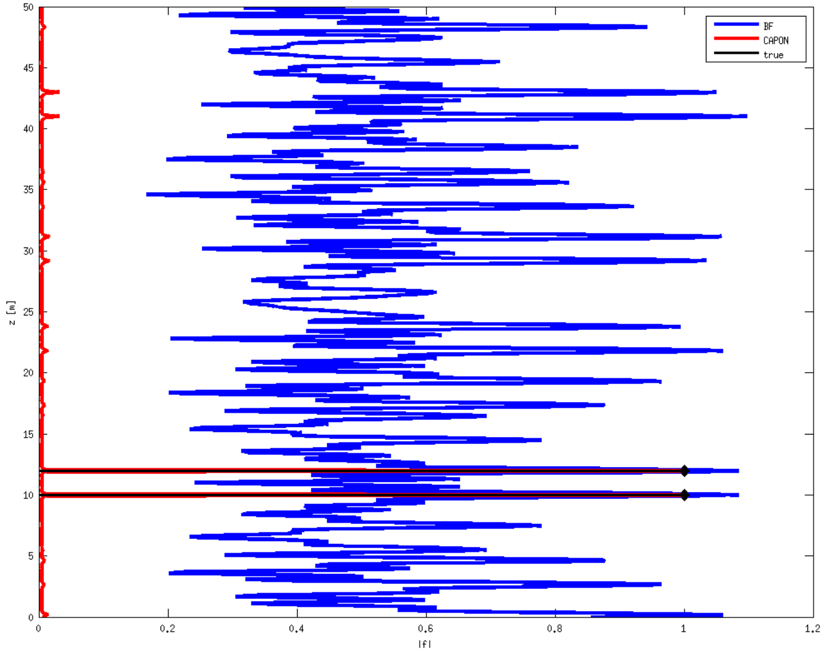

- BF: strongly affected by ambiguities
- CAPON: unsynchronized ambiguity are considered as perturbations and filtered. Good resolution performance preserved

Over speckle affected environments

- $\mathbf{w}_i^\dagger \mathbf{y},\ i = B, C$ is a Random Variable (1 realization is not representative)
- Power Spectral Density

$$P_i(z) = \mathrm{E}(|\mathbf{w}_i^\dagger \mathbf{y}|^2) = \mathbf{w}_i^\dagger \mathbf{R} \mathbf{w}_i$$

$$P_{BF}(z) = \mathbf{a}^\dagger(z)\mathbf{R}\mathbf{a}(z), \quad P_C(z) = \frac{1}{\mathbf{a}^\dagger(z)\mathbf{R}^{-1}\mathbf{a}(z)}$$

- In practice

$$\widehat{\mathbf{R}} = \frac{1}{L}\sum_{l=1}^{L} \mathbf{y}(l)\mathbf{y}^\dagger(l)$$

- BF: quite stable w.r.t L
- Capon may suffer from a poor covariance matrix conditioning

$\Rightarrow$ Diagonal Loading

$$\widetilde{\mathbf{R}} = \widehat{\mathbf{R}} + \alpha \mathbf{I}_M, \quad \alpha \geq 0$$

Tropical forest profile at P band

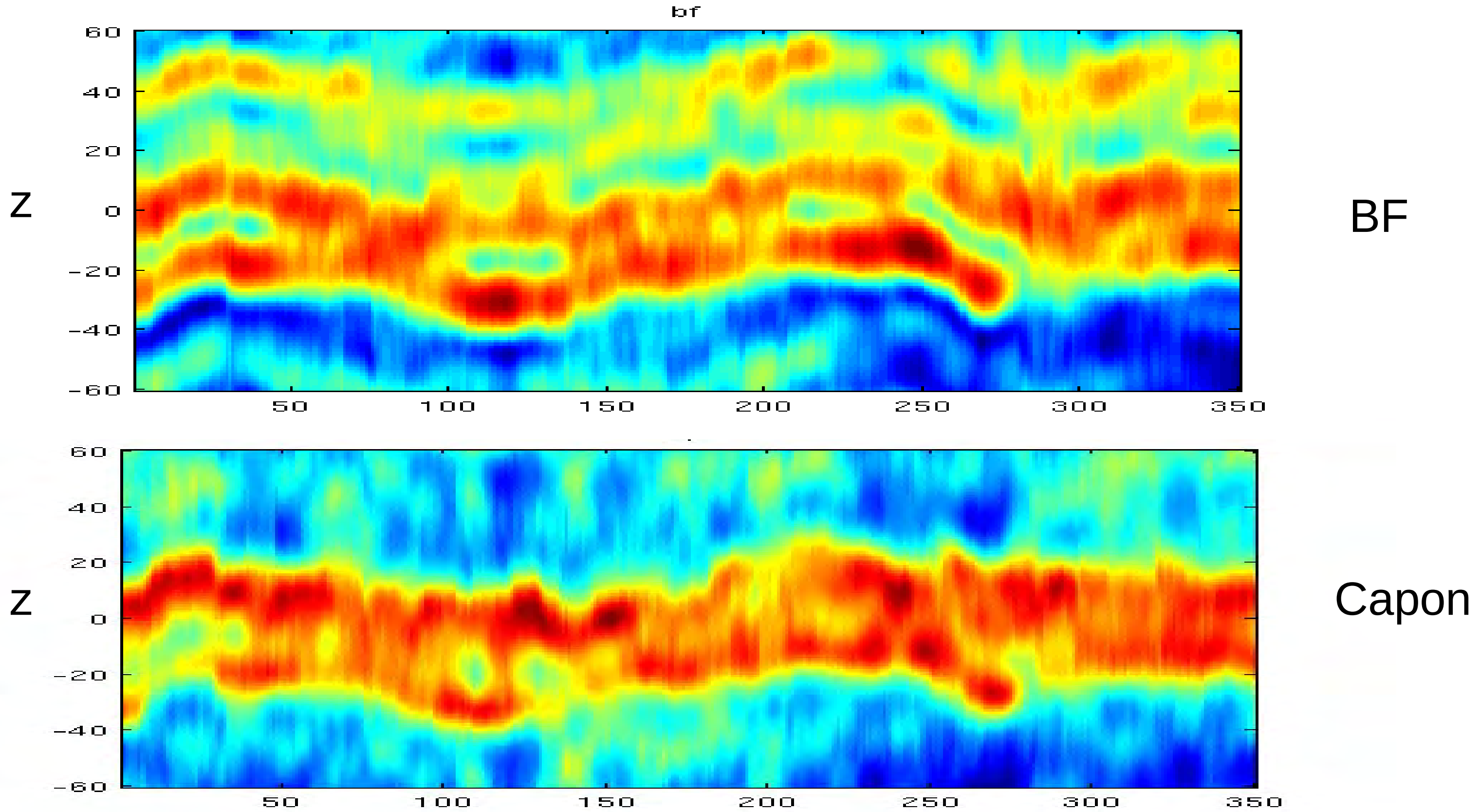

Covariance matrix model for discrete scatterers

$$\mathbf{y} = \sum_{i=1}^{N_s} s_i\,\mathbf{a}(z_i) + \mathbf{n} = \mathbf{A}\mathbf{s} + \mathbf{n} \quad \Rightarrow \quad \mathbf{R} = \mathbf{A}\mathbf{R}_{\mathbf{ss}}\mathbf{A}^\dagger + \sigma_n^2\mathbf{I}_N$$

Steering matrix $\mathbf{A} = \left[\mathbf{a}(z_1), \ldots, \mathbf{a}(z_{N_s})\right]$

Covariance matrix eigen-decomposition ($N_s < N$)

$$\mathbf{R} = \mathbf{V}\begin{bmatrix} \lambda_1 & & & & & \\ & \ddots & & & & \\ & & \lambda_N & & & \\ & & & \sigma_n^2 & & \\ & & & & \ddots & \\ & & & & & \sigma_n^2 \end{bmatrix}\mathbf{V}^\dagger = \mathbf{V}_s\begin{bmatrix} \lambda_1 & & \\ & \ddots & \\ & & \lambda_N \end{bmatrix}\mathbf{V}_s^\dagger + \sigma_n^2\mathbf{V}_n\mathbf{V}_n^\dagger$$

Covariance matrix model for discrete scatterers

$$\mathbf{y} = \sum_{i=1}^{N_s} s_i\,\mathbf{a}(z_i) + \mathbf{n} = \mathbf{A}\mathbf{s} + \mathbf{n} \quad \Rightarrow \quad \mathbf{R} = \mathbf{A}\mathbf{R}_{\mathbf{ss}}\mathbf{A}^\dagger + \sigma_n^2\mathbf{I}_N$$

Steering matrix $\mathbf{A} = \left[\mathbf{a}(z_1), \ldots, \mathbf{a}(z_{N_s})\right]$

Covariance matrix eigen-decomposition ($N_s < N$)

$$\mathbf{R} = \mathbf{V}\begin{bmatrix} \lambda_1 & & & & & \\ & \ddots & & & & \\ & & \lambda_N & & & \\ & & & \sigma_n^2 & & \\ & & & & \ddots & \\ & & & & & \sigma_n^2 \end{bmatrix}\mathbf{V}^\dagger = \mathbf{V}_s\begin{bmatrix} \lambda_1 & & \\ & \ddots & \\ & & \lambda_N \end{bmatrix}\mathbf{V}_s^\dagger + \sigma_n^2\mathbf{V}_n\mathbf{V}_n^\dagger$$

$$N = \operatorname{rank}(\mathbf{A}\mathbf{R}_{\mathbf{ss}}\mathbf{A}^\dagger) \leq N_s$$

MUSIC principle

$$\mathbf{A} = \mathbf{T}\mathbf{V}_s, \quad \mathbf{V}_s^{\dagger}\mathbf{V}_n = \mathbf{0} \quad \Rightarrow \quad |\mathbf{a}(z_i)^{\dagger}\mathbf{V}_n|^2 = 0 \, \forall \mathbf{a}(z_i) \in \mathbf{A}$$

MUSIC criterion

$$P_M(z) = \frac{1}{|\mathbf{a}(z)^{\dagger}\widehat{\mathbf{V}}_n|^2}$$

Remarks

- The noise space dimension has to be estimated
- MUSIC is well adapted to DISCRETE scatterers, not to continuous reflectivities (i.e. forest canopies)
- The values reached by the criterion DO NOT correpond to the PSD (profile intensity)
- CAPON is **NOT** HR, MUSIC **YES**

Tomographic imaging using specan

Critical configuration (**3 images**) in an urban environment at L band

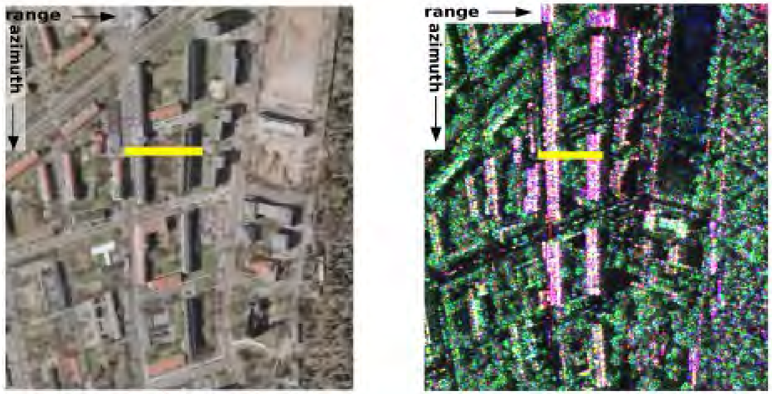

(a) Optical image (b) SAR

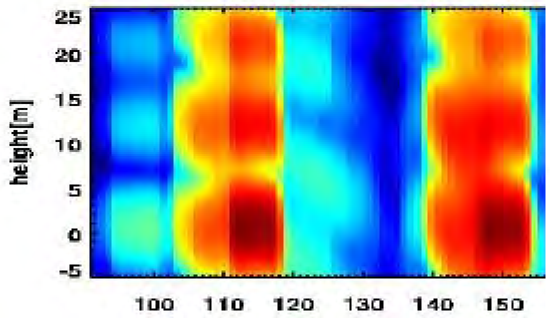

BF

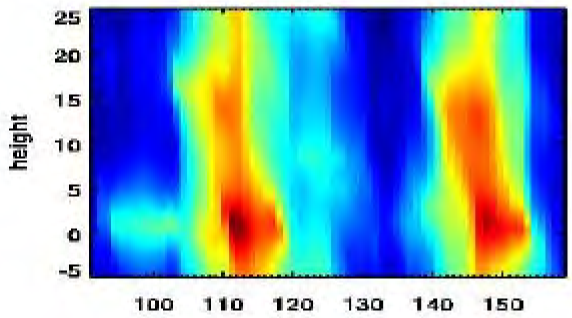

CAPON

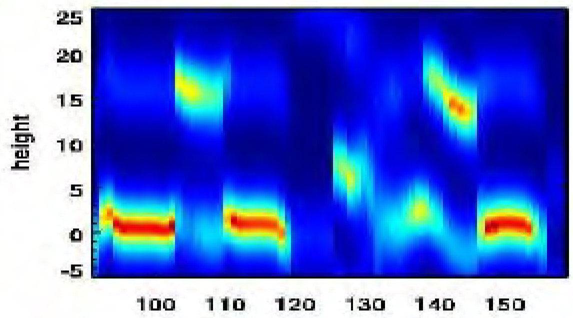

MUSIC

Strictly speaking, Capon's technique is not HR, but is very convenient and can be easily derived in the full-pol case

Case study: BIOSAR 2 data

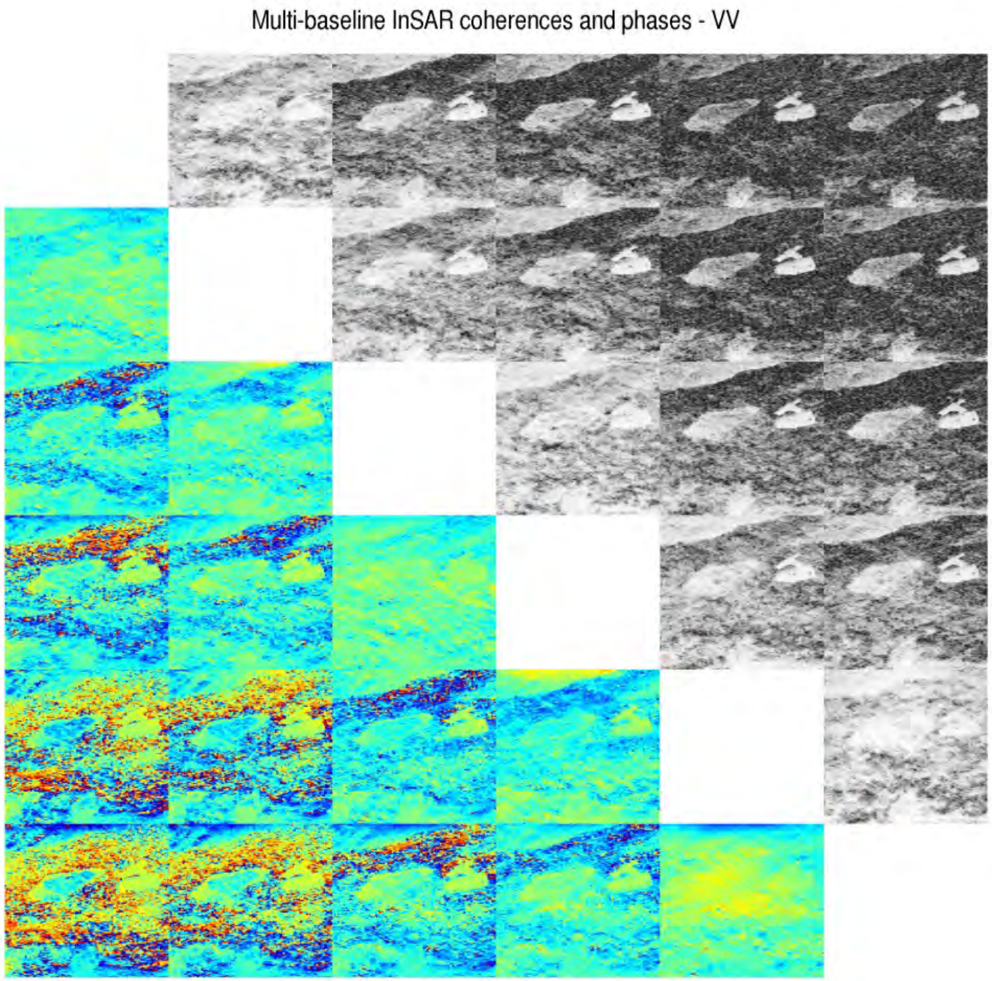

Case study: BIOSAR 2 data

BF

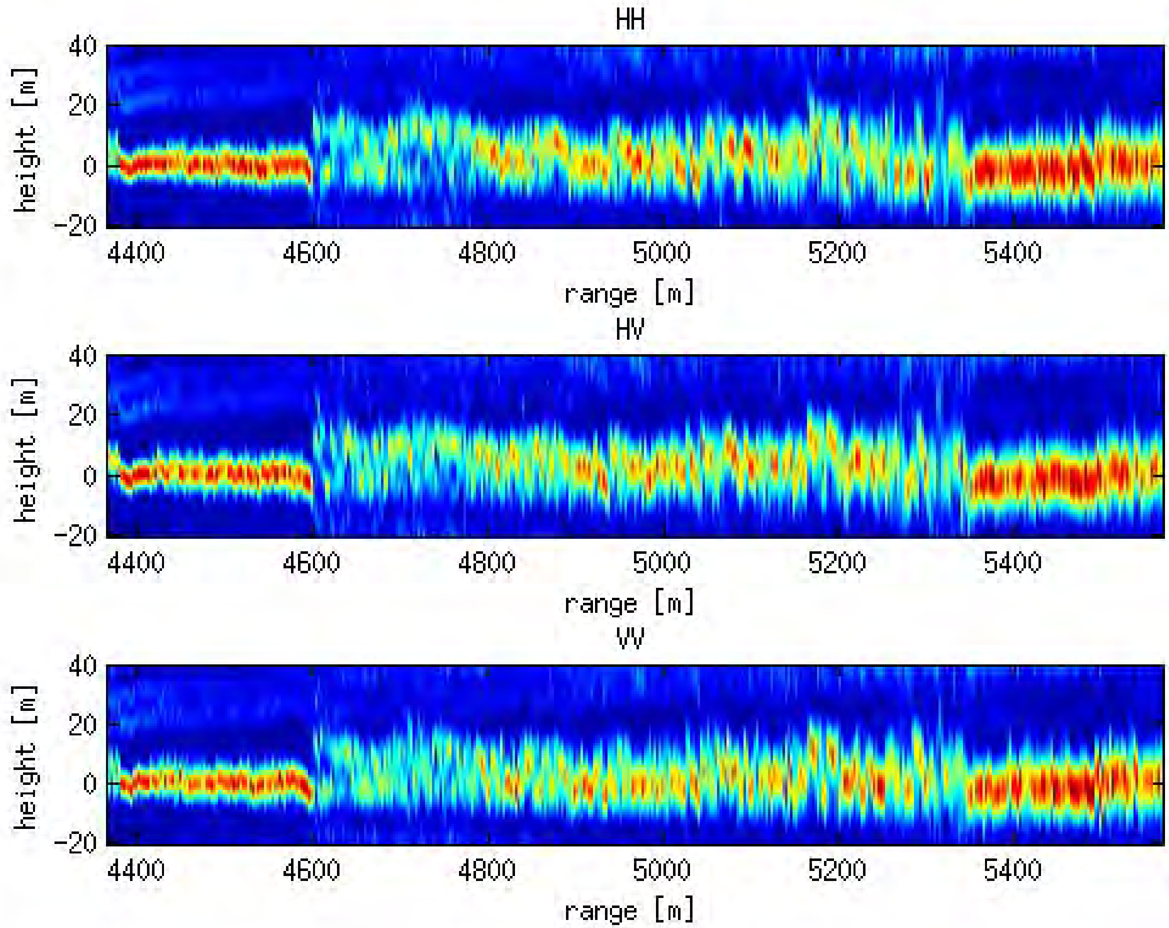

Case study: BIOSAR 2 data

CAPON: processing OK ?

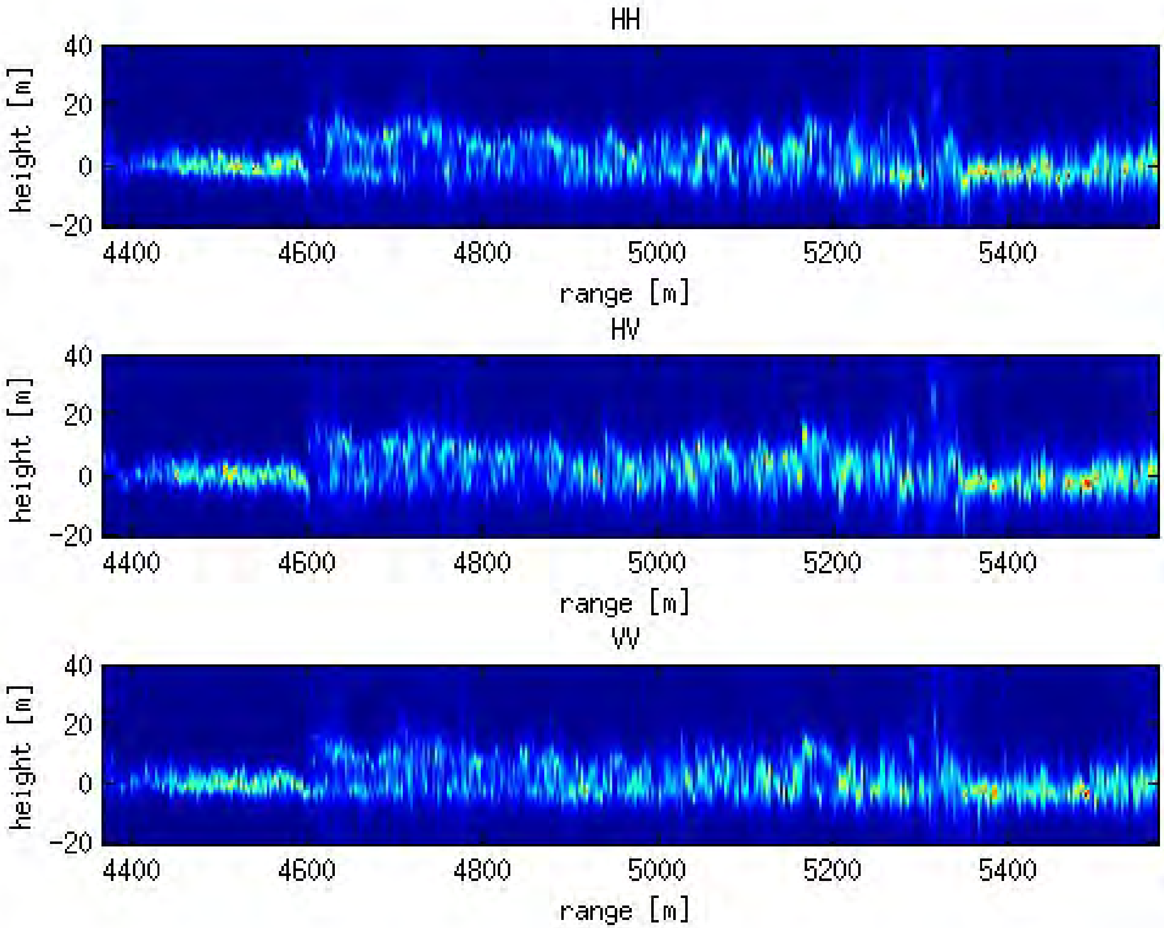

Singular covariance matrix → increase the number of samples

MUSIC: processing OK ?

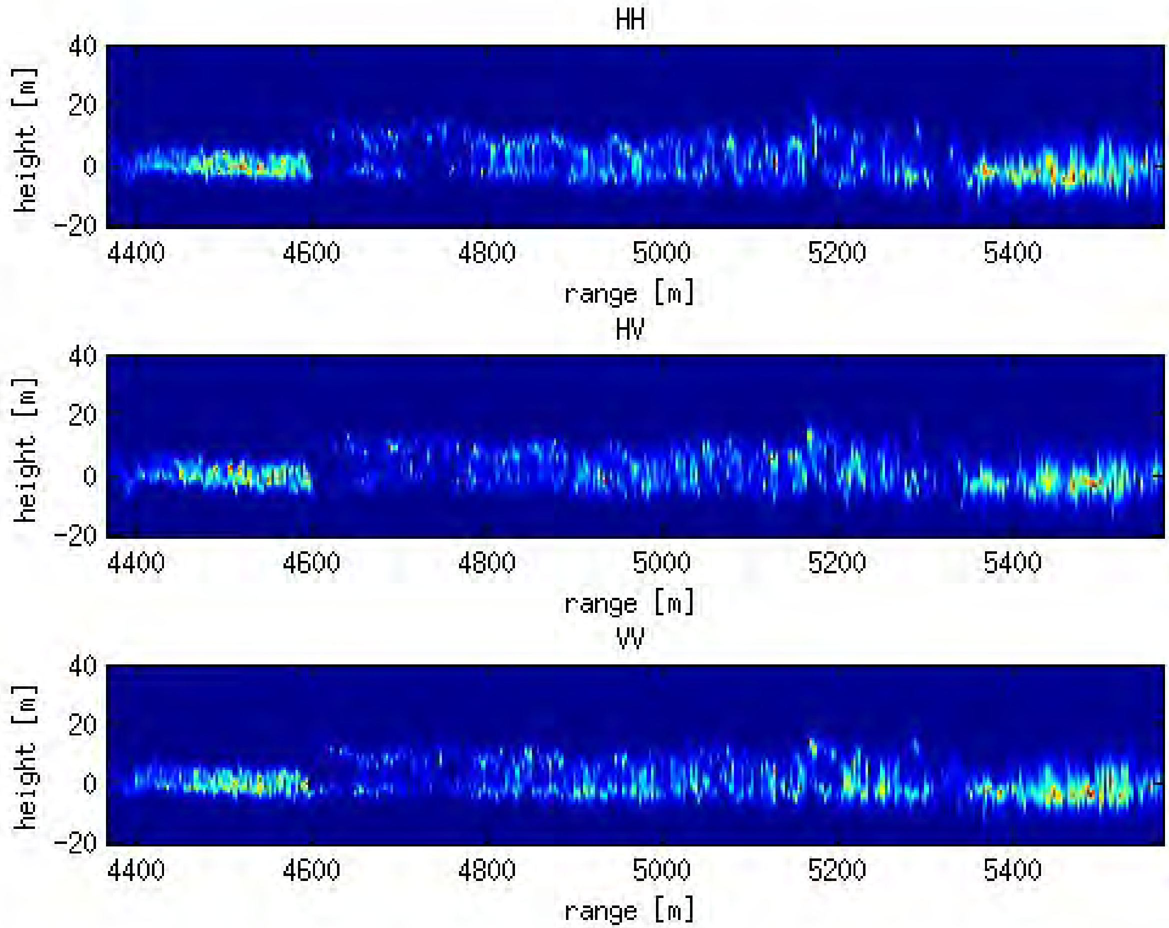

Singular covariance matrix → increase the number of samples

InSAR phases, polarization & TomSAR

L-band BIOSAR2, Capon tomograms

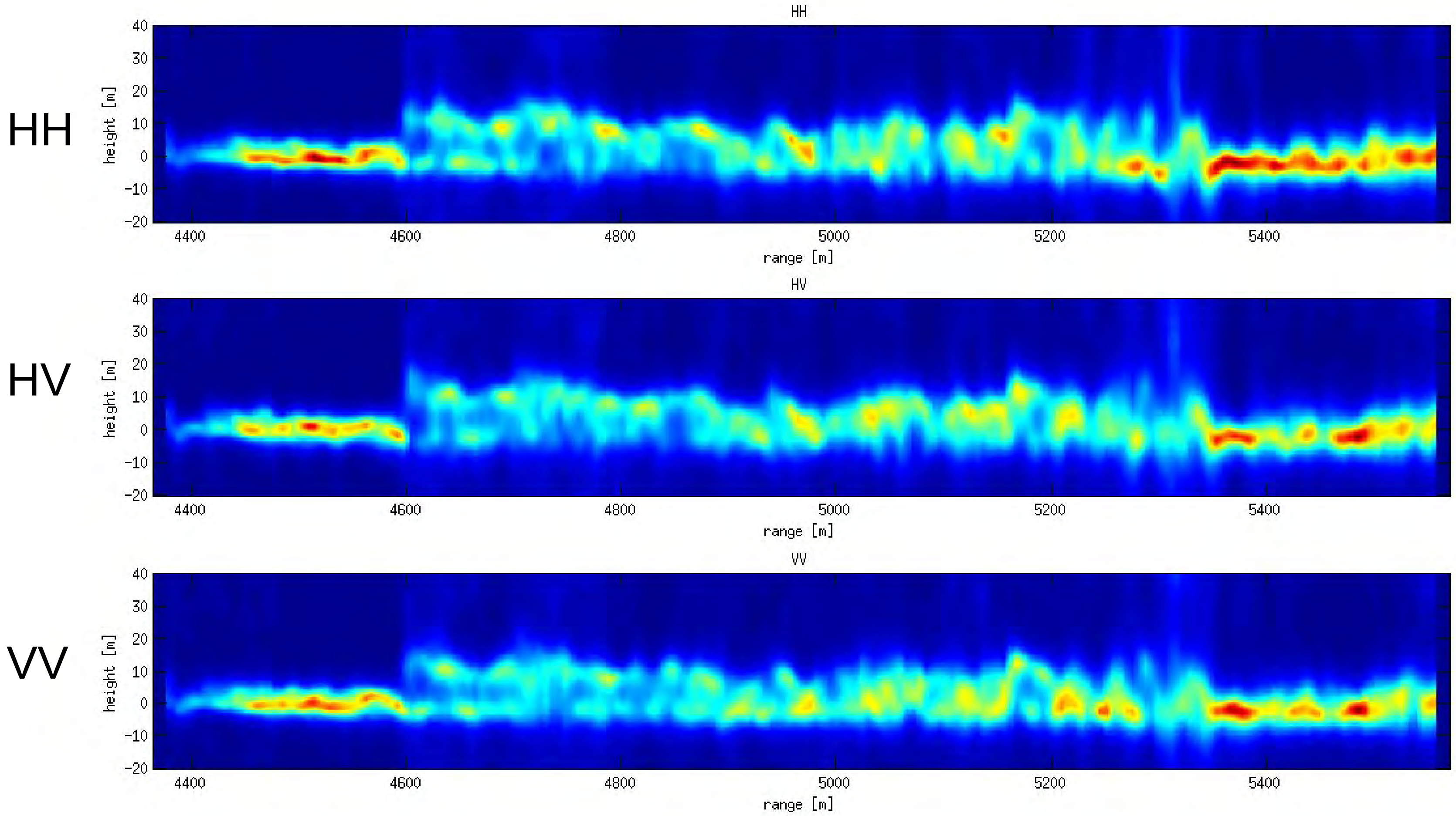

InSAR phases, polarization & TomSAR

Spatial diversity InSAR heights $h_i = \dfrac{\phi_{1i}}{k_{z_i}}$

HH

HV

VV

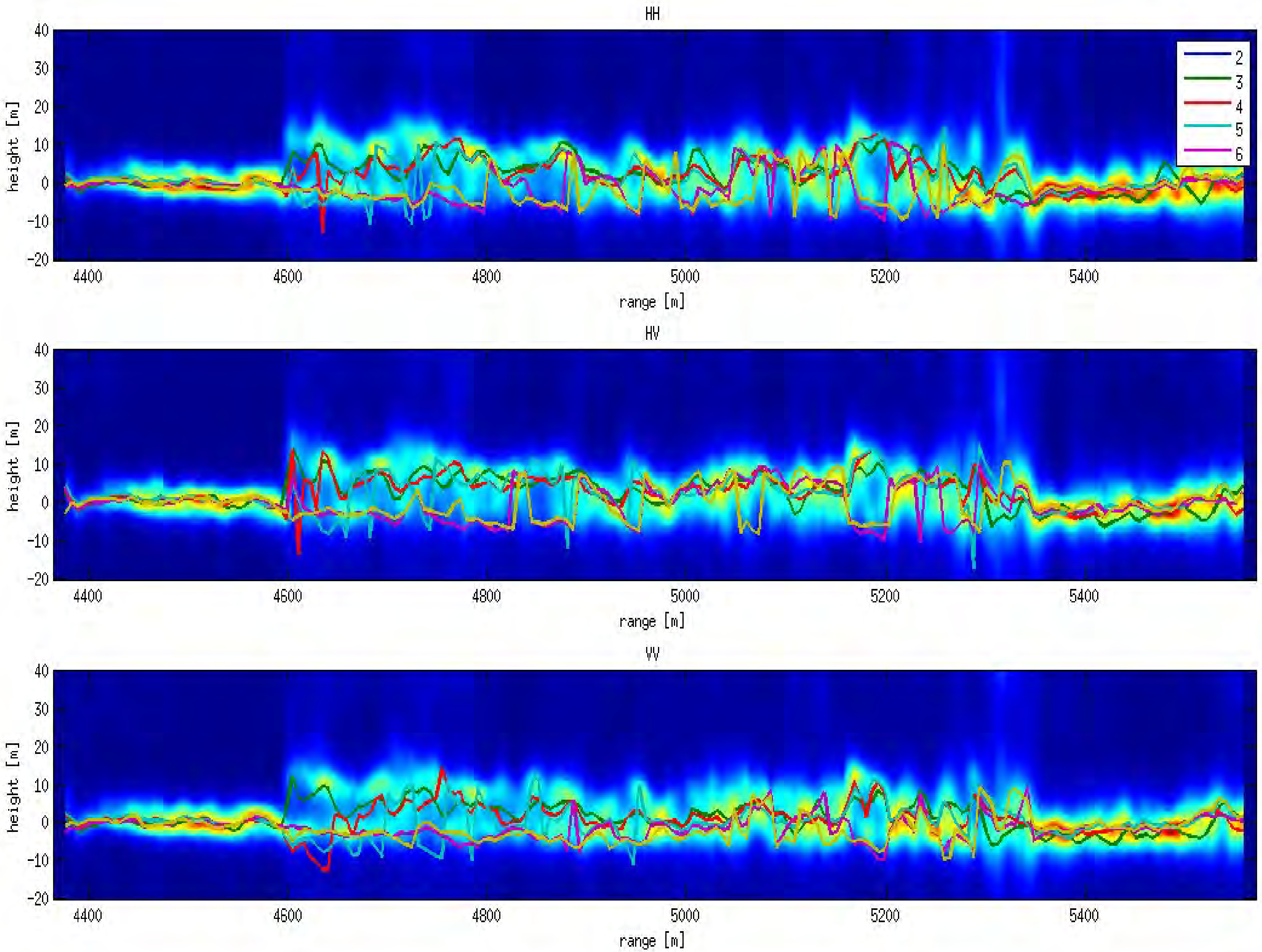

InSAR phases, polarization & TomSAR

Polarimetric diversity

POL-InSAR heights

$$h_p = \frac{\phi_{1i_p}}{k_{z_i}}$$

12

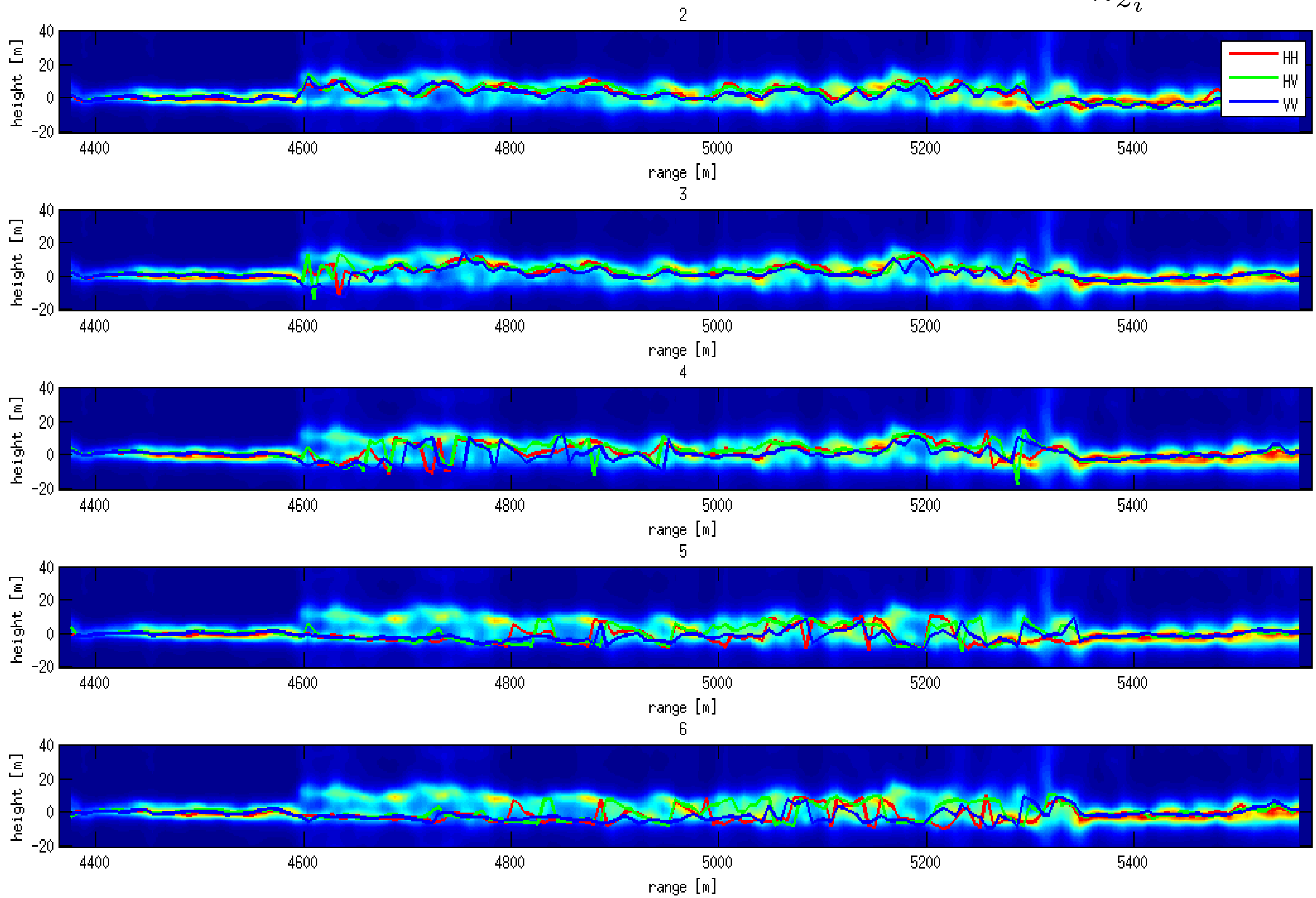

16

Strong-baseline dependence → Tomography

Need for full-rank Polarimetric SAR Tomography

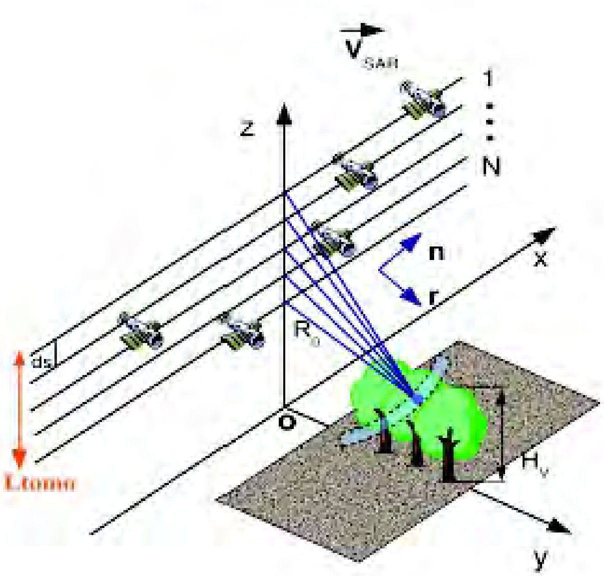

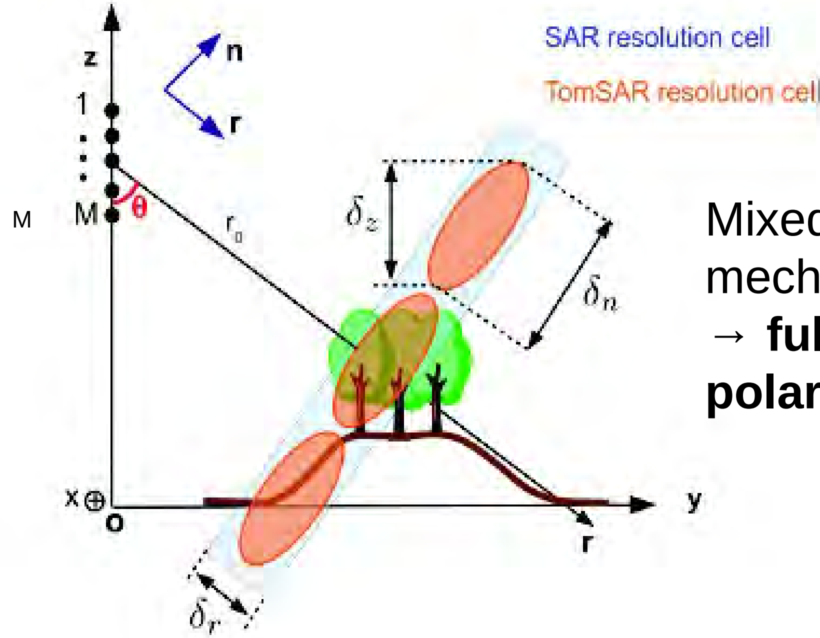

Mixed scattering mechanisms → **full rank polarimetry**

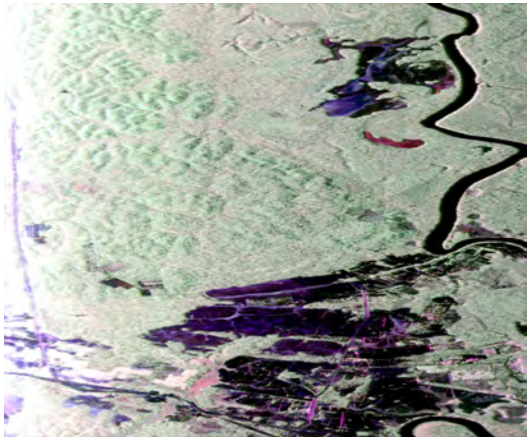

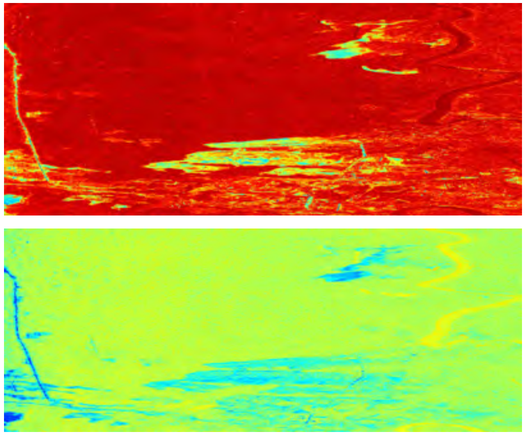

H

α

Intensity
σ(x,r)

Rank 1 polarimetry (Pauli)
k(x,r)

Full rank polarimetry
T(x,r)

M PolSAR images

$$\mathbf{y}_{PS} = \begin{bmatrix} \mathbf{y}_1 \\ \mathbf{y}_2 \\ \mathbf{y}_3 \end{bmatrix} \in \mathbb{C}^{3M}$$

$$\mathbf{R}_{PS} = \begin{bmatrix} \mathbf{R}_{11} & \mathbf{R}_{12} & \mathbf{R}_{13} \\ & \mathbf{R}_{22} & \mathbf{R}_{23} \\ & & \mathbf{R}_{33} \end{bmatrix}$$

$\gamma_{ij}(w_1, w_k)$

$\gamma_{ij}(w_2, w_k)$

$\gamma_{ij}(w_3, w_k)$

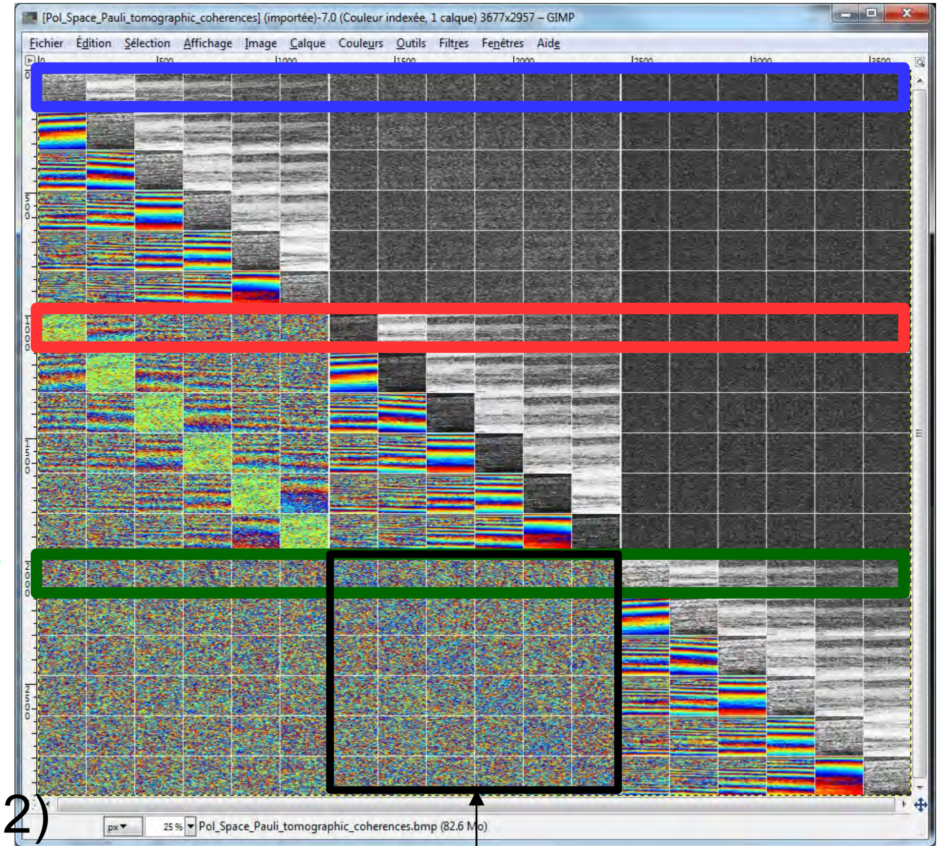

$\mathbf{R}_{ij} \in \mathbb{C}^{M \times M}$

3-D Full rank analysis strategies

- Full-rank P-Capon (BF) (LFF et al. 2012)

$$\mathbf{R}_{PS} \longrightarrow \sigma(z)\mathbf{T}(z)$$

- SKP decomposition (Tebaldini 2009)

$$\mathbf{R}_{PS} = \sum_i \mathbf{T}_{P_i} \otimes \mathbf{R}_{S_i} \longrightarrow \sum_i \sigma_i(z)\mathbf{T}_{P_i}$$

3-D POLSAR covariance matrices

Application to 3-D forest analysis

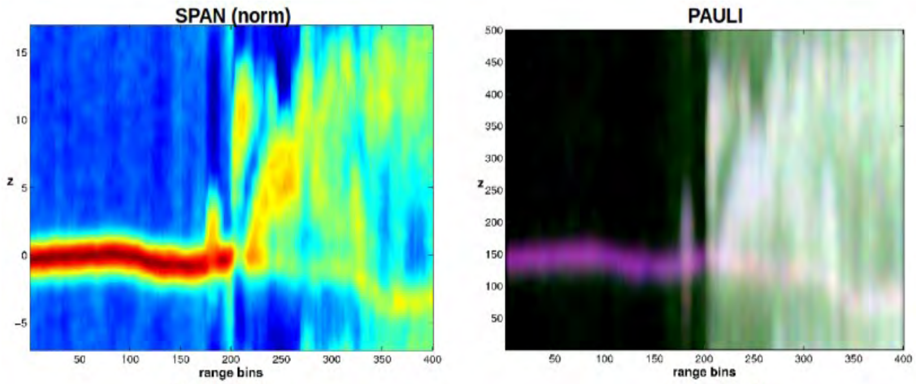

Dornstetten **airborne**

PolTomSAR data set

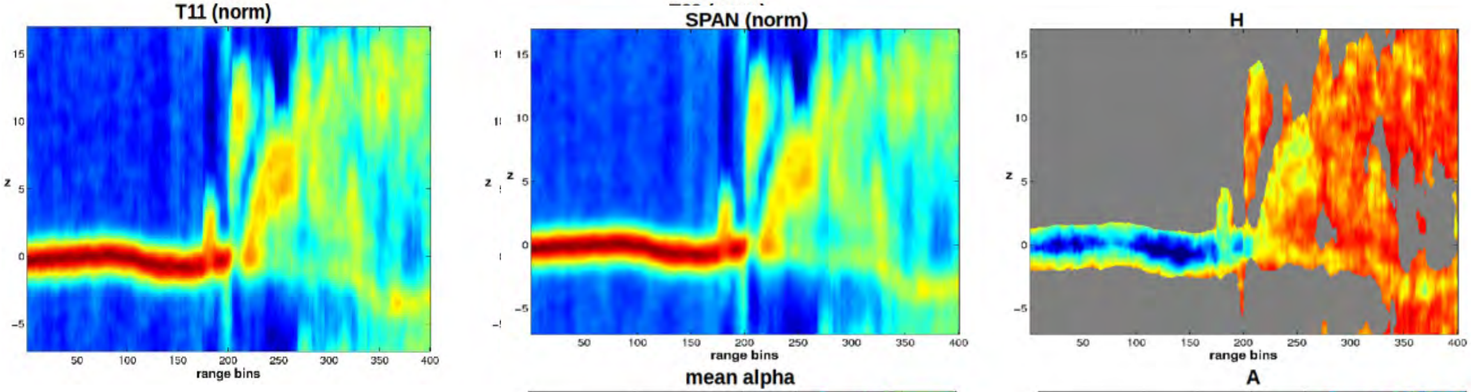

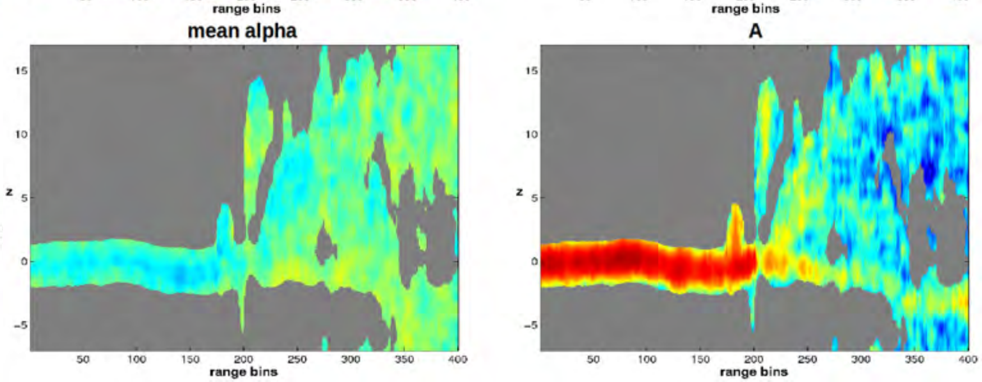

- DLR E-SAR
- L-Band
- 21 tracks: average baseline 20m
- Tomographic resolution $\delta_z = 2$m

Scattering Mechanism Decomposition

SKP decomposition

Ground-volume decomposition implies:

- Separation of Structural Properties

  => Separated Tomographic Imaging of Ground-only and Volume-only Contributions

HV

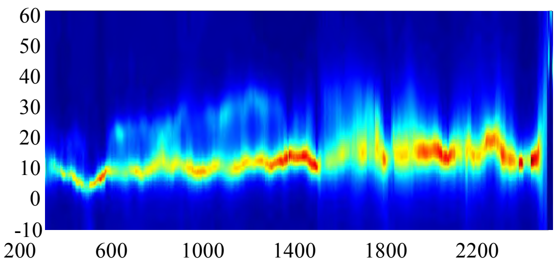

Ground

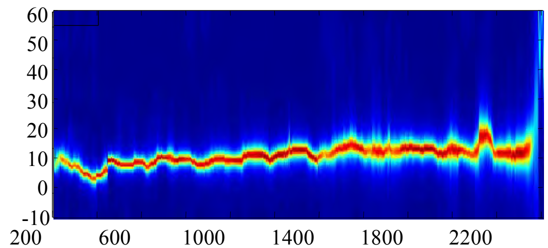

Volume

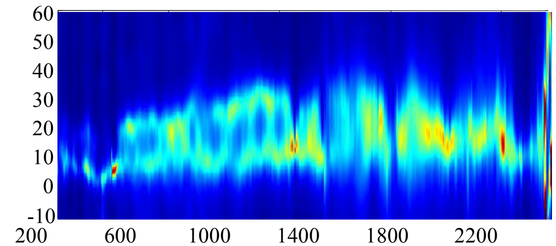

- Separation of Polarimetric Properties

  => Evaluation of the Ground to Volume Backscattered Power Ratio for each polarization

P-Band HH

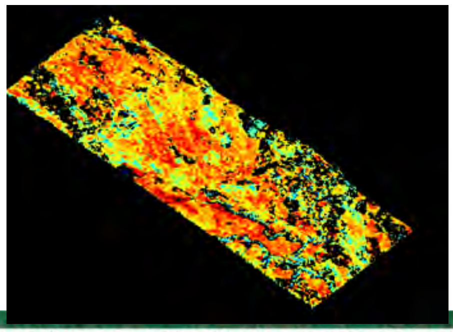

P-Band HV

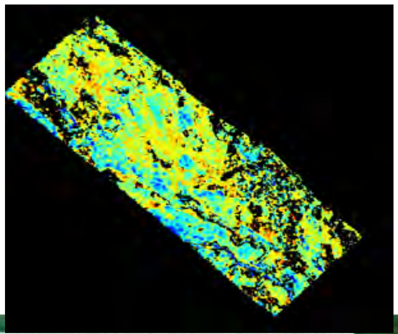

L-Band HH

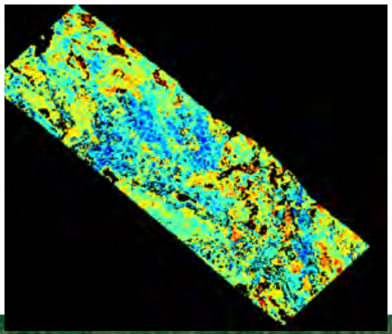

L-Band HV

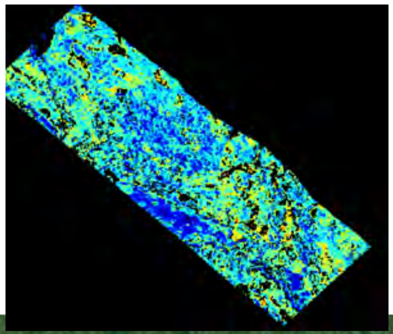

Application of PolTomoSAR to the characterization of complex media

Urban area test site

- Images over Dresden, 2000
- DLR's E-SAR at L-Band
- Resolution : 0.5 m × 2.5 m
- Fully polarimetric
- Dual-baseline InSAR

Baselines	H_{am}
10 m	55-73 m
40 m	14-18 m

3 PolSAR images

Pauli-coded SAR image

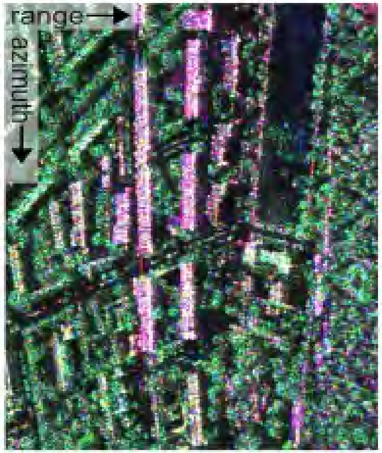

Optical image

Polarimetric SAR tomography over urban areas

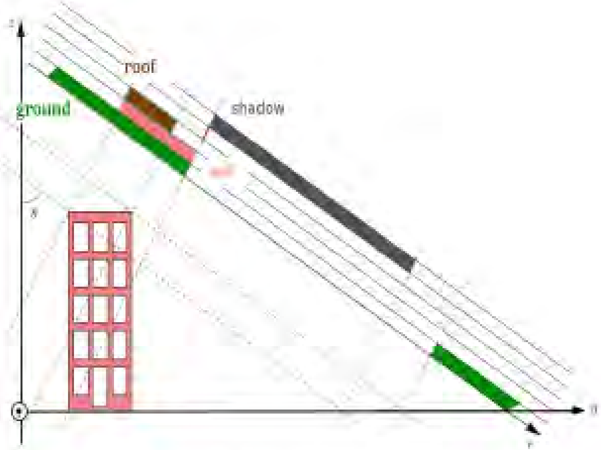

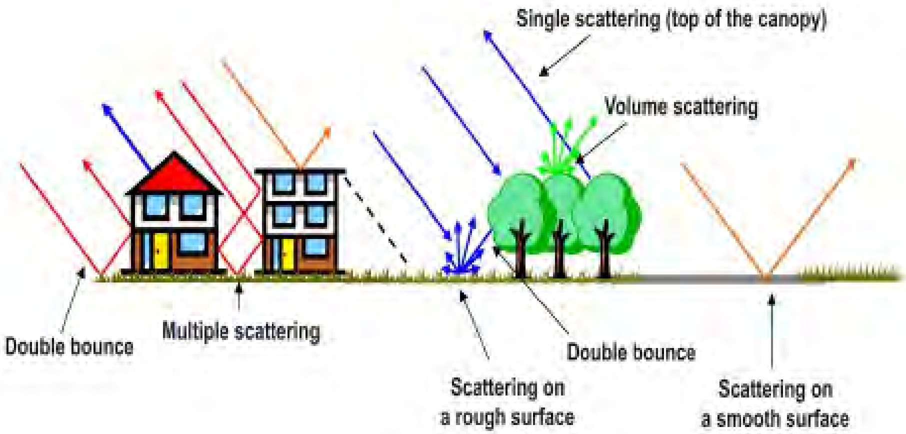

- L-band intermediate-resolution data sets
  $\Rightarrow$ High-Resolution (HR) tomographic estimators
- 3 images
  $\Rightarrow N_s = 2$
- Sum of diverse (polarimetric & statistical) contributions
  $\Rightarrow$ FP-NSF model adaptive estimator.

Polarimetric SAR tomography over urban areas

VV refectivity tomograms ($Ns = 2$)

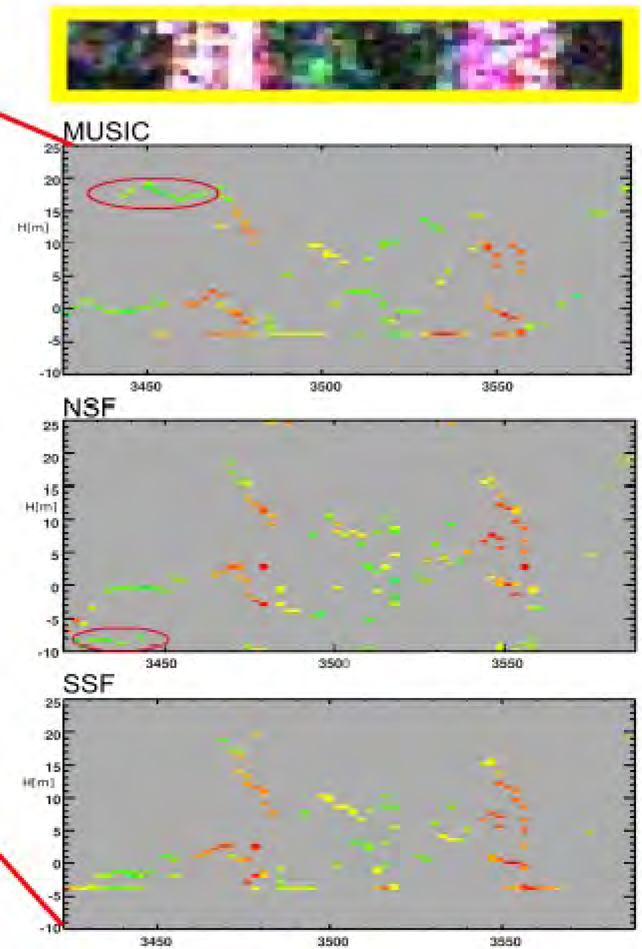

Coherent scatterers
Balconies, cars

- NSF and MUSIC: ☹
- SSF: ☺

Polarimetric SAR tomography over urban areas

SP Reflectivity tomograms

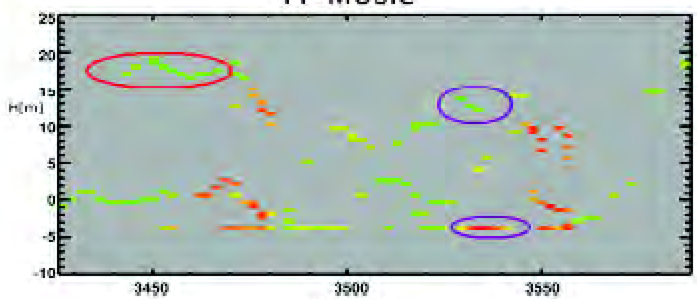

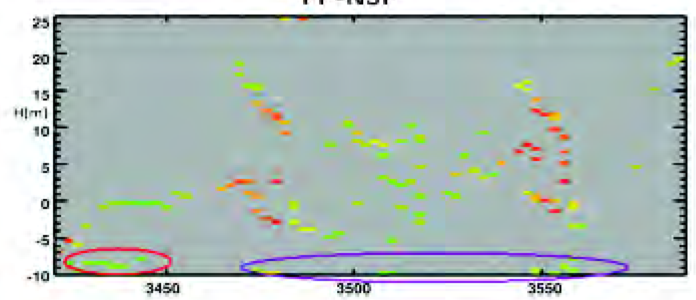

FP Reflectivity tomograms

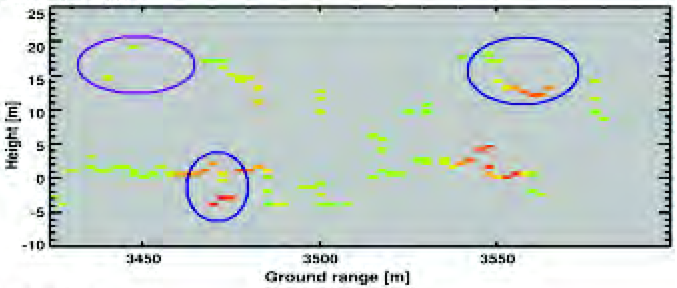

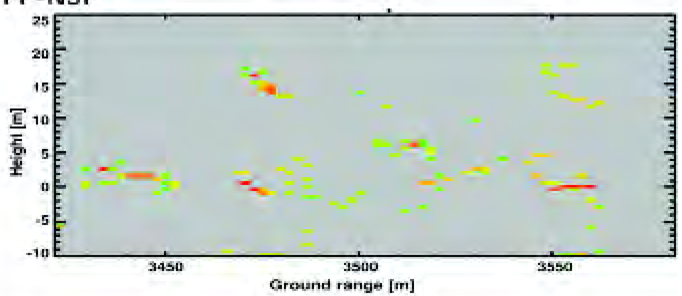

FP-NSF α tomogram

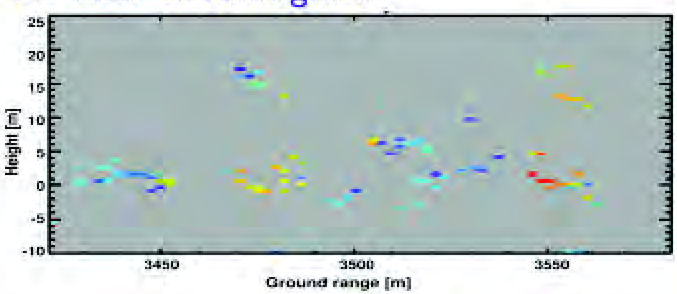

- FP-MUSIC: less sidelobes than SP case
- FP-NSF: better characterization

Polarimetric SAR tomography over urban areas

Surface elevation map

LiDAR

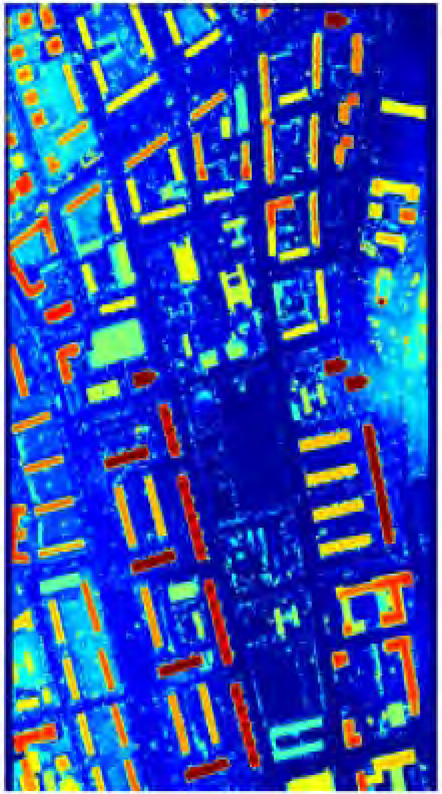

Estimated by FP-NSF ($N_s = 2$)

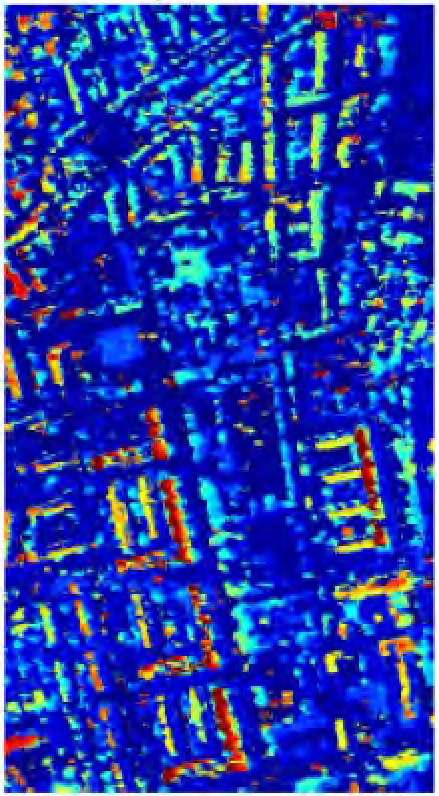

Polarimetric SAR tomography over urban areas

Building reconstruction

Google map

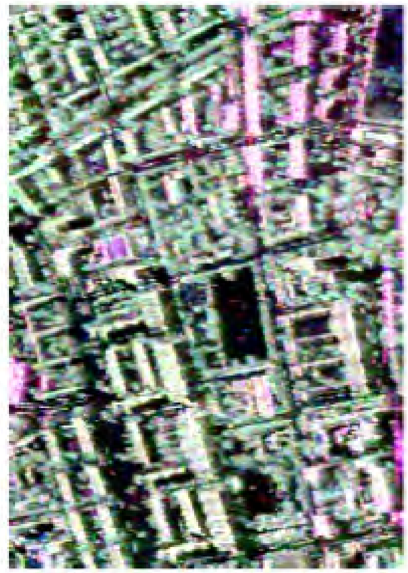

Pauli-coded

LiDAR

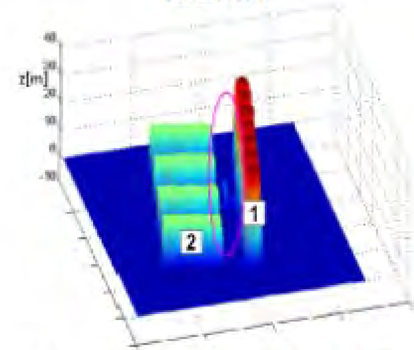

Estimated by FP-NSF
($N_s = 2$)

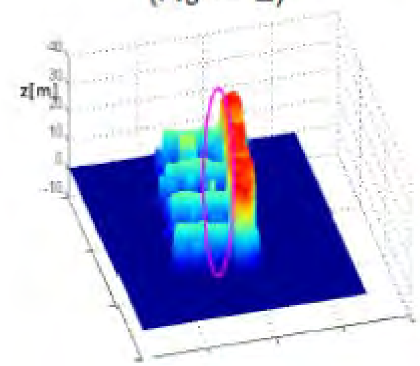

Difference between LiDAR and estimated surface

- projection of SAR imaging
- vegetation between B1 and B2

Building reconstruction


Google map


Bing map

LiDAR

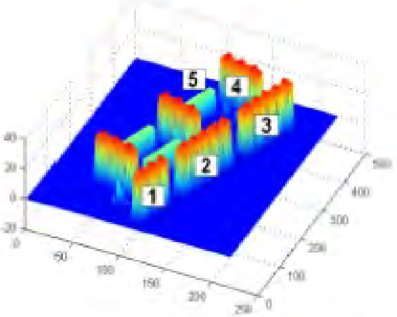

Estimated by FP-NSF
($N_s = 2$)

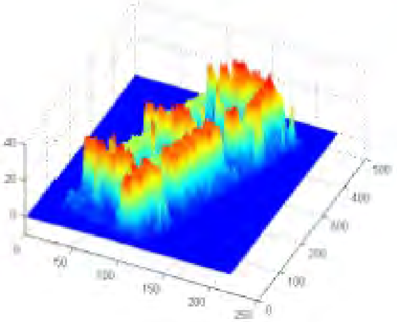

Averaged z[m]	B1	B2	B3	B4	B5
LIDAR	30.0	30.2	30.1	30.8	16.3
Estimated	27.5	27.8	27.5	27.3	16.1

POL-TOMSAR IMAGING OF CONCEALED OBJECTS

Above ground and under foliage objects observed at L band

- DLR E-SAR image over Dornstetten, Germany
- L-Band
- 21 tracks : average baseline 20m
- $\delta_z = 2\mathrm{m}$

Horizontal baseline distribution

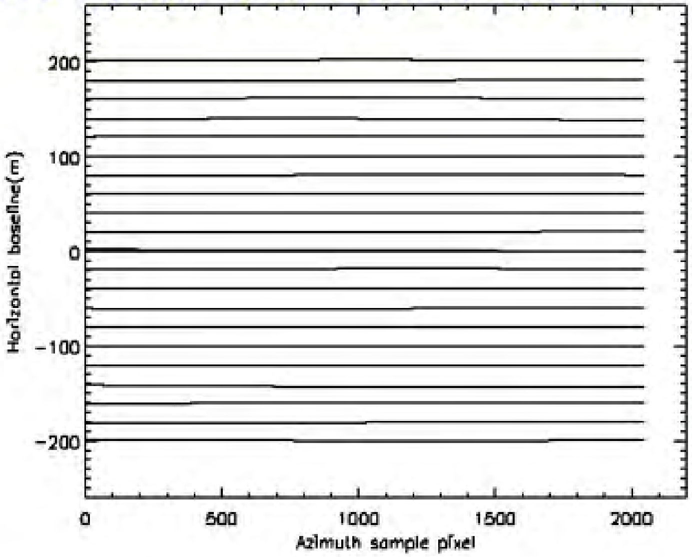

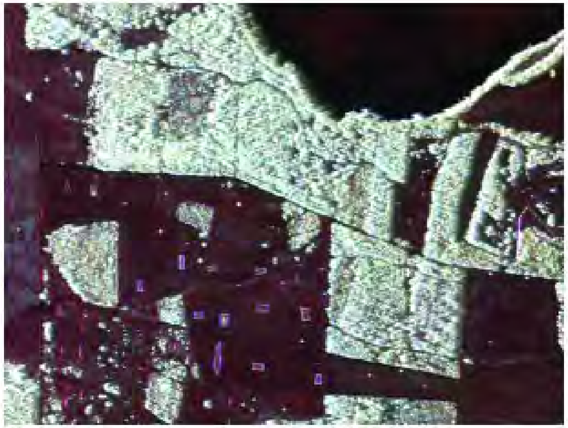

Huang, Y.; Ferro-Famil, L. & Reigber, A. "Under-Foliage Object Imaging Using SAR Tomography and Polarimetric Spectral Estimators", IEEE TGRS 2011

POL-TOMSAR IMAGING OF CONCEALED OBJECTS

VV refectivity tomograms

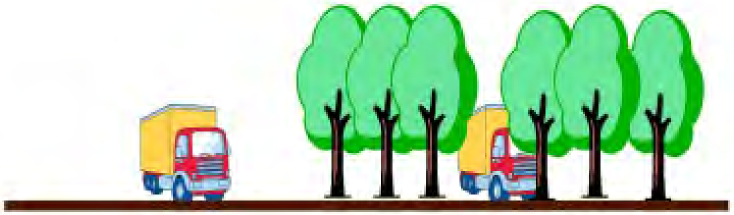

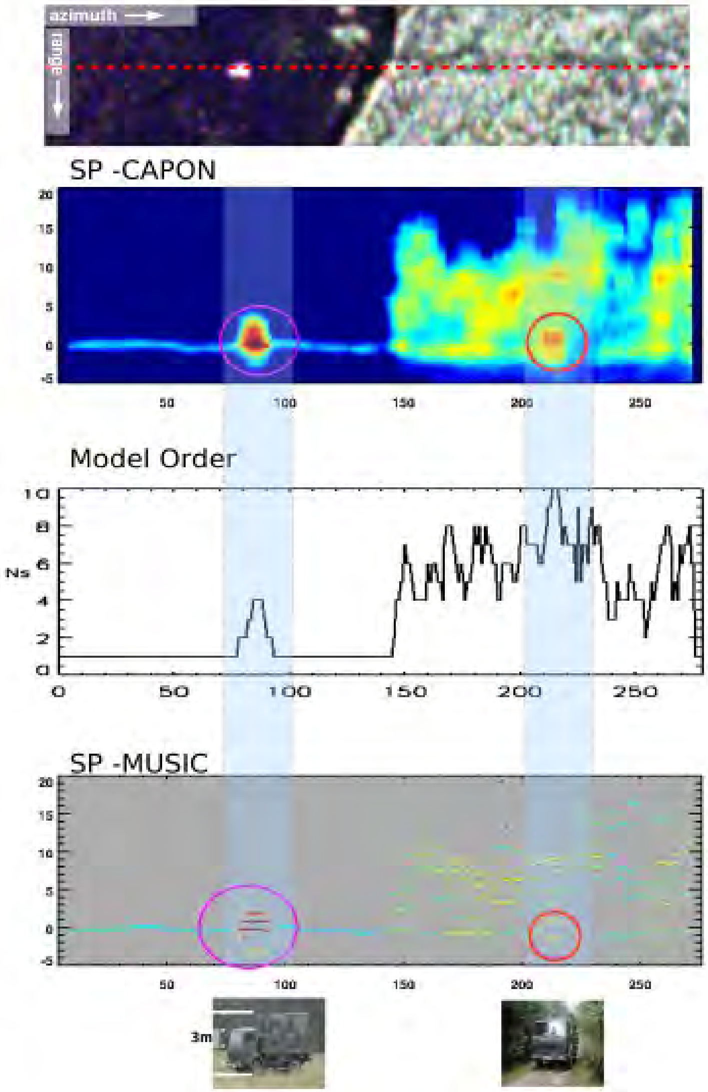

Capon :

limited resolution

$\Rightarrow$ overestimated H_{truck}

MUSIC :

- ☺ Sub-canopy truck
  $\Rightarrow$ hybrid scatterer
- ☹ Uncovered
  $\Rightarrow$ coherent scatterer
- ☹ Spurious sidelobes.

Power spectrum of a mixed environment

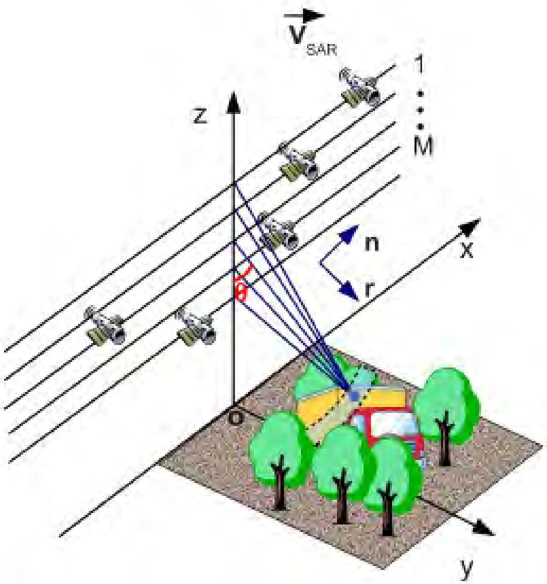

- H-distributed scatterers : Continuous Spectrum
  Forest canopy :

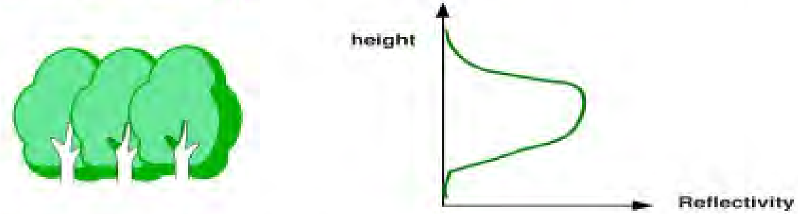

- H-localized scatterers : Discrete Spectrum
  Objects :

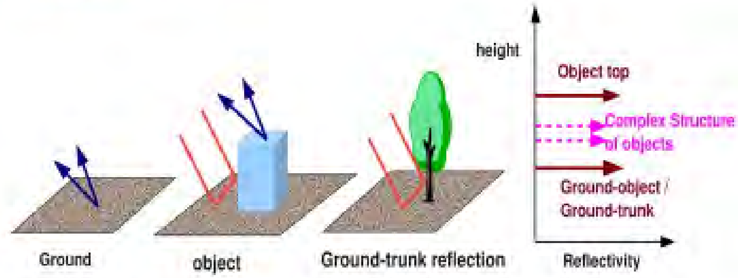

- Underfoliage objects : Mixed-Spectrum

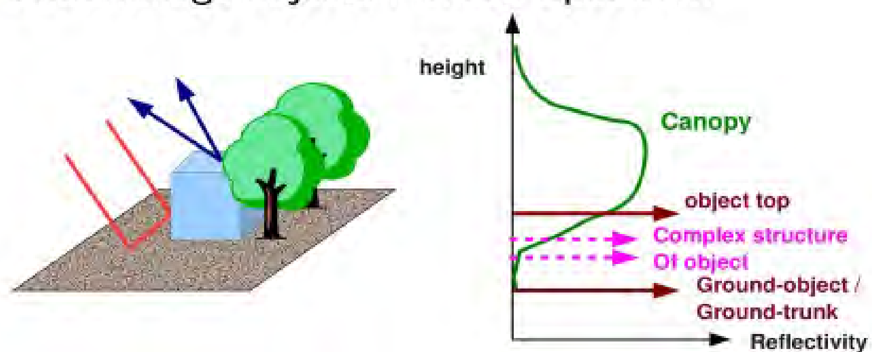

Isolated Scatterer Extraction

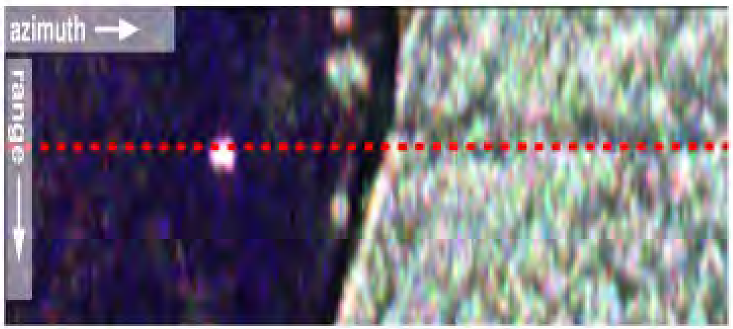

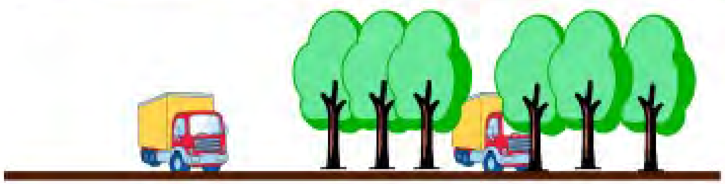

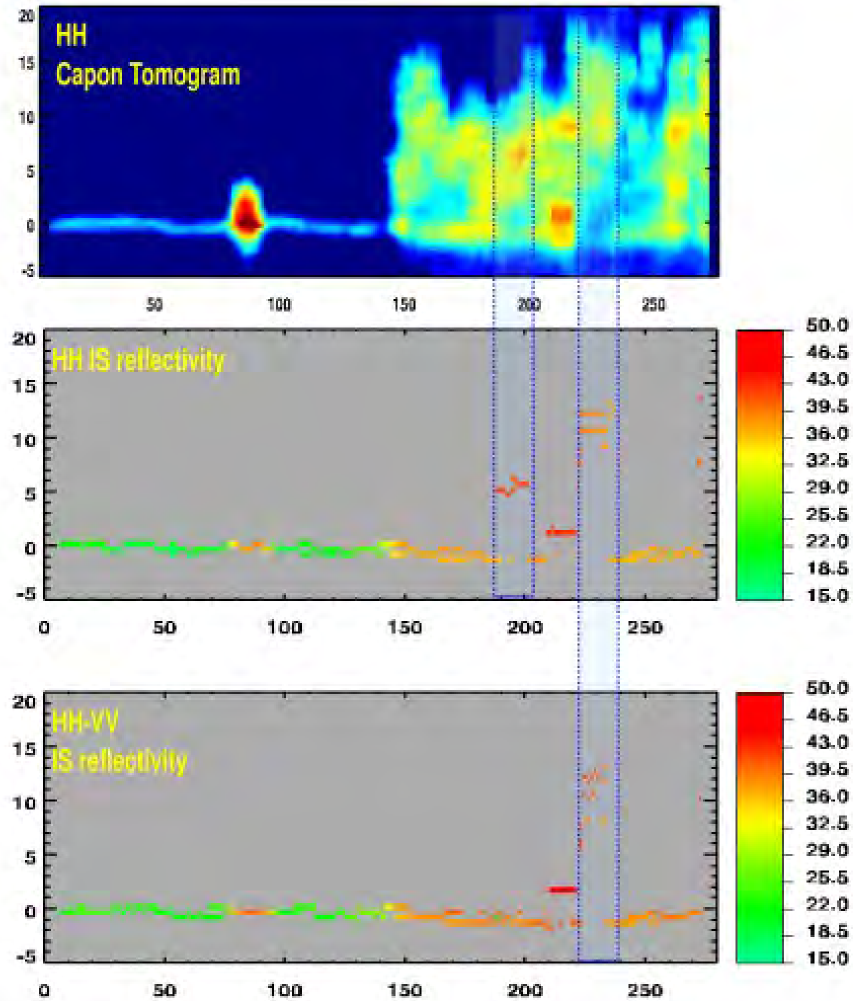

Overestimated number of IS

Overestimated IS

- Bare soil, sub-canonpy ground
- Under-foliage truck

Compressive sensing solution

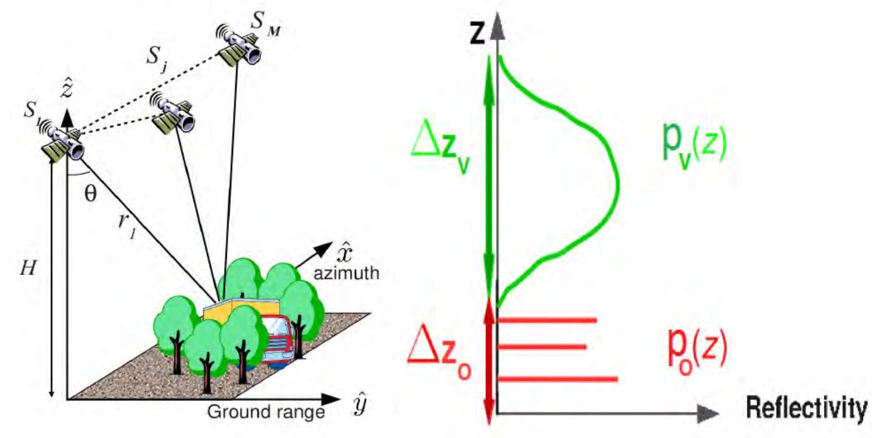

- a few wavelet components
- a few discrete contributions

$$\boxed{\min_{\mathbf{p}} ||\mathbf{B}\mathbf{p}||_1 \text{ subject to } \quad ||\mathbf{R} - \widehat{\mathbf{R}}||_F \leq \epsilon}$$

$$\mathbf{B} = \begin{bmatrix} \mathbf{I}_{(N_o \times N_o)} & \mathbf{0} \\ \mathbf{0} & \boldsymbol{\Psi}_{(N_v \times N_v)} \end{bmatrix} \in \mathbb{R}^{(N_s \times N_s)} \qquad \mathbf{p} = [\mathbf{p}_o^T \quad \mathbf{p}_v^T]^T \in \mathbb{R}^{+N_s \times 1}$$

POL-TOMSAR IMAGING OF CONCEALED OBJECTS

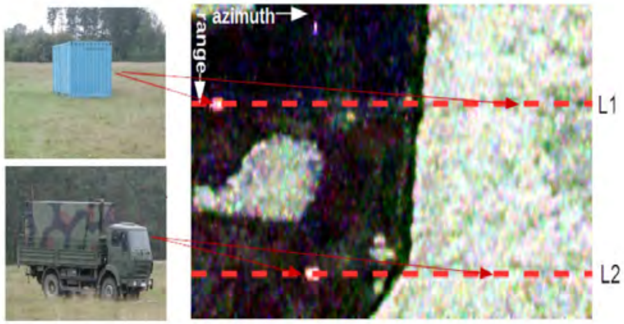

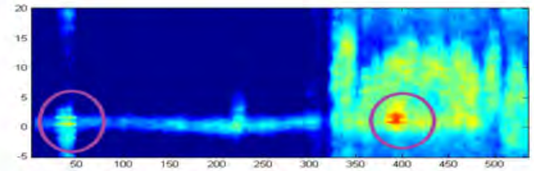

(a) Capon

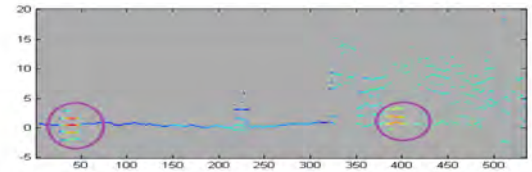

(b) MUSIC

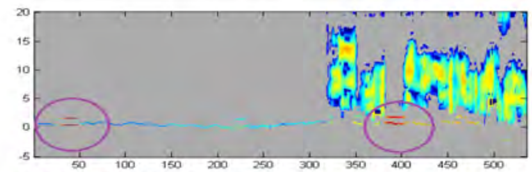

(c) Proposed method with merging

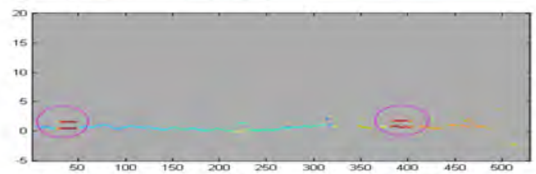

(d) Ground and underfoliage scattering ($\mathbf{p}_o$) estimated by proposed method with merging

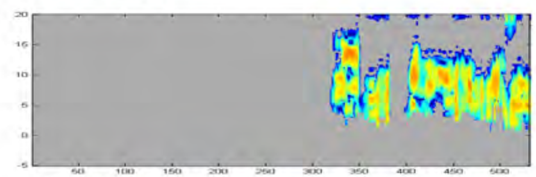

(e) Canopy power ($\mathbf{p}_v$) estimated by proposed method with merging

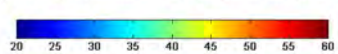

(f) dB

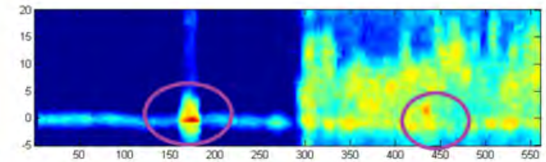

(a) Capon

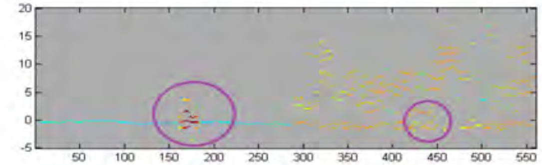

(b) MUSIC

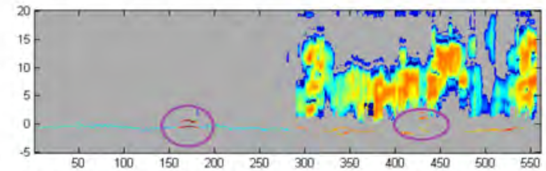

(c) Proposed method with merging

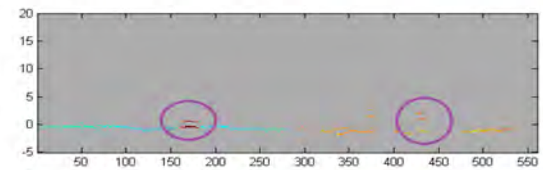

(d) Ground and underfoliage scattering ($\mathbf{p}_o$) estimated by proposed method with merging

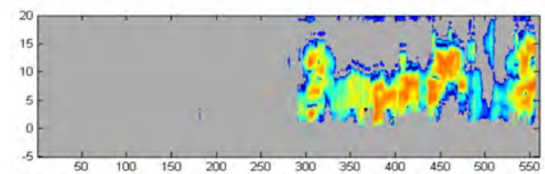

(e) Canopy power ($\mathbf{p}_v$) estimated by proposed method with merging

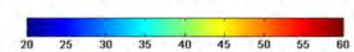

(f) dB

Tropical forest characterization

Tropical forest test site and objectives

- TropiSAR Campaign, 2009
- ONERA SETHI
- P-Band
- 6 tracks
- $\delta_{az} = 1.245m$
  $\delta_{rg} = 1m$
- $\delta_z = 12.5m$
- Ground truth
  - LiDAR data
  - Biomass measurements for 16 ROIs

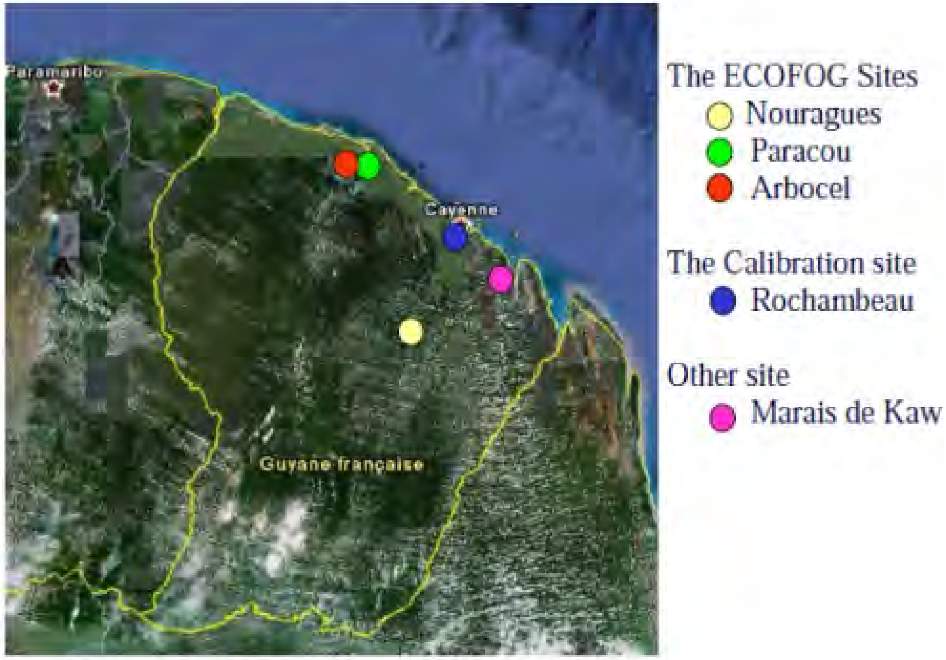

Courtesy ONERA

Objectives

- Tree height,underlying ground topography estimation
- Forest vertical structure characterization
- Biomass monitoring

Tropical forest characterization

Tropical forest test site : Paracou

Optical image | SAR image | LiDAR z_g | LiDAR z_{top}

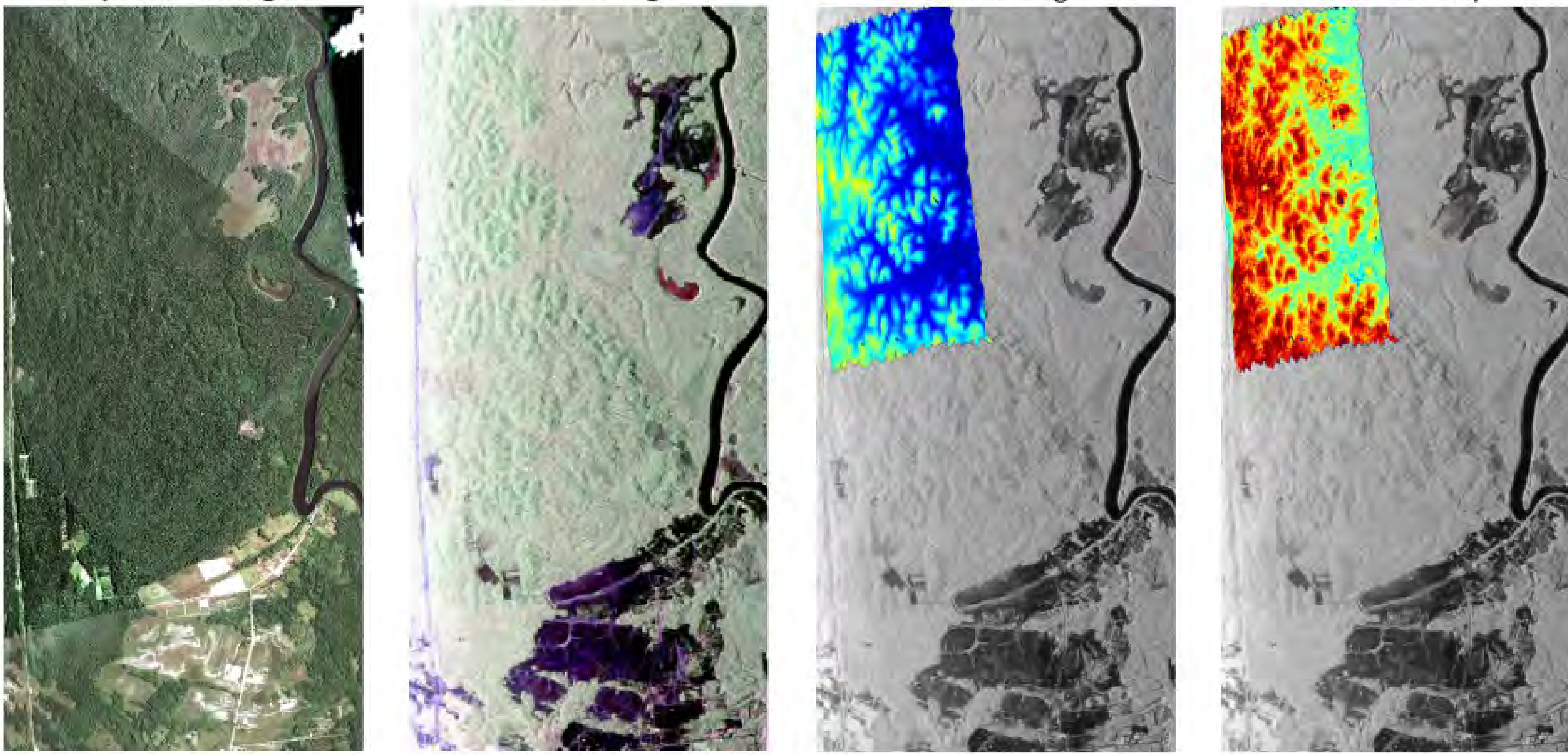

- Tropical forest environments
(savannah, undisturbed forests, logged plots...)

- Highly varying ground topography

Tropical forest characterization

Tree height and ground topography estimation

Hybrid spectral approach

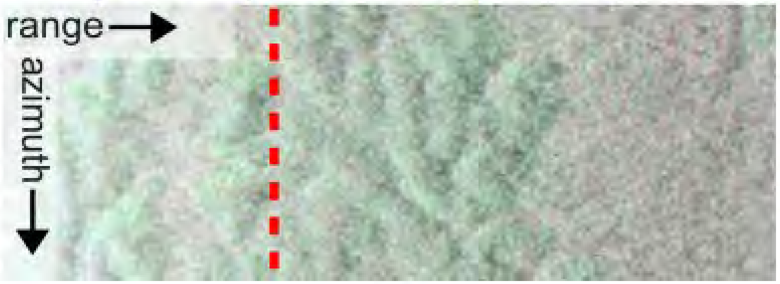

- Estimated profiles match LiDAR
- HH profiles : similar to FP case

LiDAR TomSAR

HH

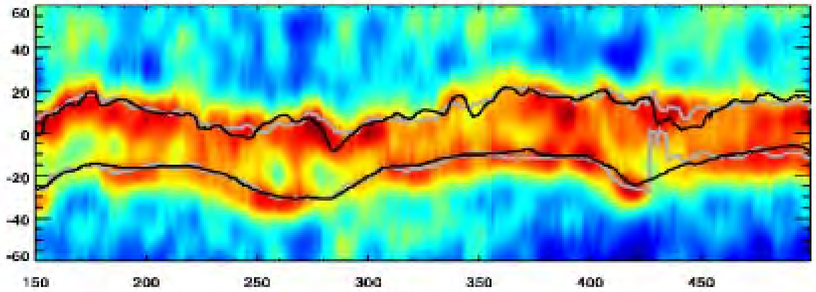

VV

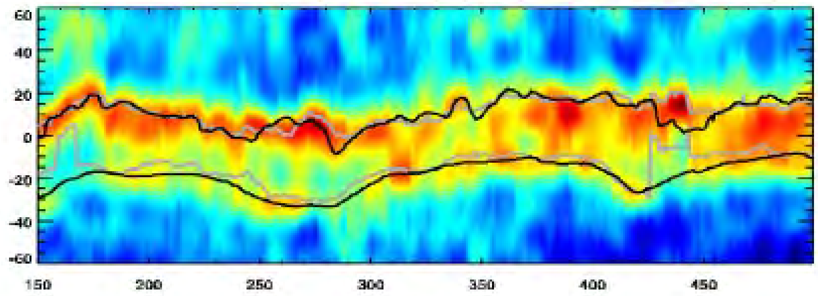

HV

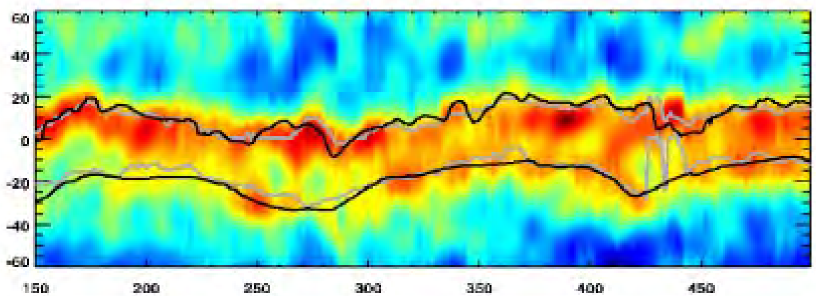

FP

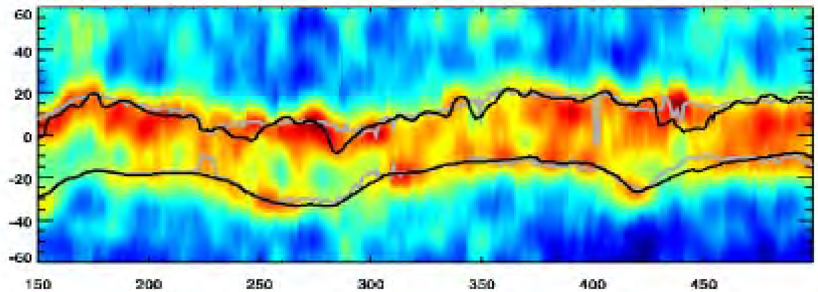

Tropical forest characterization

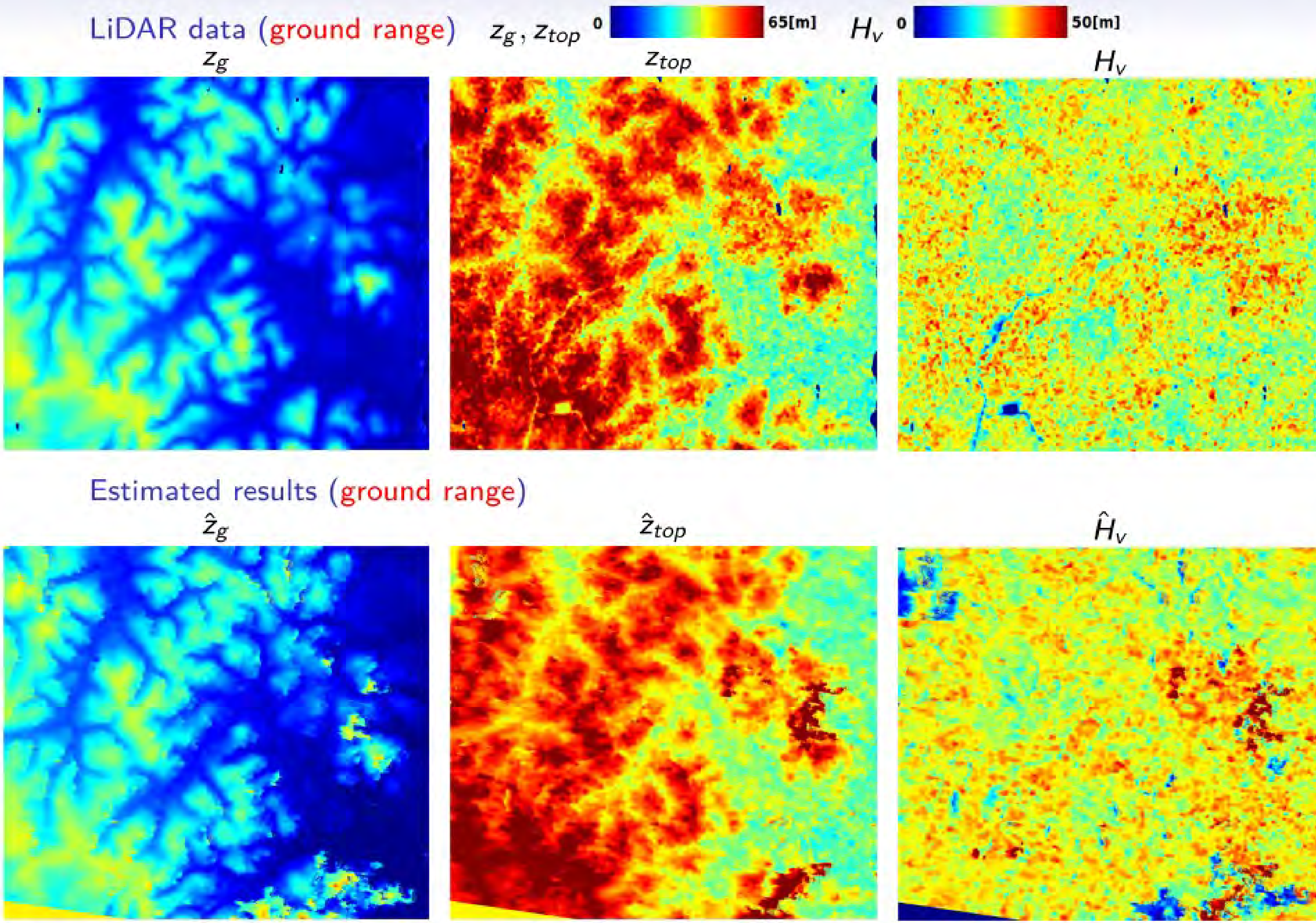

Tropical forest characterization

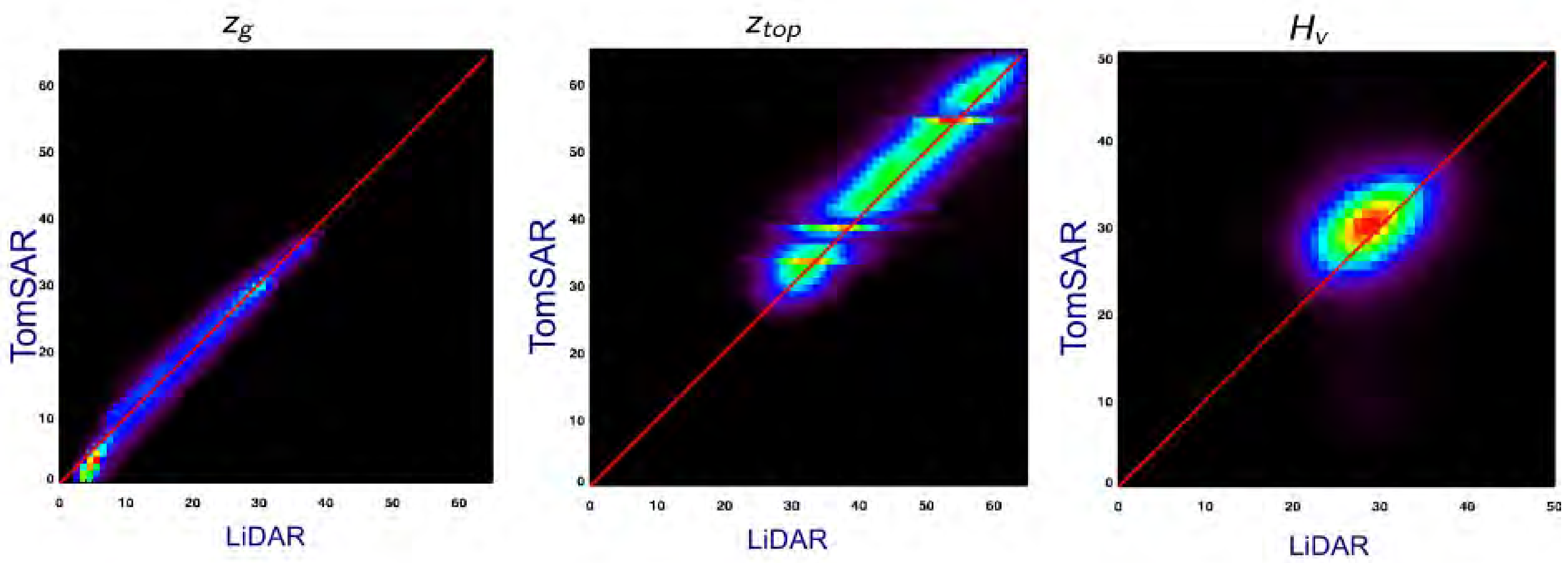

TomSAR-LiDAR [m]	Mean	Std
Δz_g	0.005	4.6
Δz_{top}	1.6	7.4
ΔH_v	0.9	7.7

Tropical forest biomass estimation

Ground/Volume separation:

PolTomSAR data → (A posteriori phase calibration) → Pol/Space covariance matrix → (SKP2 decomposition) → Ground Pol/Space covariance matrices; Volume Pol/Space covariance matrices

Ground/tree top heights estimation:

Ground spatial covariance matrix → (Tomography)

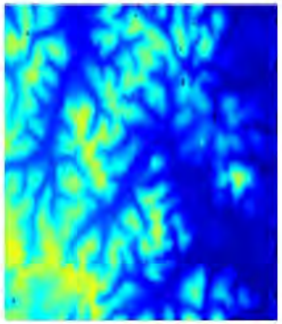

Volume spatial covariance matrix → (Tomography)

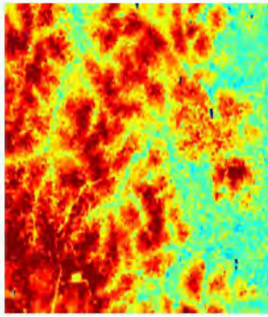

Biomass estimation:

Volume SKP2 solution → (Tomographic focusing)

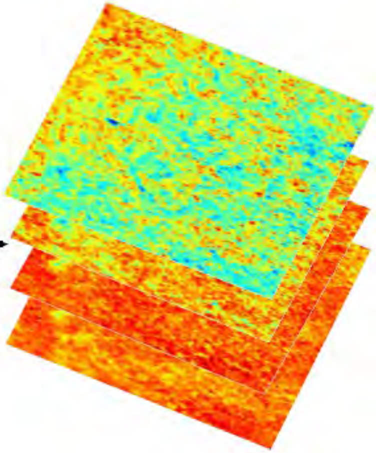

→ (Slices/canopy height Adaptation)

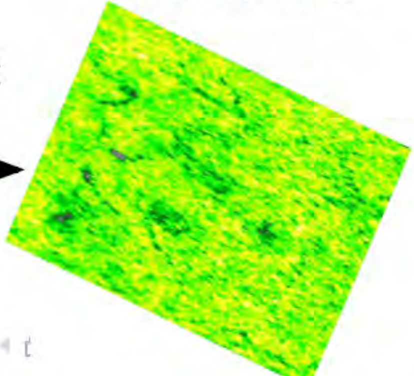

Tropical forest biomass estimation

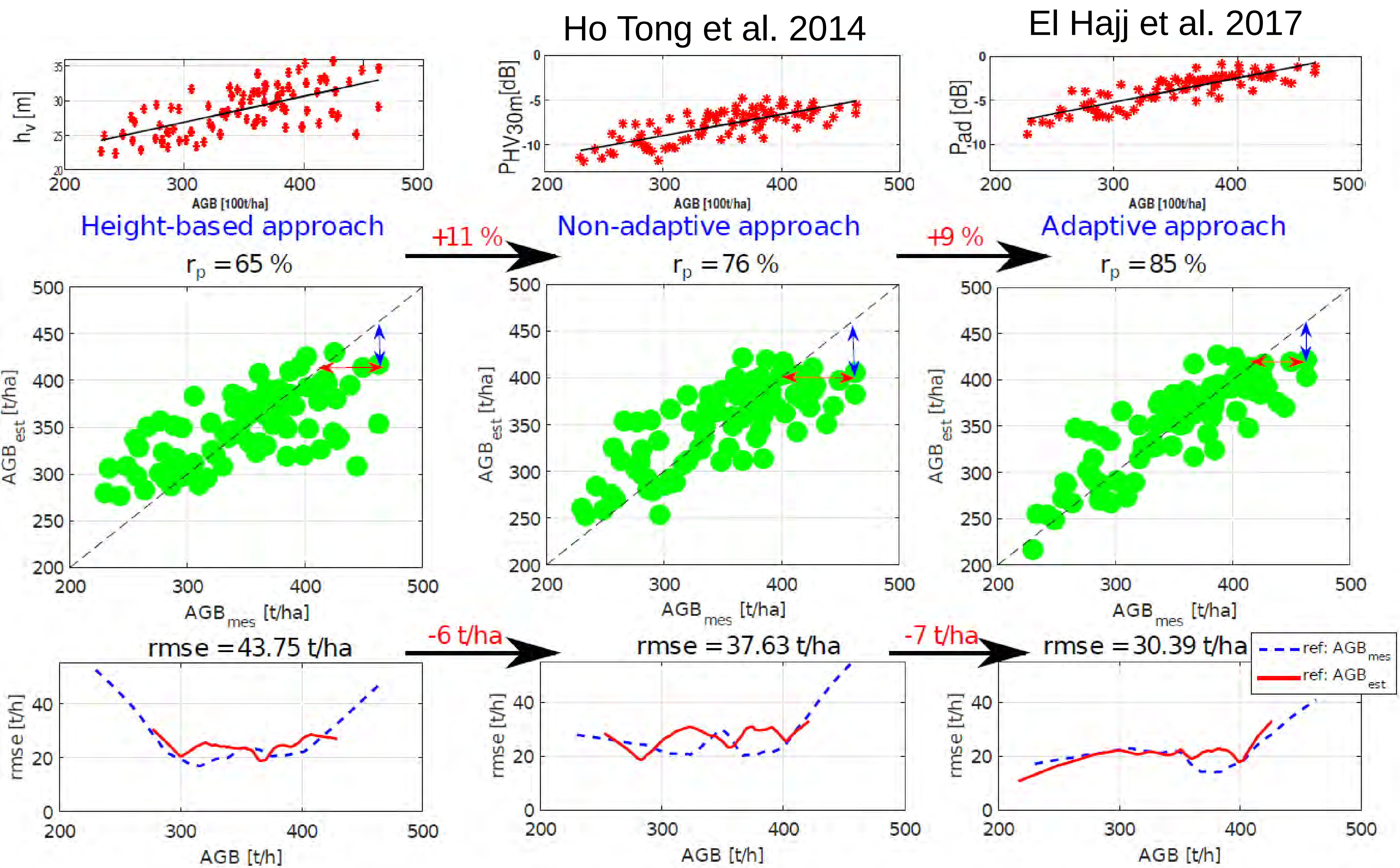

Some objecives of PolTomoSAR remote sensing

SAR remote sensing: important asset for environmental monitoring

- Coverage, resolution, penetration, robustness
- EM properties ↔ physical features
- Towards systematic and highly frequent space observations at low cost
  → model-based approaches, assimilation, big data ...

EM scattering from dense (snow, ice) multi-component (forest) media: may be complex

- Exaggeratedly numerous physical parameters vs. simplistic description
- Arbitrary level of computing complexity, simplifying assumptions
- Some parameters cannot be measured at a sufficient scale
- → EM “radar ground truth” needed

Direct characterization of complex EM responses

→ SAR Tomography (TomoSAR): High-Res 3D imaging
→ SAR Polarimetry (PolSAR): dielectric, structure (roughness, volume) properties
→ enhanced component separation

Ground Based-SAR, airborne campaigns

→ VHR (cm up to m) local properties, EM “ground truth”
→ **preparation of spaceborne missions**.

Ground Based SAR

Measurements by a Ground based Synthetic Aperture Radar system,
developed and implemented by the SAPHIR team at the University of Rennes 1

- Signal Tx and Rx controlled by a VNA
- Available frequency bands: 3 GHz to 35 Ghz (C,X,Ku bands)
- Dynamic range ≈ 90 dB
- Sealed in a metallic box when operating works under a snow fall
- Box + VNA = 40 Kg

Ground Based SAR

○ 2D synthetic antenna by collecting parallel passes → 3D imaging (TomSAR)

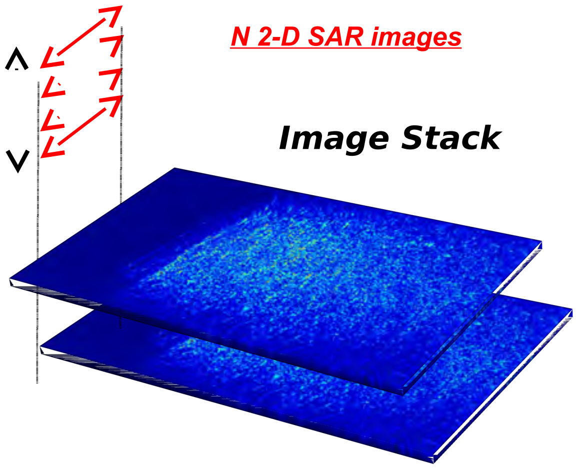

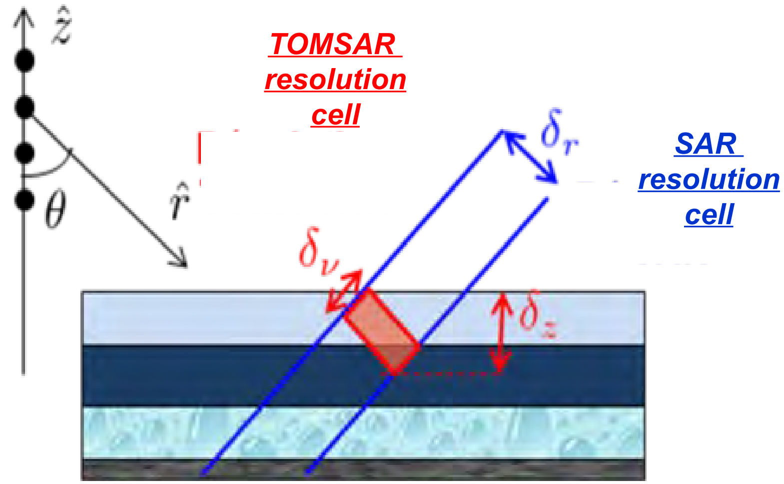

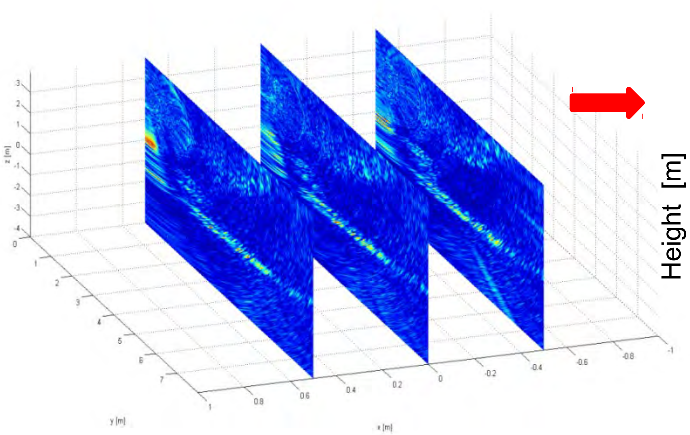

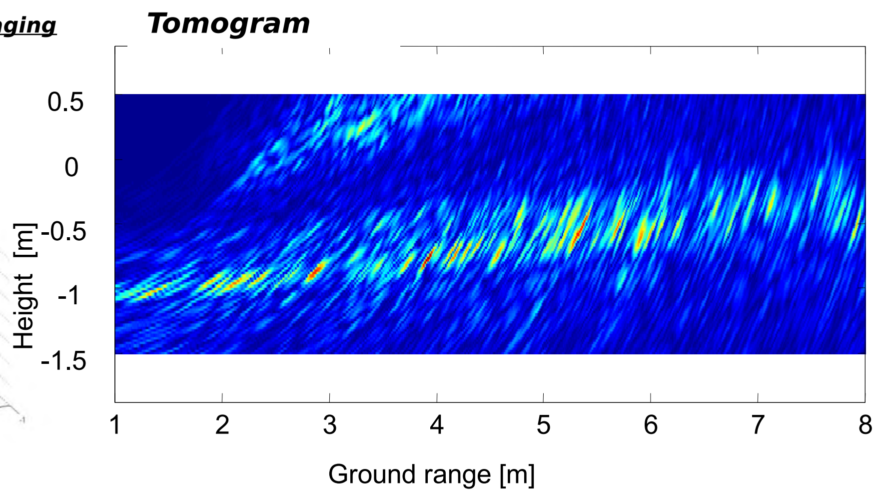

The IETR GBSAR system allows to obtain multiple parallel passes in three ways:

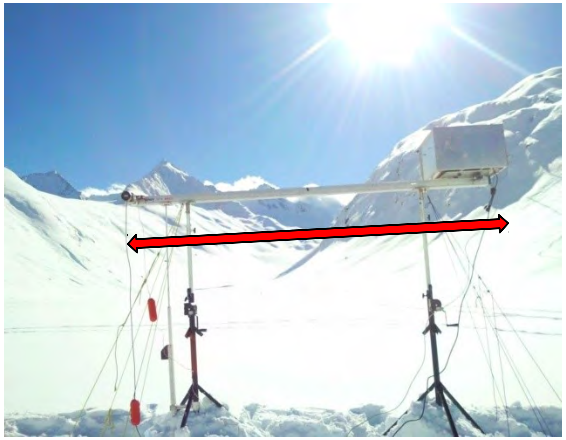

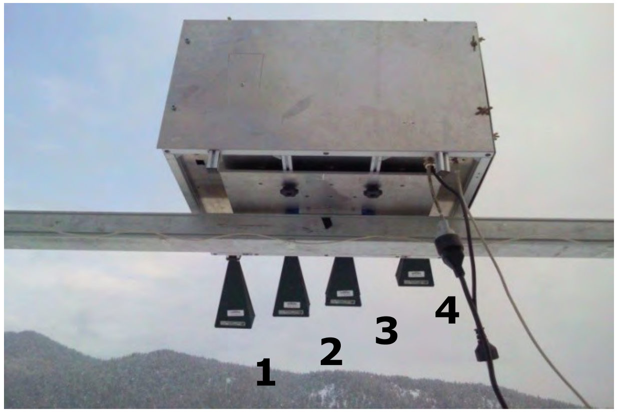

6 equivalent tracks

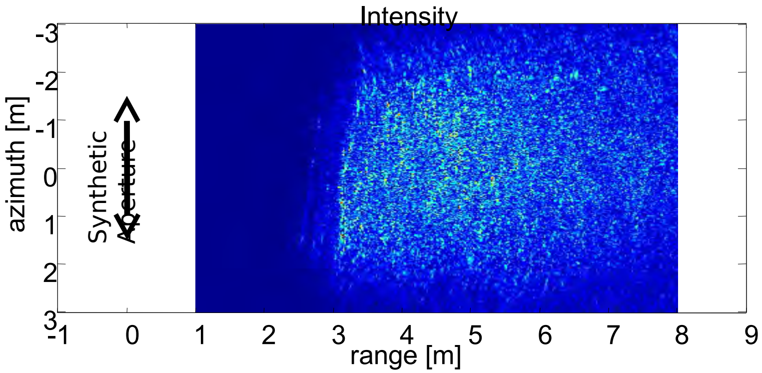

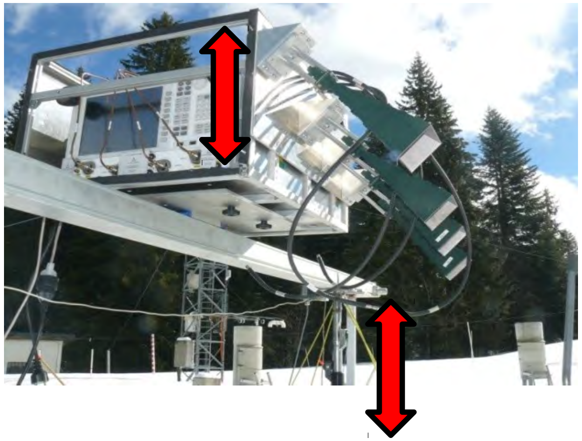

Additional tracks

Snowpit data:
- snowpack depth 1.4m
- horizontal layers

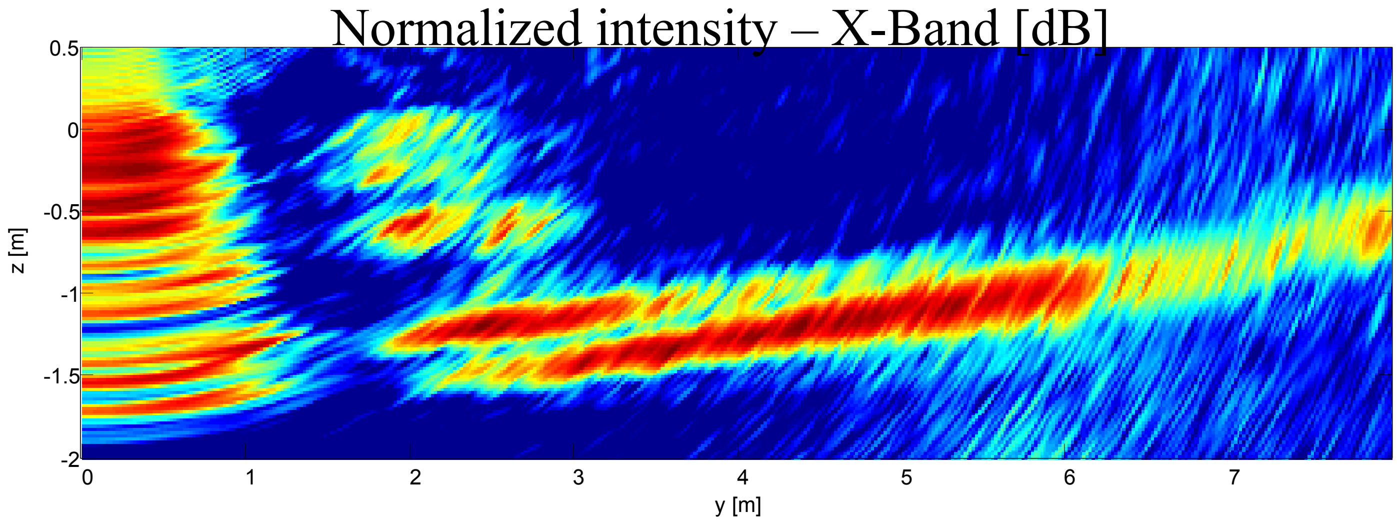

Dense dielectric medium

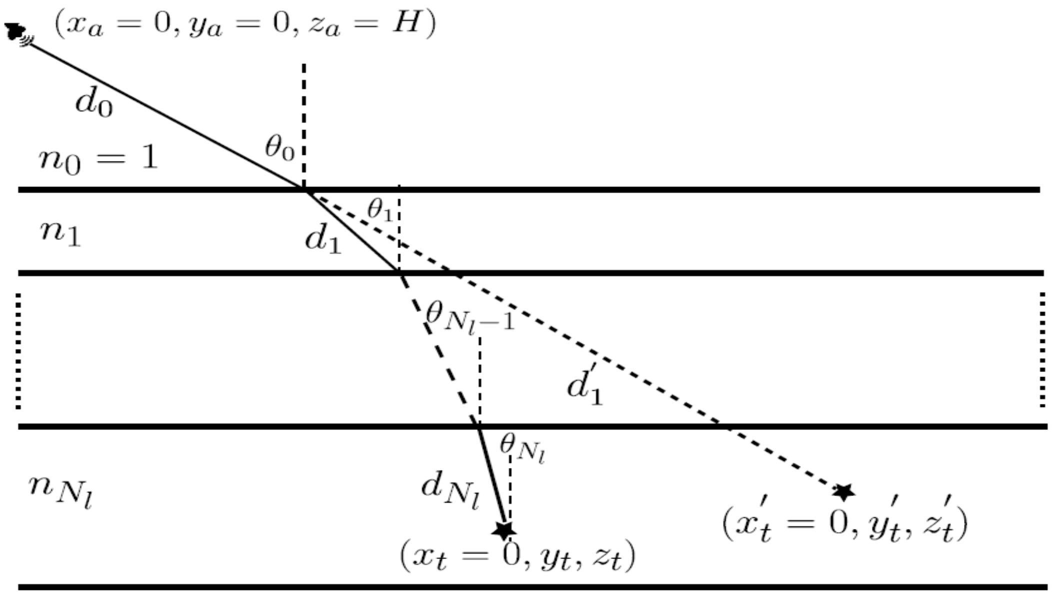

Refractive index estimation

Iterative procedure for estimation of refractive indices (hyp. horizontal layers):

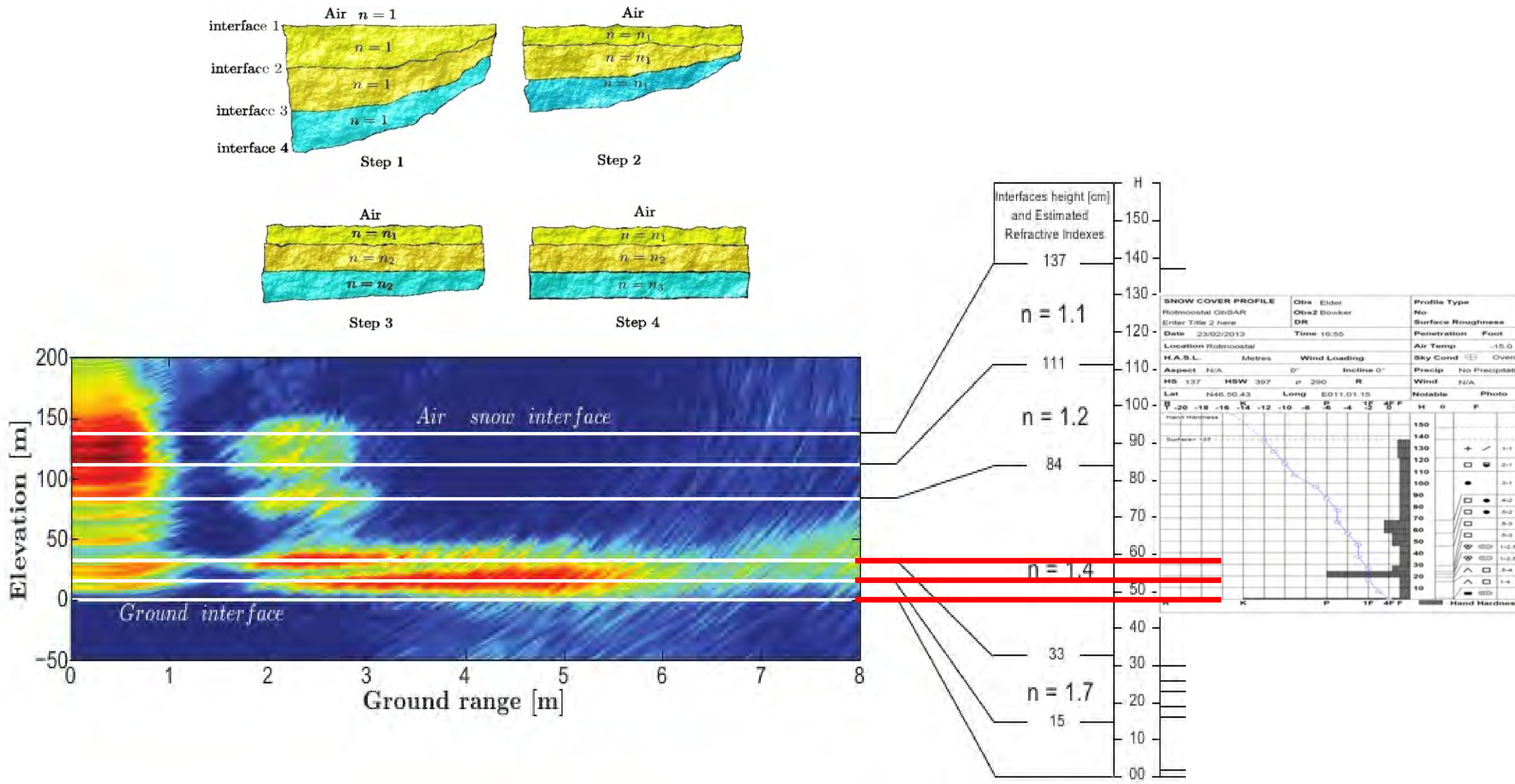

- Distance computation : numerical resolution of the Eikonal Equation

$$\left\|\vec{\nabla} d(\vec{r}, \vec{r_a})\right\|^2 = n^2(\vec{r})$$

- Usual scattering models may overestimate volume contribution

- Key geophysical factor: snow hardness

SAR Tomography over fjord ice

Data acquisition carried out in March 2013 at the Kattfjord, Tromsø, Norway

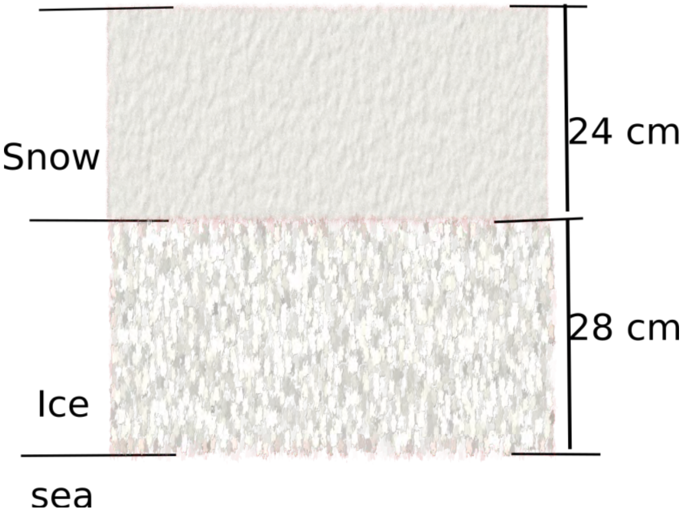

- Seasonal ice – life of 3-4 months
- Tomographic X-band measurements at VV and HV
- Temperature from -8° to -2°
- The fjord ice: low salinity sea ice
- Dry snow cover on top
- Significant amount air bubbles within the ice layer
  - 0.5 mm to 7 mm diameter
  - Irregularly shaped
  - Randomly oriented

SAR Tomography over fjord ice

- Same tilt effect as snow-pack tomography
- Corrected assuming
  - refractive index of snow = 1.4
  - refractive index of fjord ice = 1.7
- Normalized intensity is presented to highlight contrasts (interfaces)

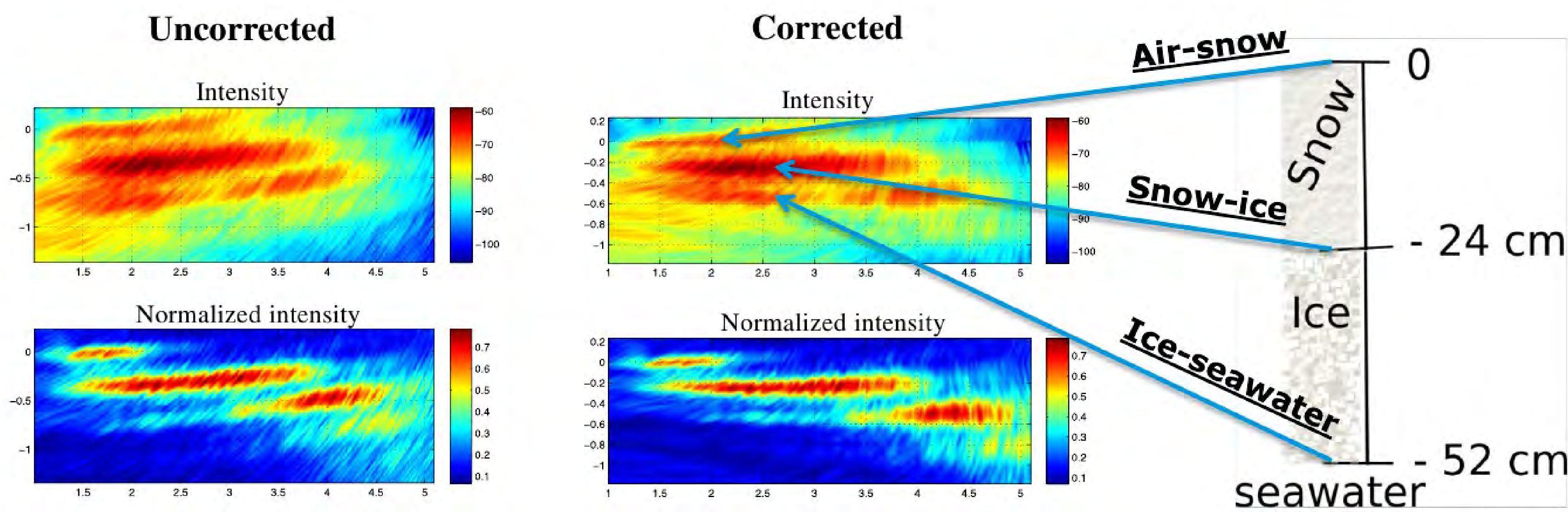

- Three clearly visible interfaces
  - Air/snow
  - Snow/ice
  - Ice/seawater

SAR Tomography over fjord ice

- VV & HV tomography

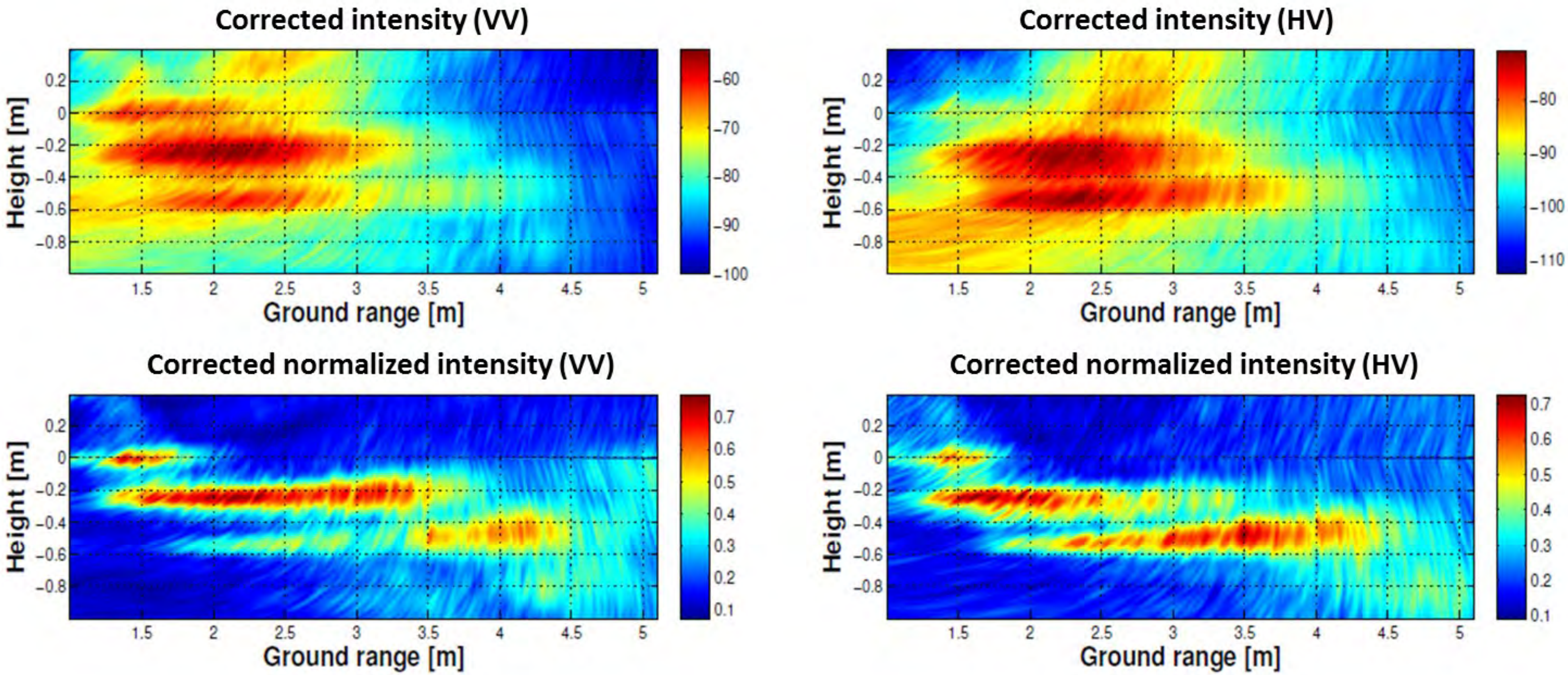

- Weaker air/snow and stronger snow/ice and ice/seawater scattering at HV than at VV

⇒Mostly polarized contributions from regular spherical snow grains
⇒Depolarized contributions from irregular air bubbles in the ice layer

3-D imaging of a dry glacier

***Test site*:** Mittelbergferner, Austrian Alps

- temperate glacier at the main ridge of the Alps in Tyrol
- main test area is a flat plateau in the upper part of the glacier between 3000 and 3200 m

3D Focusing

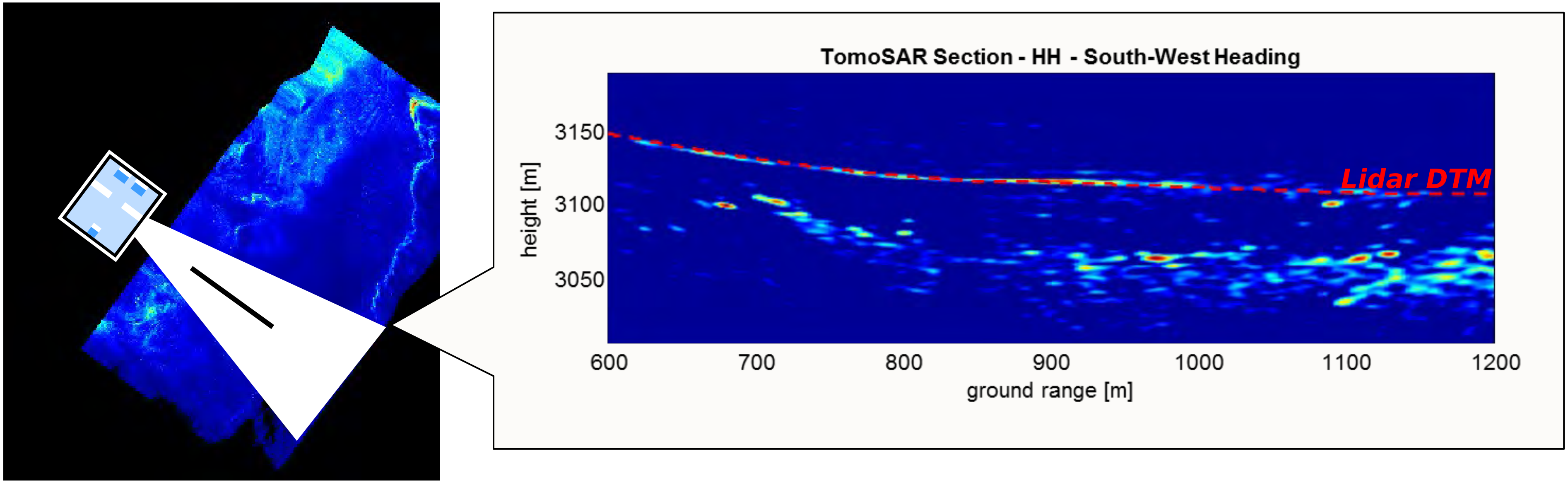
TomoSAR Section - HH - South-West Heading
height [m]
3150
3100
3050
600
700
800
900
1000
1100
1200
ground range [m]
Lidar DTM

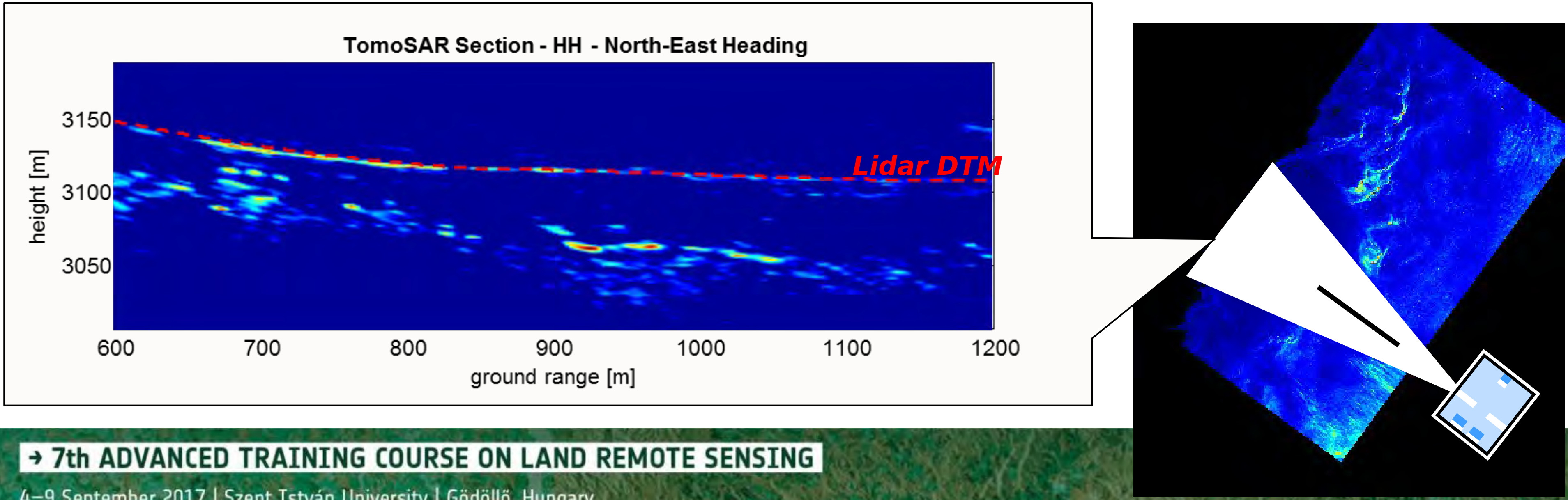
TomoSAR Section - HH - North-East Heading
height [m]
3150
3100
3050
600
700
800
900
1000
1100
1200
ground range [m]
Lidar DTM

3D Focusing

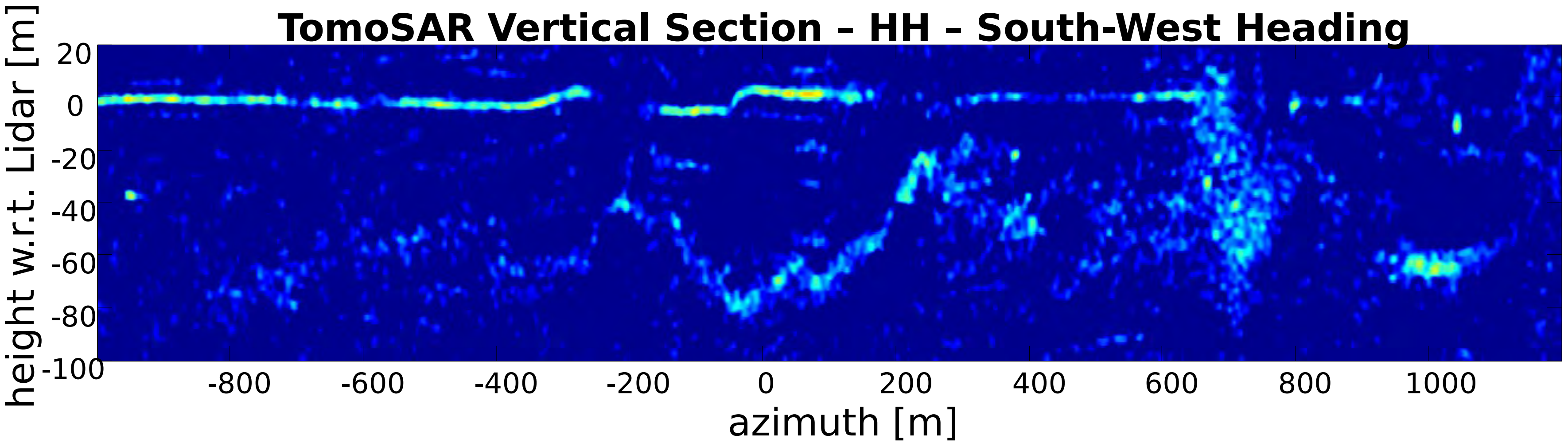
TomoSAR Vertical Section – HH – South-West Heading
height w.r.t. Lidar [m]
20
0
-20
-40
-60
-80
-100
-800
-600
-400
-200
0
200
400
600
800
1000
azimuth [m]

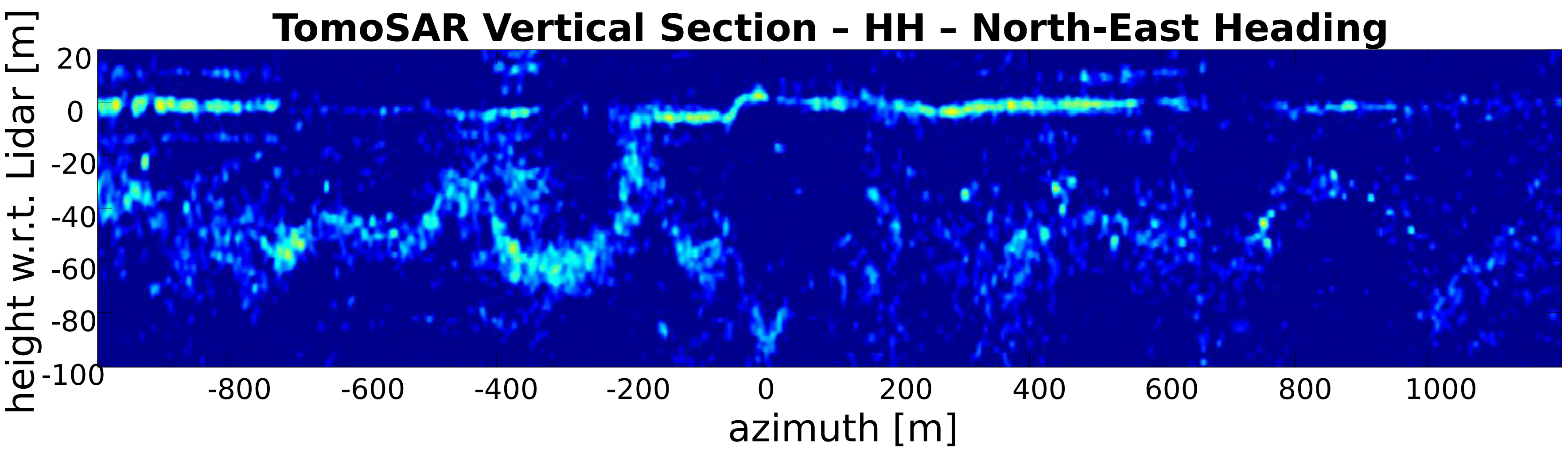
TomoSAR Vertical Section – HH – North-East Heading
height w.r.t. Lidar [m]
20
0
-20
-40
-60
-80
-100
-800
-600
-400
-200
0
200
400
600
800
1000
azimuth [m]

Comparison to 200 MHz GPR Transects

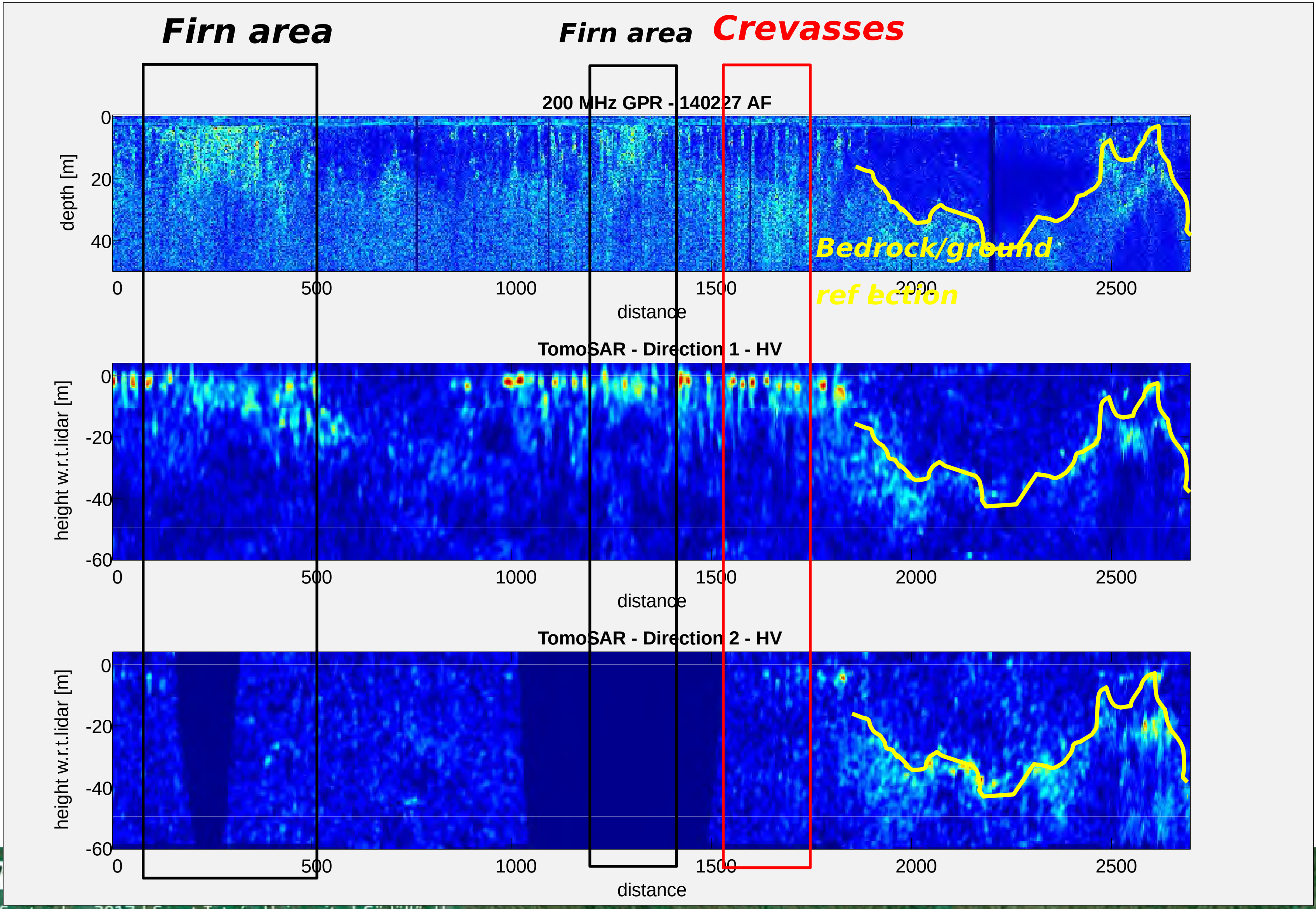

3D Polarimetry

(normalized) HH - red
(normalized) HV – green
(normalized) VV - blue

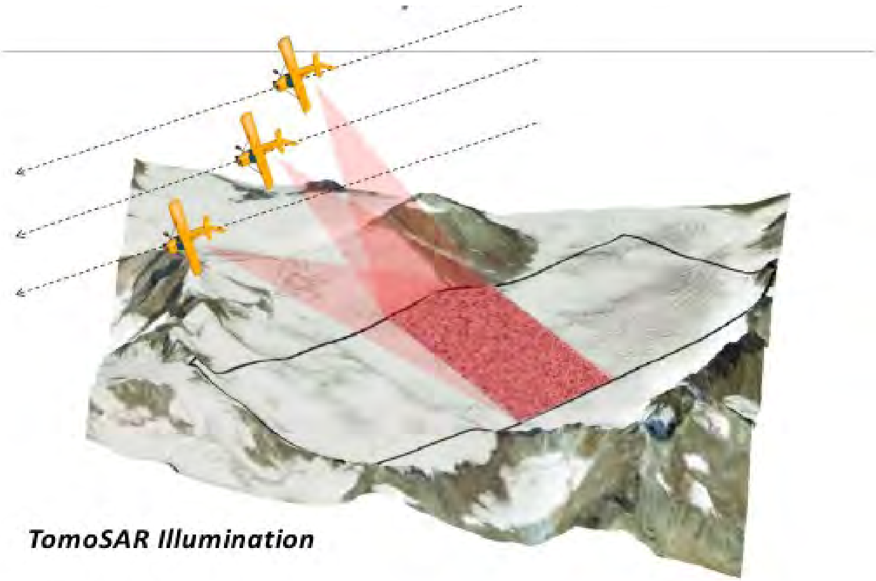

TomoSAR Illumination

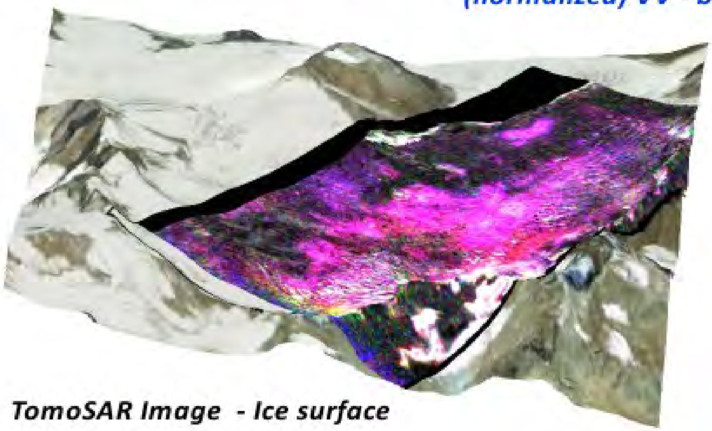

TomoSAR Image - Ice surface

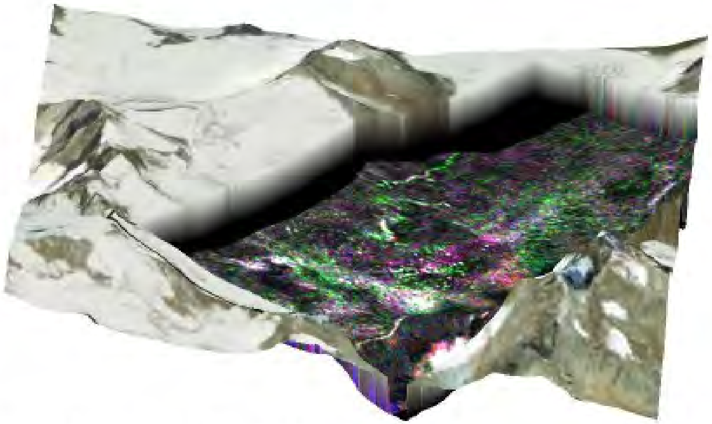

TomoSAR Image - 25 m below the Ice surface

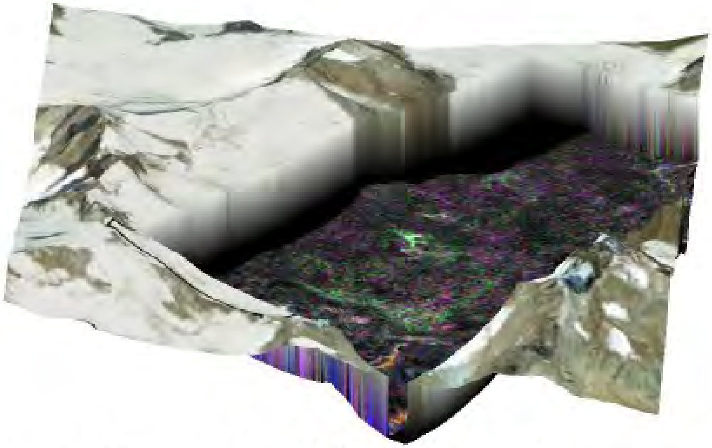

TomoSAR Image - 50 m below the Ice surface

Towards <u>spaceborne</u> SAR tomography

Coherent vs Incoherent TomoSAR

Current paradigm for forested areas: **retrieve the *vertical distribution of backscattered power* based on the observed *InSAR coherences***

SLC data

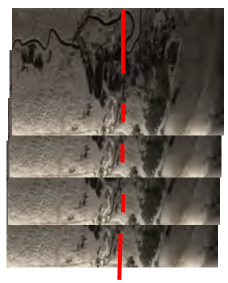

Complex data vector (Nx1)

$$\mathbf{d} = \begin{bmatrix} d_1 \\ d_2 \\ \vdots \\ d_N \end{bmatrix}$$

Coherence matrix (NxN)

$$\mathbf{R} = \begin{bmatrix} 1 & \gamma_{12} & \cdots & \gamma_{1N} \\ \gamma_{21} & 1 & & \\ \vdots & & \ddots & \vdots \\ \gamma_{N1} & & \cdots & 1 \end{bmatrix}$$

TomoSAR processing

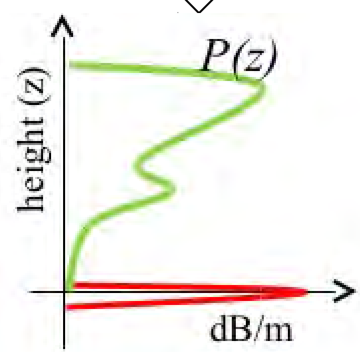

Remarks:

- **R is (semi-)positive definite => *P*(z) ≥ 0 physically consistent !**
- Equivalent to coherent focusing if inversion is carried out using linear methods (Fourier)
- **Non-linear methods can be used to achieve super-resolution/ side-lobe rejections**

Coherent vs Incoherent TomoSAR

Spaceborne SARs collect multiple baselines are usually collected by flying multiple passes

⇒The illuminated scene is required to be stable over time

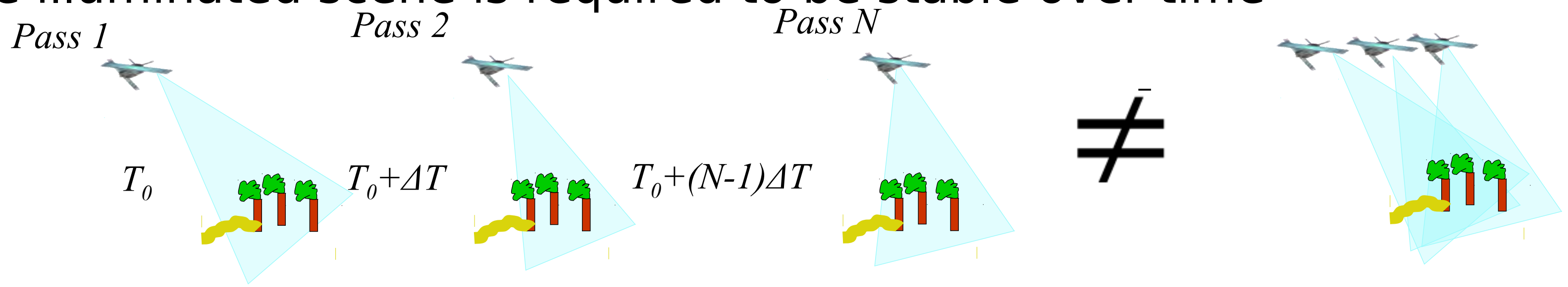

Random motions on the order of a fraction of a wavelength are prohibited !!!

Urban tomography: motion due to subsidence/wind/thermal dilation

⇒ can be accounted for using suitable models

Forest tomography: random motion of scattering element within the vegetation, changing water content, terrain moisture

- P-Band scattering: larger branches, trunks → coherence may be preserved at few days
- L-Band (and higher frequencies) scattering: need for simultaneous acquisitions

Coherent vs Incoherent TomoSAR

Single pass InSAR: a way out of temporal decorrelation

- ***Tandem-L***
- ***SAOCOM-CS***

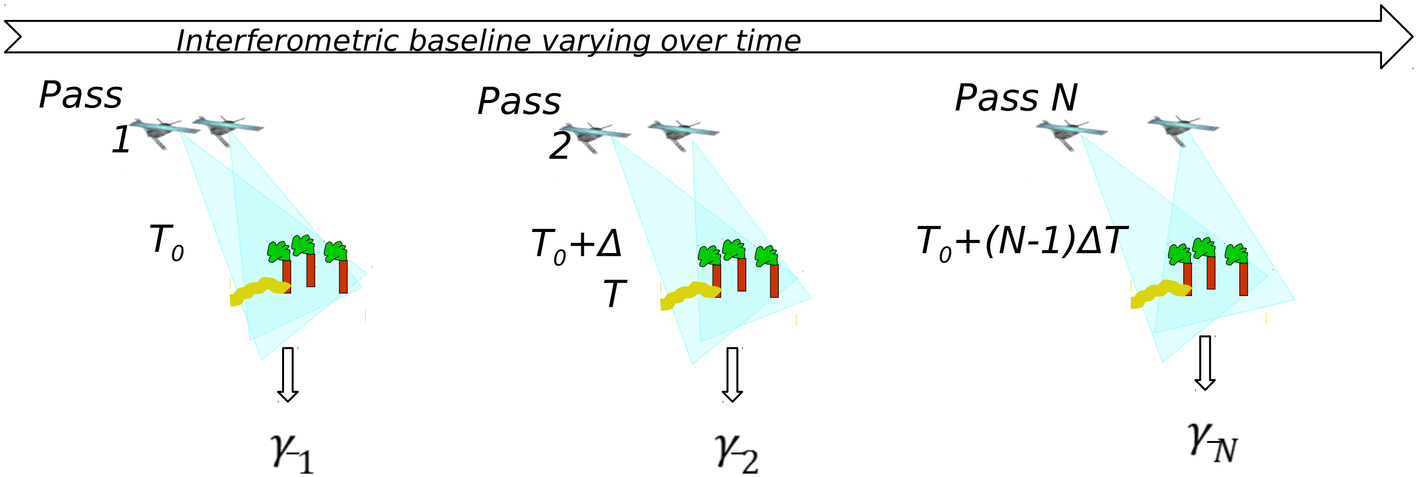

Coherence vector (Nx1)

$$\boldsymbol{\gamma} = \begin{bmatrix} \gamma_1 \\ \gamma_2 \\ \vdots \\ \gamma_N \end{bmatrix}$$

TomoSAR processing

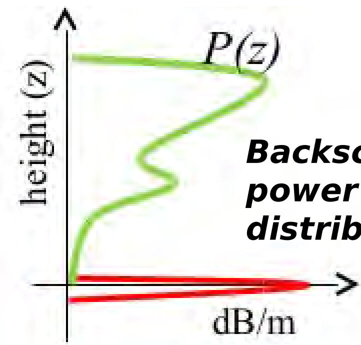

Backscattered power distribution

<u>Incoherent</u> processing

Intrinsically robust to temporal decorrelation, since the images forming each interferometric pair are acquired nearly simultaneously.

Coherent vs Incoherent TomoSAR

Coherent Tomography

$$\mathbf{R} = \begin{bmatrix} 1 & \gamma_{12} & \cdots & \gamma_{1N} \\ \gamma_{21} & 1 & & \\ \vdots & & \ddots & \vdots \\ \gamma_{N1} & & \cdots & 1 \end{bmatrix} \Rightarrow \boxed{\textit{TomoSAR processing}} \Rightarrow$$

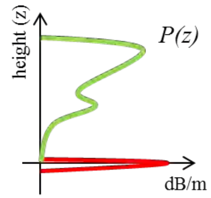

- **R** is (semi-)positive definite => ***P*(z) ≥ 0** → **physically consistent !**
- Equivalent to coherent focusing if inversion is carried out using linear methods (Fourier)
- Assumption: **Frozen Forest = Stable Scatterers**

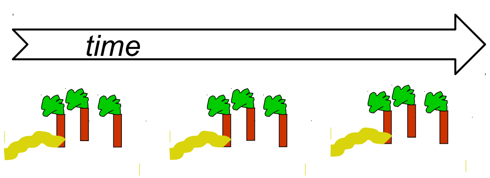

Frozen stationary forest

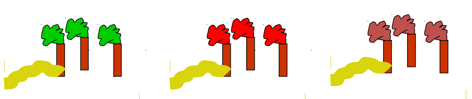

Non-frozen stationary forest
→ Temporal decorrelation

Physical source: motion and EM changes of scattering elements

Incoherent Tomography

$$\boldsymbol{\gamma} = \begin{bmatrix} \gamma_1 \\ \gamma_2 \\ \vdots \\ \gamma_N \end{bmatrix} \Rightarrow \boxed{\textit{TomoSAR processing}} \Rightarrow$$

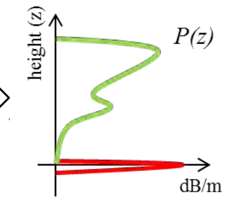

- **The solution is no guaranteed to be ≥ 0**

⇒ Countermeasures needed to enforce positive definitiveness

- Not equivalent to coherent focusing – convergence in expected value if proper weighting is applied
- Assumption: **Stationary Forest = Stable Structure**

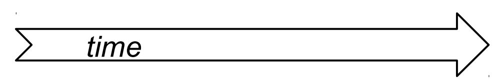

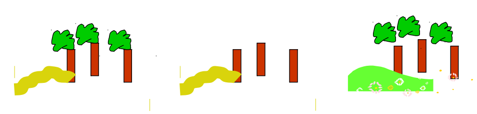

Non-frozen, non-stationary forest
→ Structural variations

Physical source: seasonality, weather conditions, soil moisture, forest growth, …

L band spaceborne mission project

SAOCOM-CS: a passive Companion Satellite to SAOCOM

In 2013, ESA received an offer from the National Commission for Space Activities of Argentina (CONAE) to launch a small satellite with the SAOCOM-1b satellite, and to collaborate during the mission exploitation phase

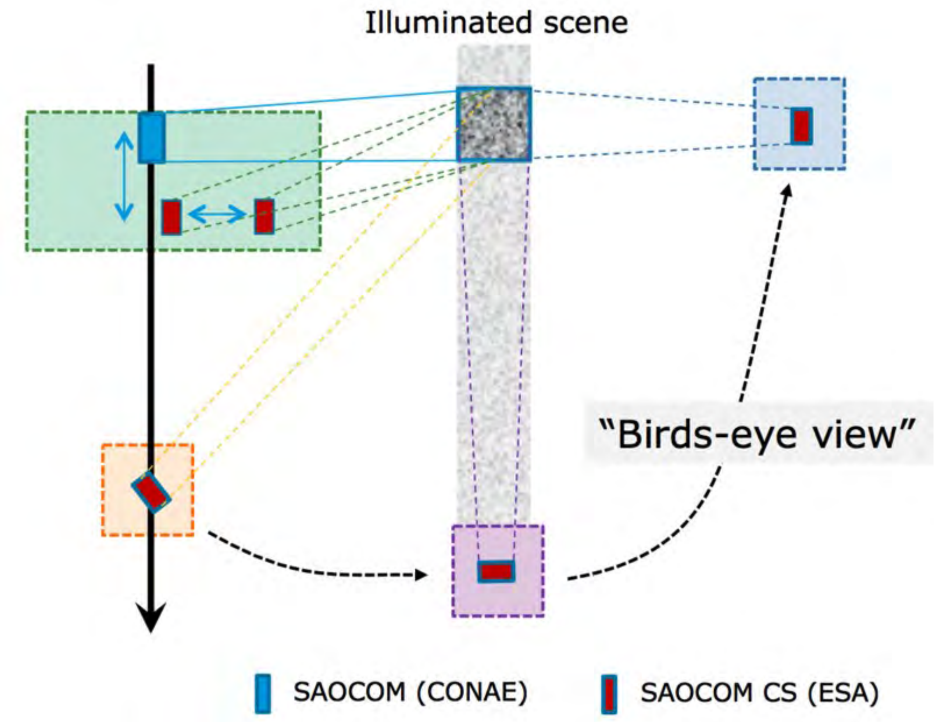

PARSIFAL

ESA EE9 Mission proposal

L band spaceborne mission proje

SAOCOM parameters	Description
Orbit	Sun-synchronous nearly circular frozen polar orbit
Repeat cycle	16 days (one satellite)
Mission lifetime	5 years
Payload	L-band fully-polarimetric SAR
Central frequency	1275 MHz
Incidence angle	20–50°
Spatial resolution	5 m (Stripmap)
Bandwidth	Up to 45 MHz
Noise Equivalent Sigma Zero (NESZ)	−27.9 (Stripmap single-polarisaton worst case)

SAOCOM-CS Application Field	Measurement Geometry	Maturity Level
Boreal forests	**Tomographic**	Science driver
Tropical forests	**Tomographic**	In-orbit demonstrator
3D ice motion	AT Bistatic, Perp. Bistatic	In-orbit demonstrator
Surface and asset deformation	AT Bistatic, Perp. Bistatic	In-orbit demonstrator
Soil moisture	Perp. Bistatic, Specular	In-orbit demonstrator
Ice subsurface structure	**Tomographic**	In-orbit experiment
Arid zones	Perp. Bistatic	In-orbit experiment
Other experiments	All	In-orbit experiment

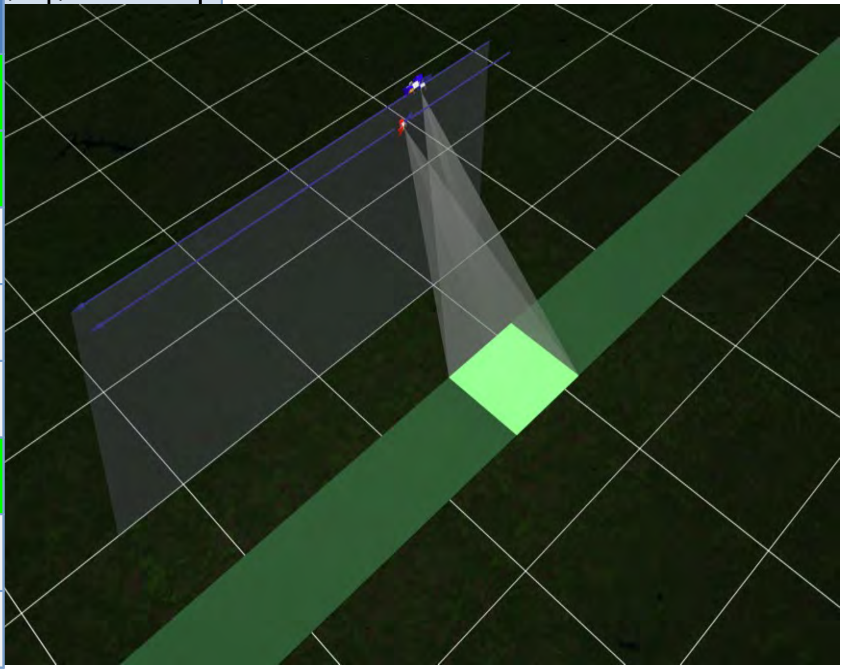

L band spaceborne mission project

Campaign	BioSAR 2008 - ESA
System	E-SAR - DLR
Site	Krycklan river catchment, Northern Sweden
Scene	Boreal forest Pine, Spruce, Birch, Mixed stand
Topography	Hilly
Tomographic Tracks	6 + 6 – Fully Polarimetric (South-West and North-East)
Carrier Frequency	P-Band and L-Band
Slant range resolution	1.5 m
Azimuth resolution	1.6 m
Vertical resolution (P-Band)	20 m (near range) to >80 m (far range)
Vertical	6 m (near range) to 25 m (far

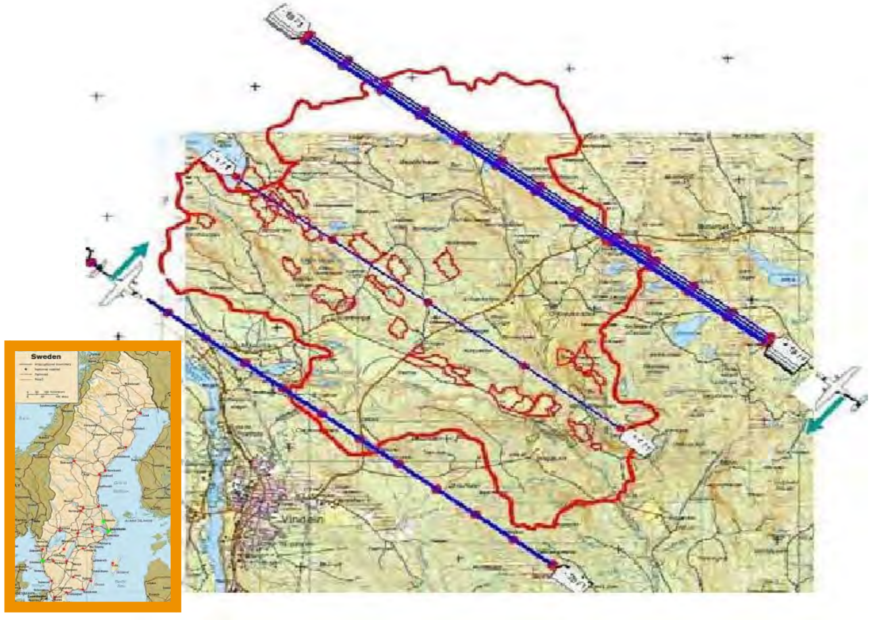

SAOCOM-CS Tomography (from airborne data)

Data simulation

- Range filtering from 100 MHz to 40 MHz
- Degraded azimuth resolution from 1.6 m to 8 m

Tomographic pre-processing

- Incoherent processing based on 5 InSAR pairs (w.r.t. a common Master)
- Coherence interpolation onto a regular baseline grid

Tomographic focusing

- **Beamforming** approach with triangular weights
- **Capon filtering** to achieve super-resolution capabilities

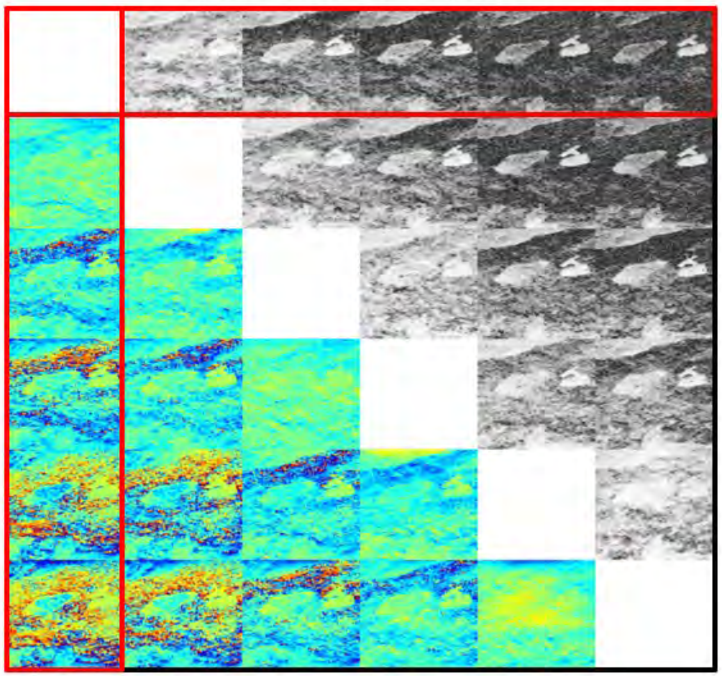

Coherence vector (Nx 1)

$$\boldsymbol{\gamma} = \begin{bmatrix} \gamma_1 \\ \gamma_2 \\ \vdots \\ \gamma_N \end{bmatrix}$$

⇨ *Interpolation on a regular baseline grid* ⇨

Regularized coherence vector (N x 1)

$$\tilde{\boldsymbol{\gamma}} = \begin{bmatrix} \tilde{\gamma_1} \\ \tilde{\gamma_2} \\ \vdots \\ \tilde{\gamma_N} \end{bmatrix}$$

⇨

Reconstructed coherence matrix (N+1 x N+1)

$$\mathbf{R} = \begin{bmatrix} 1 & \tilde{\gamma_1}^* & \cdots & \tilde{\gamma_N}^* \\ \tilde{\gamma_1} & 1 & & \\ \vdots & \tilde{\gamma_1} & \ddots & \vdots \\ \tilde{\gamma_N} & & \cdots & 1 \end{bmatrix}$$

⇨ *TomoSAR focusing*

Vertical sections

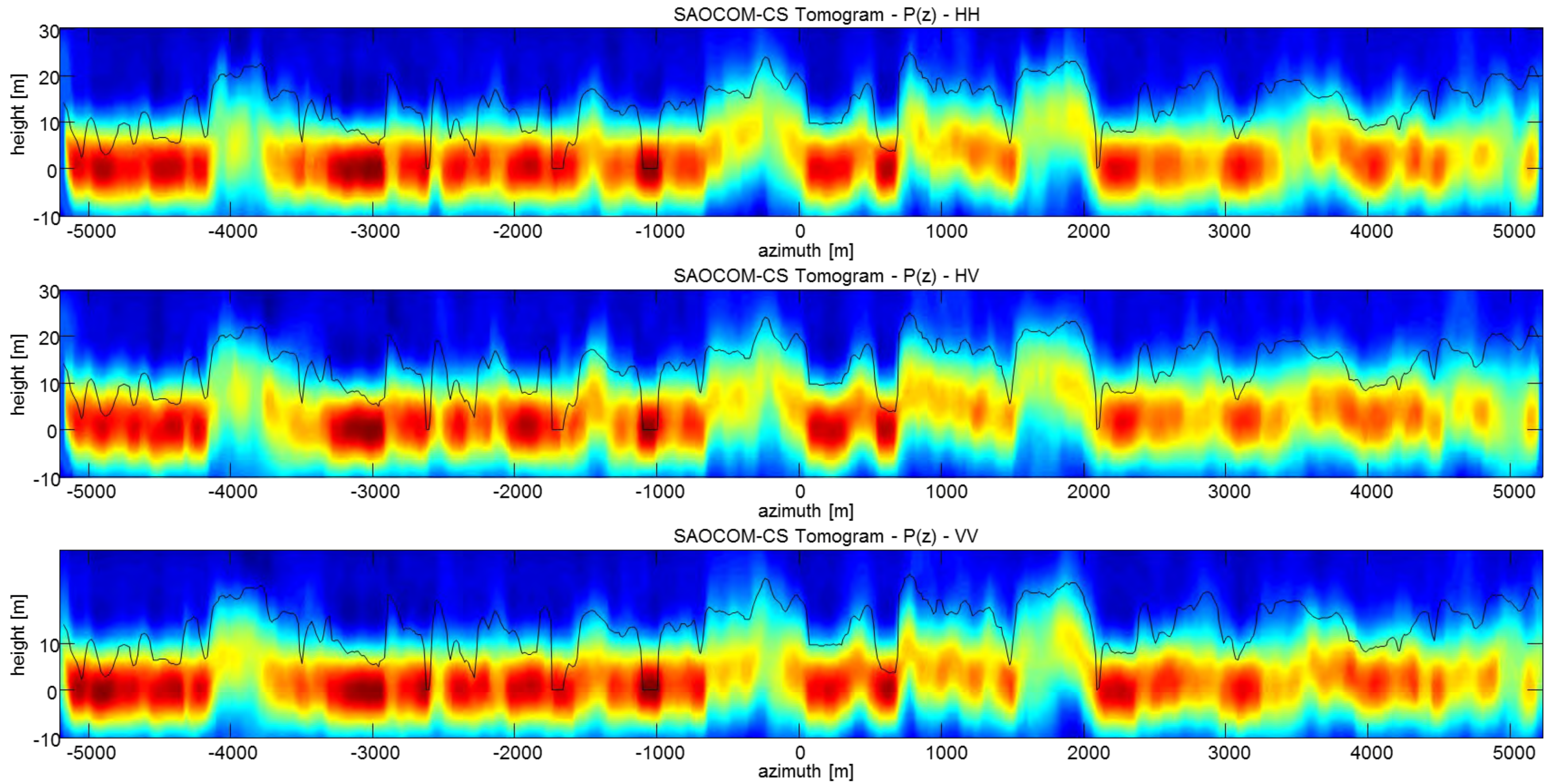

Focusing method: Beamforming

Vertical sections

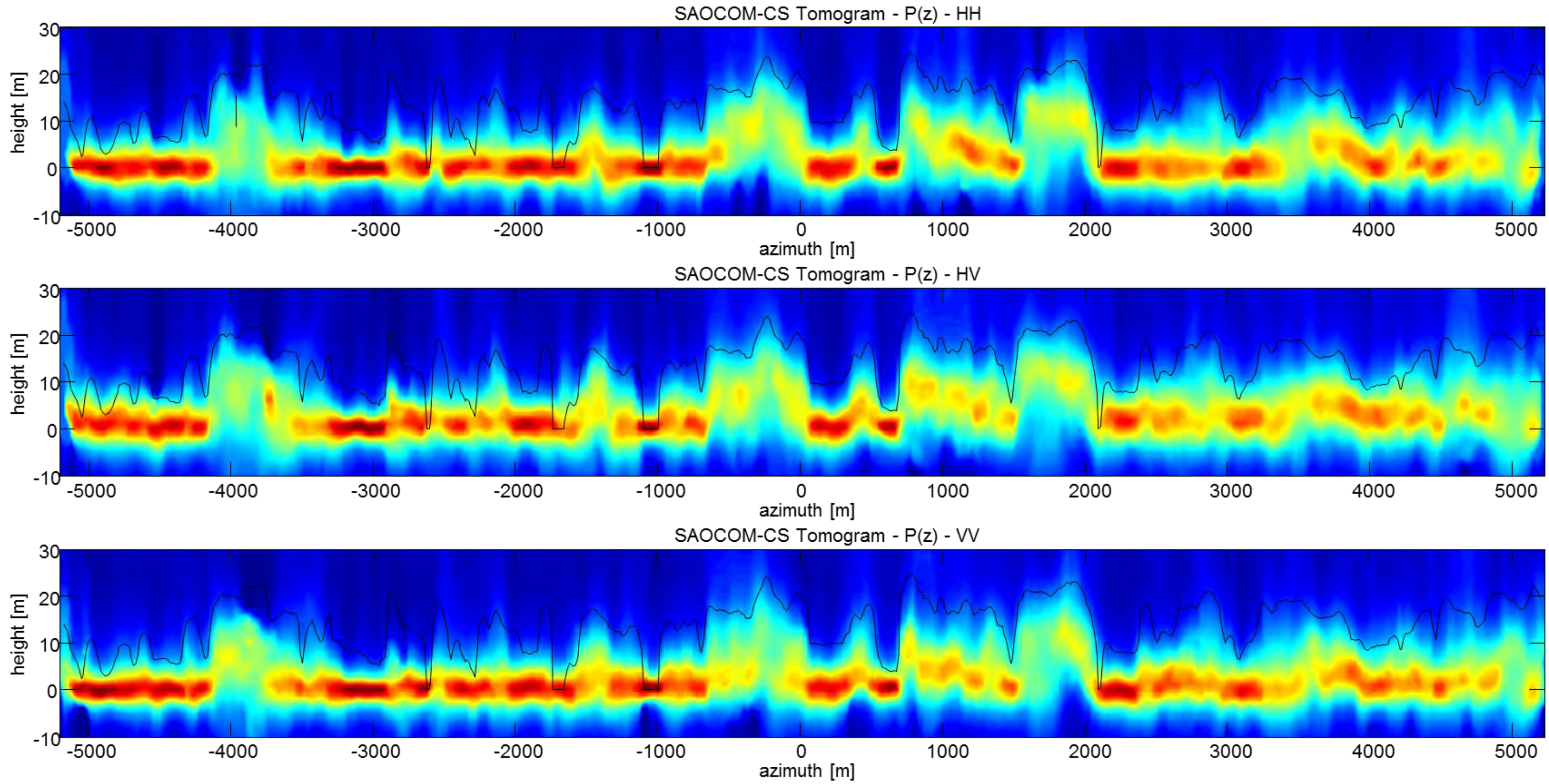

Focusing method: Capon

Height retrieval performance

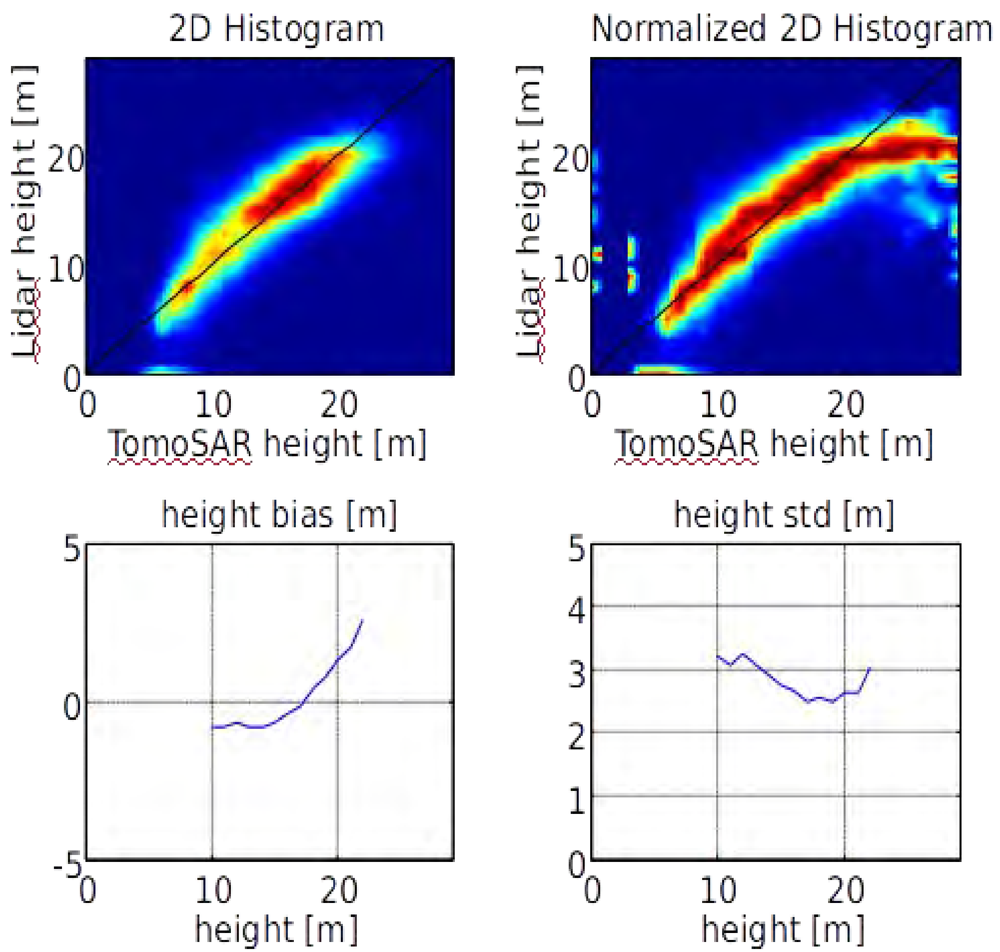

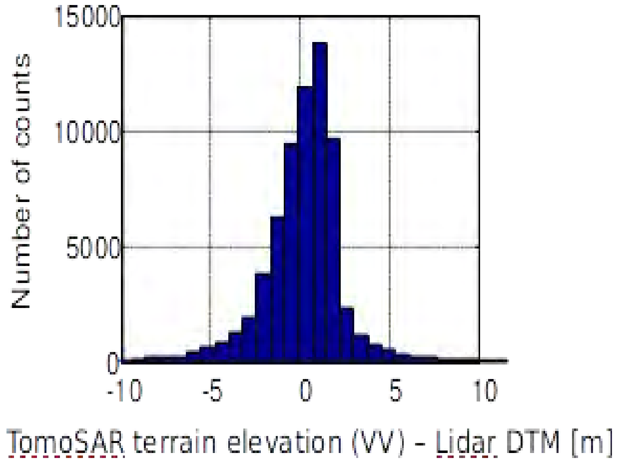

! " # $ # % & ' ( ) * ! + ' , - . ,

((/ - . ' " - # 0 ! # 1 ! 2 # / 3 # $ # !

3 # 4 ' & 5 , ! , (' . 6 + # & 0 6 ! ! " # $ #

. 7 0 # 4 / 6 5 % 6 $ 6 0 " ,

! ! , . ' " " 6 & 6 & ! / # . ' , "@ 5 5 D - $ > 5) ! (# 0 - 6 ! 9 0 ,

$$s_{r_i}(\pm\Delta x_a) = a_{c_i}\, e^{-jk\sqrt{r_i^2+(x_0\mp\Delta x_a)^2}} \longrightarrow x_0, a_c$$

! 6 A 6 & ' / ! , . ' " " 6 & 6 & , ; ! ! $ ' 0 * ! ' D - $ > ") ! (# , -

$$\delta x = \frac{\lambda_c}{4\sin\left(\frac{\Delta\phi}{2}\right)}$$

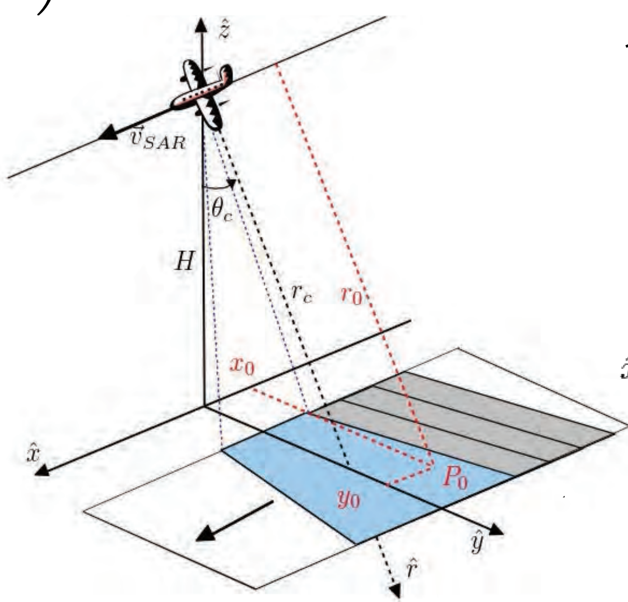

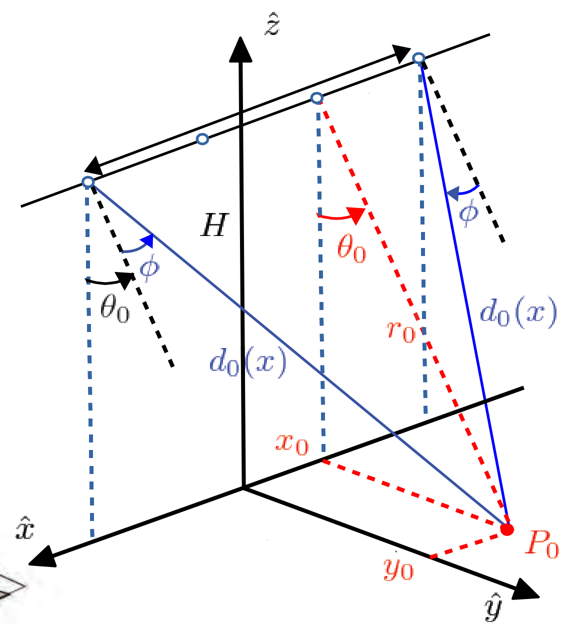

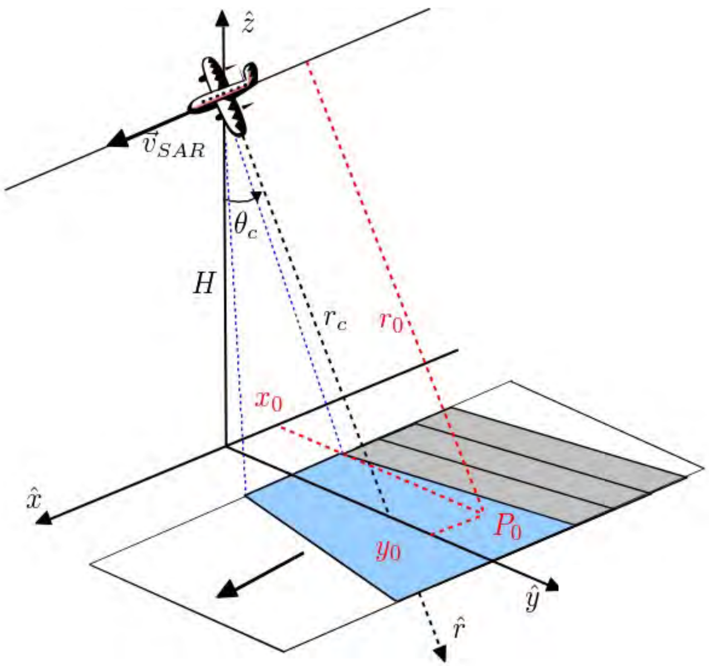

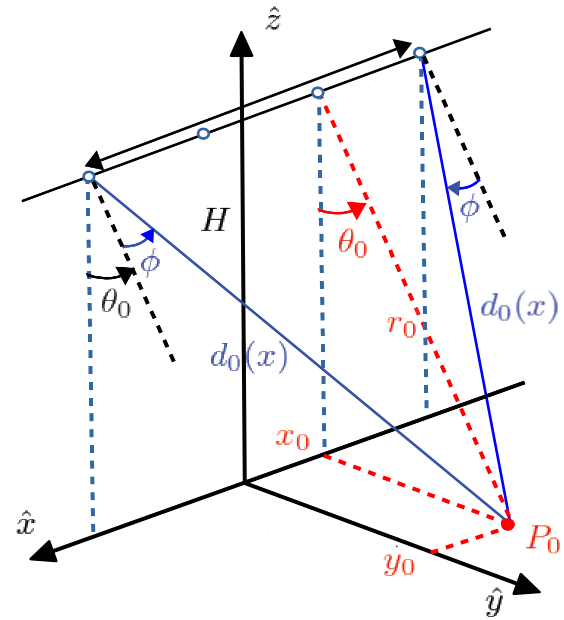

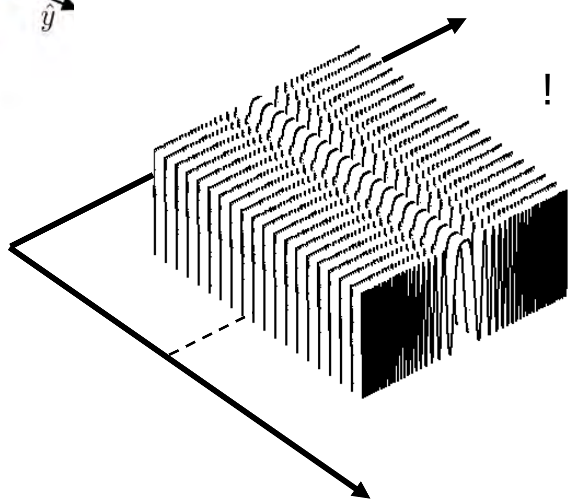

- ; B * ! " > %4%>?' #) +*%#C

2) & $\tau = \dfrac{2d}{c}$

5 & 3 2 6 & %7 ! $p(\tau)\,\mathrm{rect}\left(\dfrac{\tau}{T_p}\right)$

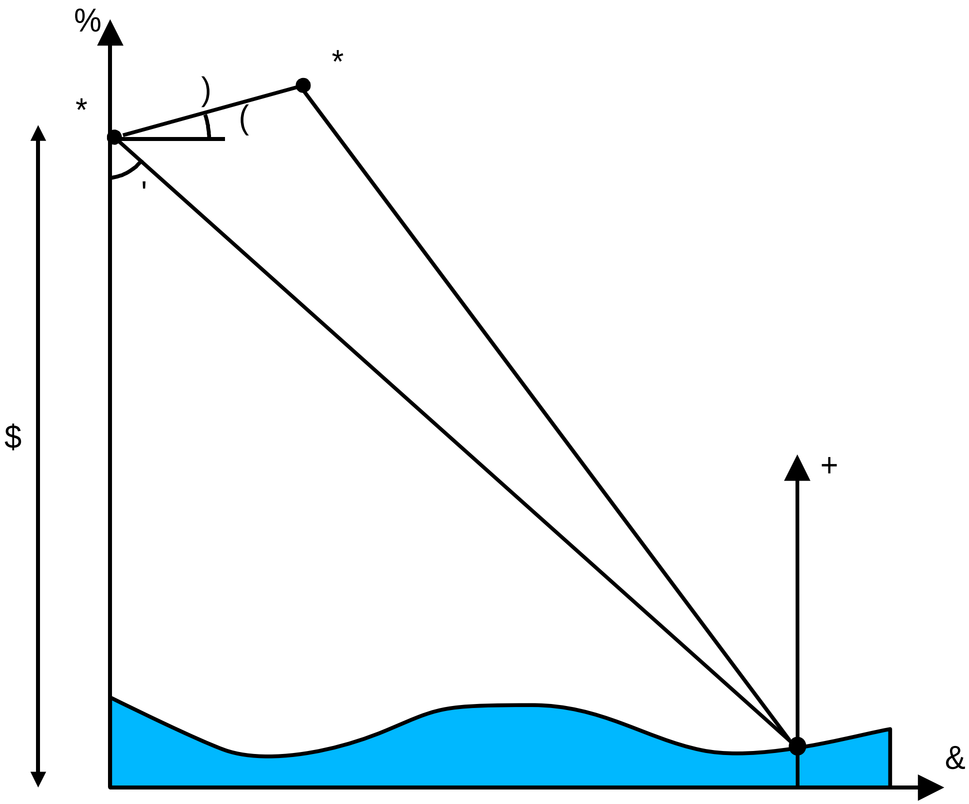

A ' H " ! " # $ %* # 6 ' !) $ * ' #

$$s_1 = |a_{c_1}| \exp\left(-j\frac{4\pi}{\lambda_c} r_1 + j + \phi_{obj_1}\right)$$
$$s_2 = |a_{c_2}| \exp\left(-j\frac{4\pi}{\lambda_c} r_2 + j + \phi_{obj_2}\right)$$

0 # , - 1 % 4 4) = $ * ' # 4 %C 4)

$$|a_{c_1}| \approx |a_{c_2}|, \quad \phi_{obj_1} \approx \phi_{obj_2}$$

0 # , - 1 %= H 4 " %> * 6 6 " ! " # ; '

$$\phi_{12} = \arg(s_1 s_2^*) = \frac{4\pi}{\lambda_c}(r_2 - r_1) = k_c \Delta r_{12}$$

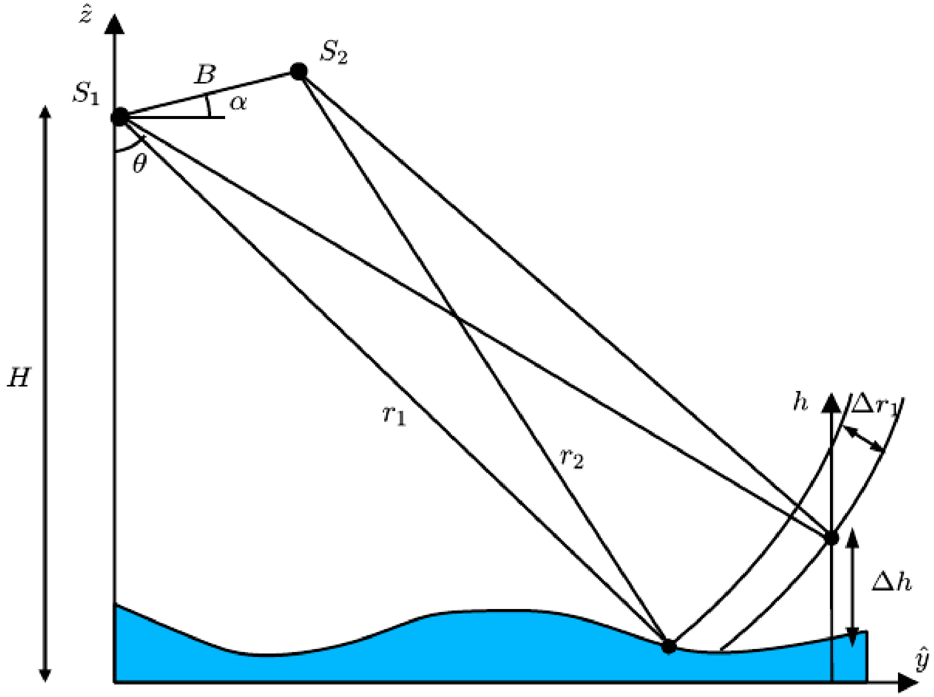

& ! (6 * " + > % " D J J %4 E * ' # %

$$\phi_{12} = k_c B \sin(\alpha - \theta)$$

, " # 4 * $ * 3 * $ 5 %$ ' %$ " ! ! *

$$\theta = f(H, r_1, h)$$

' ; + %+ * # " ! * K $ * ' #

$$\boxed{\begin{aligned} \Delta\phi_{12} &= k_z \Delta h + k_{fe} \Delta r_1 \\ &= \Delta\phi_{topo} + \Delta\phi_{fe} \end{aligned}}$$

$$k_z = \frac{k_c B_\perp}{r_1 \sin\theta}, \quad k_{fe} = k_z \cos\theta$$

0 5 " - (. - ' . " & < " " = + , " $ > # ! #

F - & 6 . " ! K E F ! - $ ' % - 0 % ! # 1 ! ' 0

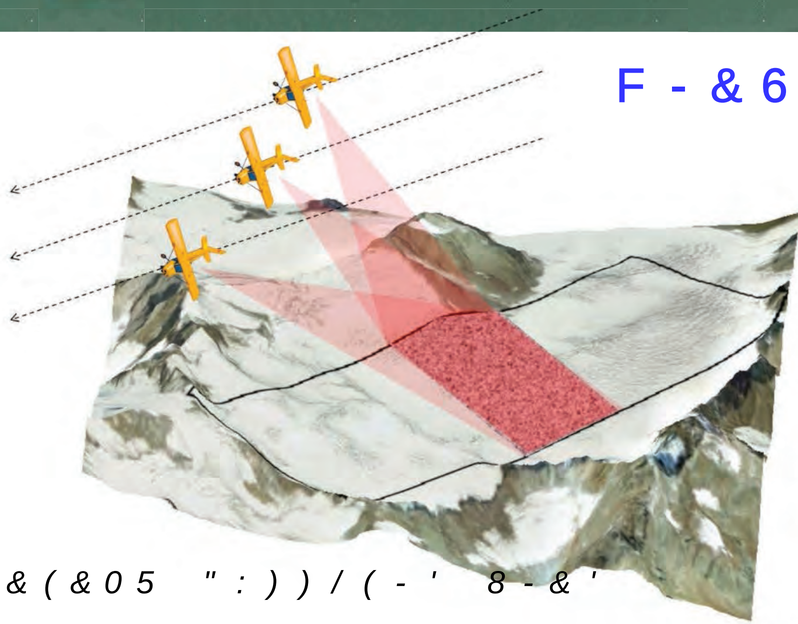

4 & (& 0 5 " :)) / (- ' 8 - & '

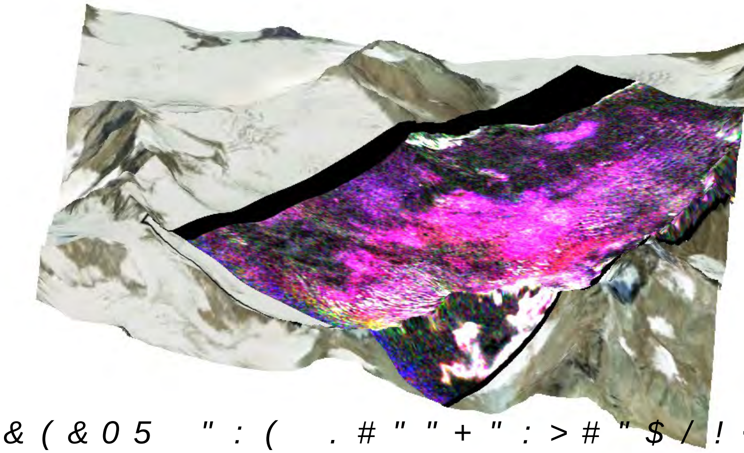

4 & (& 0 5 " : (. # " " + " : > # " $ / ! < #

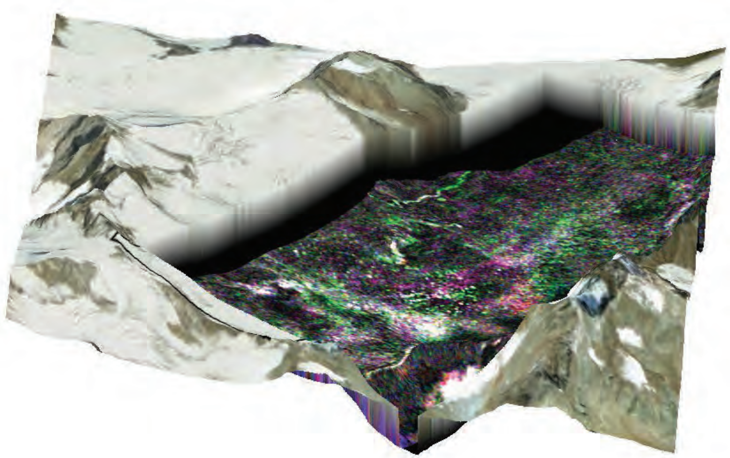

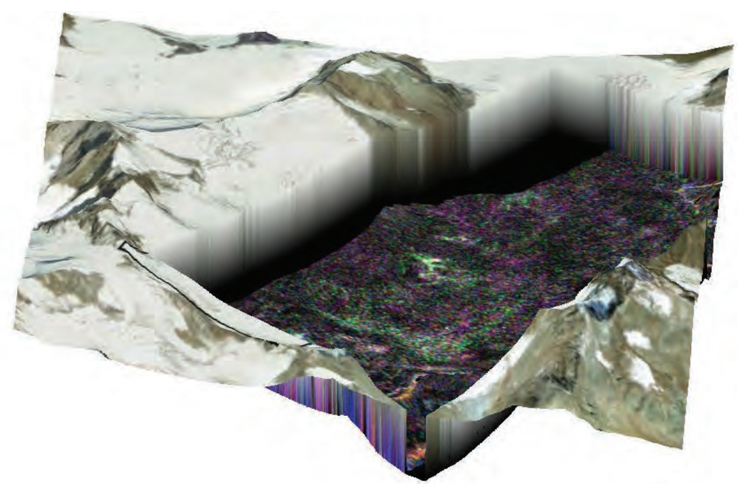

4 & (& 0 5 " : (. # " " + " ; @ " (" A #) & B " 8 4 & (& 0 5 # " " $ / (! < # > " # " + " @ C " (" A #) & B ?

Multiple baselines : Illumination from multiple points of view

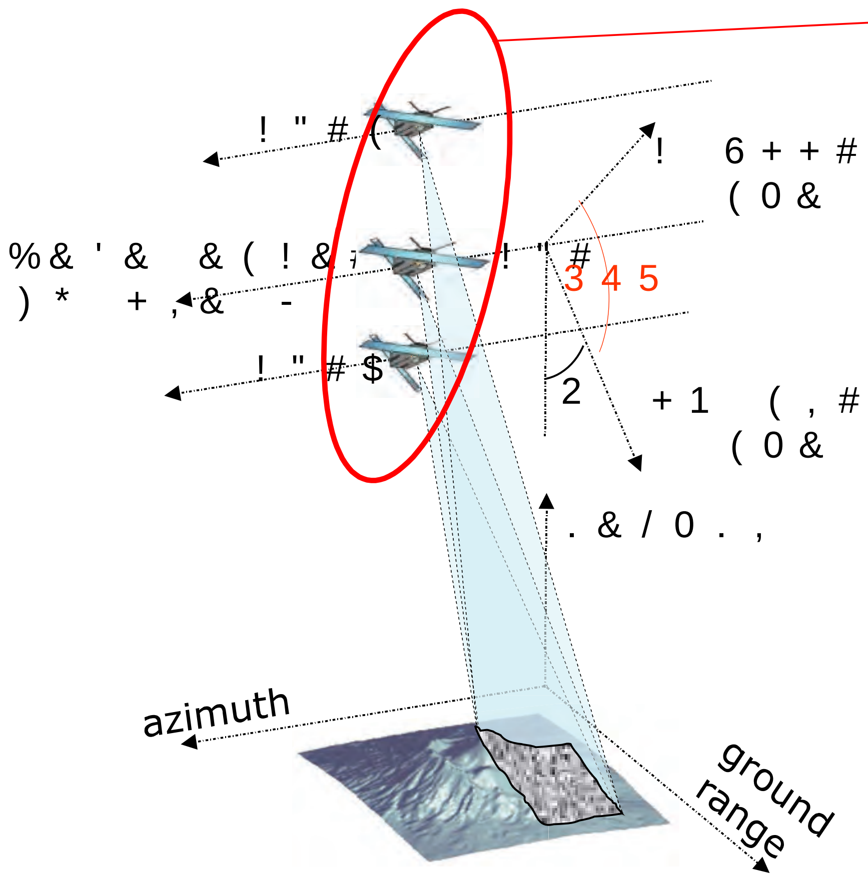

" 2 3 4 5 0 4 3 % ! 6 , 5 7 3 1 + 1 % + , %
/ 4 1 1 8 4) , * 3 % 9 + 4 3 / 5 + ,
⇒ : 4 1 1 8 4) , * 3 % 4 3 1 ; 0 5 +
/) 2) < + ; + 5 + 3 1